Journal of Energy Storage 21 (2019) 801–825

Contents lists available at ScienceDirect

Journal of Energy Storage

journal homepage: www.elsevier.com/locate/est

Review of supercapacitors: Materials and devices

Poonam[a], Kriti Sharma[b], Anmol Arora[a], S.K. Tripathi[a,*]

[a] Department of Physics, Centre for Advanced Study in Physics, Panjab University, Chandigarh, 160014, India
[b] Department of Physics, Goswami Ganesh Dutta Sanatan Dharma College, Sector 32-C, Chandigarh, 160014, India

ARTICLE INFO

Keywords:
Supercapacitor
Specific capacitance
Energy density
Power density
Novel electrode materials
New energy devices

ABSTRACT

Supercapacitors have gained a lot of attention due to their unique features like high power, long cycle life and environment-friendly nature. They act as a link for energy-power difference between a traditional capacitor (having high power) and fuel cells/batteries (having high energy storage). In this perspective, a worldwide research has been reported to address this and rapid progress has been achieved in the advancement of fundamental as well as the applied aspects of supercapacitors. Here, a concise description of technologies and working principles of different materials utilized for supercapacitors has been provided. The main focus has been on materials like carbon-based nanomaterials, metal oxides, conducting polymers and their nanocomposites along with some novel materials like metal-organic frameworks, MXenes, metal nitrides, covalent organic frameworks and black phosphorus. The performance of nanocomposites has been analysed by parameters like energy, capacitance, power, cyclic performance and rate capability. Some of the latest supercapacitors such as electrochromic supercapacitor, battery-supercapacitor hybrid device, electrochemical flow capacitor, alternating current line filtering capacitor, micro-supercapacitor, photo-supercapacitor, thermally chargeable supercapacitor, self-healing supercapacitor, piezoelectric and shape memory supercapacitor have also been discussed. This review covers the up-to-date progress achieved in novel materials for supercapacitor electrodes. The latest fabricated symmetric/asymmetric supercapacitors have also been reported.

1. Introduction

Energy is vital for human development. Energy consumption and production, which depend on combustion of fossil fuels, is going to affect the world economy and ecology severely. So, there has been an increasing demand for environment-friendly, high-performance renewable energy storage devices. Electrochemical energy is an unavoidable part of the clean energy portfolio. Batteries, supercapacitors (SCs) and fuel cells are unconventional energy devices working on the principle of electrochemical energy conversion. SCs have gained much attention on account of high specific capacitance (C_s), long life cycle, high power density (P_d), being almost maintenance free, experiencing no memory effect, safe and function as a bridge for power-energy difference that exists between capacitor (high P_d) and fuel cells/batteries (large energy storage) [1–4]. These present a viable solution for providing energy in rural areas, where no public grids are available or where a heavy cost of wiring and providing electricity is involved. SCs can also be utilized as power supplies for portable devices like mobile

Abbreviations: SC, supercapacitor; SCs, supercapacitors; ASCs, asymmetric supercapacitors; C_s, specific capacitance; P_d, power density; E_d, energy density; EDLCs, electric double layer capacitors; ACs, activated carbons; CNTs, carbon nanotubes; CDC, carbide derived carbon; TMOs, transition metal oxides; MOs, metal oxides; CPs, conducting polymers; PANI, polyaniline; PPy, polypyrrole; PVA, polyvinyl alcohol; PEDOT, poly34-ethylene-dioxythiophene; PSS, poly (4-styrene sulfonate); PPV, poly-phenylene vinylene; PW, potential window; MOFs, metal organic frameworks; COFs, covalent organic frameworks; ACFM, activated carbon fibre material; SSA, specific surface area; ILs, ionic liquids; CFC, carbon fibre cloth; MWCNTs, multi walled carbon nanotubes; PVDF, poly-vinylidene fluoride; PTFE, poly tetrafluoroethylene CVD chemical vapour deposition; GO, graphene oxide; SILAR, successive ionic layer adsorption and reaction; HPCNTs, hierarchical porous carbon microtubes; GMAs, graphene macro assemblies; AQ, anthraquinone; CMG, chemically modified graphene; SWCNTs, single walled CNTs; Pind, polyindole; NWs, nanowires; NS, nanosheets; ESR, equivalent series resistance; rGO, reduced graphene oxide; DMF, N N-dimethyl formamide; TGA, thermogravimetric analysis; SEM, scanning electron microscopy; η, coulombic efficiency; CV, cyclic voltammetry; CoS_2-rGO, cobalt disulphide-reduced graphene oxide; N-CNFs, nitrogen functionalized carbon nanofibres; NFs, nanofibres; rGO@HTC, N-doped hydrothermal carbon coated graphene; PpPD, poly (phenylenediamine); HEG, hydrogen exfoliated graphene; CQDs, Carbon Quantum Dots; +ve, positive; -ve, negative; photo-SCs, photosupercapacitors; DSSC, dye-sensitized solar cells; ATO, anodic titanium oxide; PSSH, polystyrene sulfonic acid; PEO-NaOH, NaOH-treated polyethylene oxide; BC, biochar; SMSC, shape memory supercapacitor; FESEM, field effect scanning electron microscopy; XRD, X-ray diffraction; TEM, transmission electron microscopy; CD, charge-discharge; NF, nickel foam

* Corresponding author.
E-mail address: surya@pu.ac.in (S.K. Tripathi).

https://doi.org/10.1016/j.est.2019.01.010
Received 5 October 2018; Received in revised form 9 January 2019; Accepted 9 January 2019

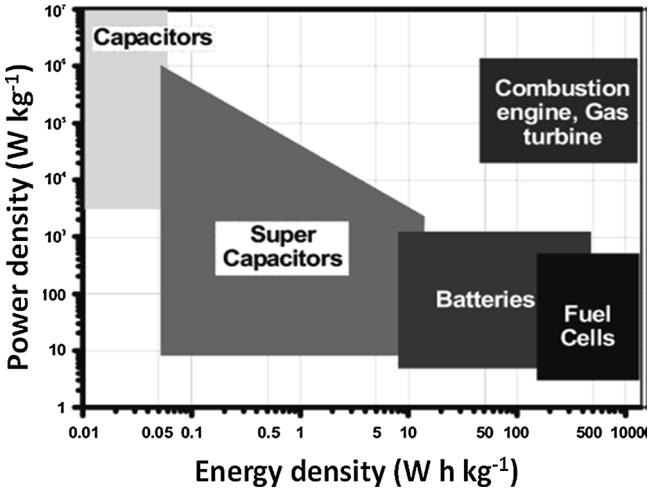

Fig. 1. Ragone plot of different electrochemical energy conversion systems, combustion engine, turbines and traditional capacitors [5]. (Reproduced with permission from Ref. [5] Copyright American Chemical Society (2004)).

phones, notebook computers, digital cameras etc. -being small, lightweight and flexible. In electric and hybrid vehicles, SCs may be used to offer high P_d required for short-term acceleration along with recuperation of energy during braking, hence saving energy and shielding the batteries from the high frequency rapid charging-discharging process (dynamic operation). The P_d and energy density (E_d) are represented by Ragone plot (Fig. 1). This plot explains that the fuel cells are high-energy systems; whereas SCs are high-power systems. Batteries have intermediary power and energy capabilities. There exists some overlap in E_d and P_d of fuel cells and SCs with batteries. Also, it is apparent from the figure that any single electrochemical device cannot compete with an internal combustion engine. So E_d and P_d of electrochemical devices have to be increased to compete with the combustion engine [5].

The credit for the beginning of capacitor technology goes to the invention of the Leyden Jar (1745–1746) which was made up of a glass vessel with metal foils. The metal foils acted as electrodes and the jar acted as a dielectric. In the charging process of the above mentioned device, positive (+ve) charges accumulated on one electrode and negative (-ve) charges on the other. When these two charges were connected using a metal wire, a discharging process would take place. The first electrolytic capacitor came in the 1920s. In 1957, the first supercapacitor (electric double layer capacitors-EDLCs) was patented by General Electric using activated charcoal as the plates. In EDLCs, charge storage takes place electrostatically (non-Faradaic) i.e. no shifting of charge takes place between electrode and electrolyte (which makes them highly reversible along with high cycling stability). Carbon nanomaterials, like carbon aerogels, activated carbons (ACs), carbon nanotubes (CNTs), graphene, carbide-derived carbon (CDC) etc. are unique structures for EDLCs with the huge specific surface area (SSA), great mechanical and chemical stability and good electrical conductivity. To increase the C_s of SCs, new electrochemically active materials had been investigated for pseudocapacitors (Faradaic charge transfer).

During 1975–1980, B. E. Conway explored RuO_2 pseudocapacitors extensively. These capacitors store charge through electrosorption, oxidation-reduction reactions and intercalation mechanism [6]. These faradaic processes would let pseudocapacitors attain higher C_s and E_d compared to EDLCs. Pseudocapacitance is linked to the electron charge-transfer among electrolyte and electrode impending from de-solvated and adsorbed ion. The adsorbed ions do not react with the atoms of the material, but only the transfer of charge occurs. The capacity of electrodes to achieve pseudocapacitance effect depends on the chemical affinity of materials to the ions adsorbed on the surface of the electrode along with the structure and the dimension of the electrode pores. The charge storage increases linearly with the applied voltage. Materials that exhibit redox behaviour and used in pseudocapacitors are transition-metal oxides (TMOs) eg. IrO_2, RuO_2, Fe_3O_4, MnO_2, NiO, V_2O_5, Co_3O_4 etc. transition metal sulphides and conducting polymers (CPs) eg. polyaniline (PANI), polythiophene, polypyrrole (PPy), polyvinyl alcohol (PVA), poly (3,4-ethylene dioxythiophene) (PEDOT), polyacetylene, poly (4-styrene sulfonate) (PSS), poly-phenylene-vinylene (PPV) etc.

Li-ion capacitors (hybrid capacitors) were explored by FDK in 2007. In such capacitors, a carbon electrode was combined with a Li-ion electrode which increased the capacitance, lowered the anode potential with enhanced cell voltage and hence increased the E_d. In such systems, the faradaic electrode, with high C_s, provides higher E_d and the non-faradaic electrode provides higher P_d. Hence, research has been focussed on hybrid capacitors such as composites (coupling of carbon materials with either CPs or TMOs) and battery type (coupling a supercapacitor (SC) electrode with a battery electrode) etc. Table 1 shows the comparison of EDLC, pseudocapacitor and hybrid supercapacitor [7].

The traditional capacitors have a rigid and massive structure and hence are not suitable for future applications. Thinner, lighter, flexible, transparent SCs with a number of novel features and functions are required for multifunctional consumer electronics. The ACs and TMOs are still the generally used electrode materials. The ACs possess non-regular morphologies, feebly graphitized frameworks with wide pores, whereas TMOs exhibit low electronic conductivity, which is not able to keep pace with high rate energy storage environments [8]. So, new materials for SC electrodes have been explored such as covalent organic frameworks (COFs), metal-organic frameworks (MOFs), MXenes, metal sulphides, metal nitrides, mixed conductors, 2-D materials etc. [9–11].

The key challenge for supercapacitor is the small E_d. As the E_d of capacitors is directly proportional to C_s and the square of the voltage (V), so to increase E_d, either C_s or potential or both of these quantities should be increased. This can be accomplished by using electrode materials having high C_s, electrolytes having broad potential windows and optimization of the structure of integrated systems. Even though the fabrication of individual components (like electrode materials, electrolytes) of the SCs is relatively simple, but to promote their combined effect, the compatibility between the pore size and structure of electrode material with the electrolyte ion size is essential. Electrolytes/solutions play an essential role in setting up important properties like

Table 1
Comparison of EDLC, pseudocapacitor and hybrid capacitor [7].

Electrochemical double layer capacitor (EDLC)	Pseudocapacitor	Hybrid capacitor
1. Carbon is used as electrode material.	MOs and CPs are used as electrode material.	A combination of carbon and MOs/CPs is used.
2. Charge storage mechanism is through the electrochemical double layer formation (non-Faradaic process).	The charge is stored through the redox reactions (Faradaic process).	The charge is stored both by Faradaic and non-Faradaic processes.
3. Low E_d, good rate capability, good cyclic stability, low C_s.	High C_s, High E_d, high P_d, low rate capability.	High E_d, high P_d, good cyclability, polymer/carbon composite has moderate cost and moderate stability, Li/Carbon capacitors are of high cost.

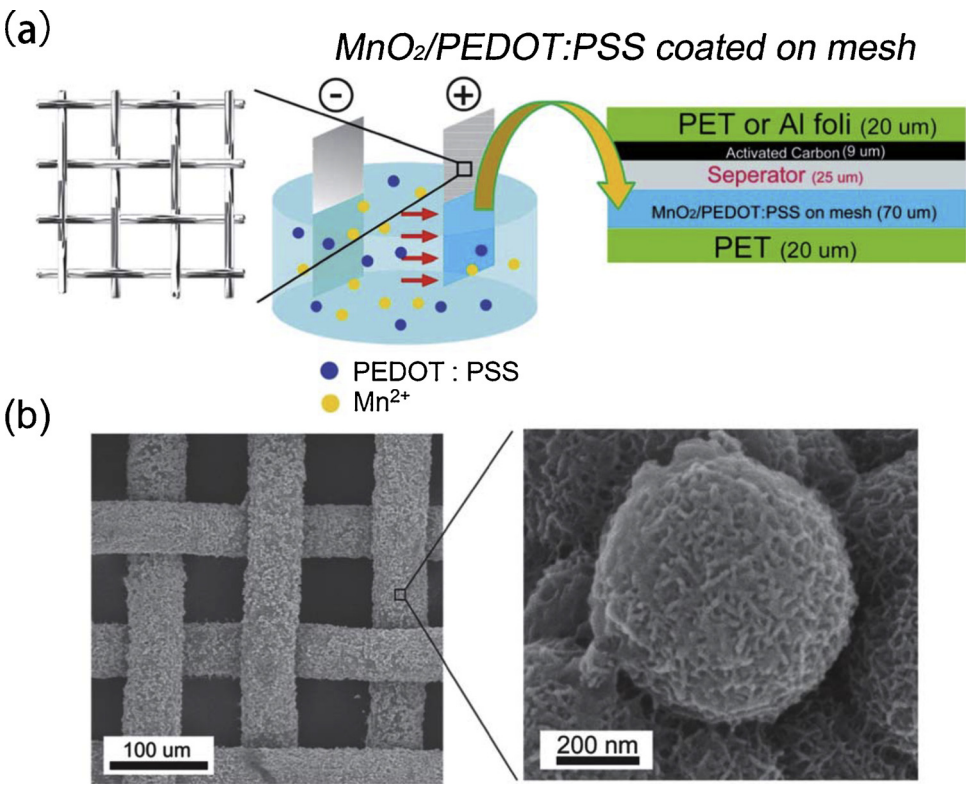

Fig. 2. (a) Schematic of the fabrication process of MnO_2-PEDOT: PSS nanostructured composite by co-electrodeposition on the stainless steel mesh and its fabrication as an asymmetrical supercapacitor (b) SEM images of MnO_2-PEDOT: PSS at diverse magnifications [23]. (Reproduced with permission from Ref. [23] Copyright Royal Society of Chemistry (2013)).

P_d, temperature range and conductivity. Other requirements of electrolytes for SC are: a wide potential window (PW), high ionic concentration, good electrochemical stability, low equivalent series resistance (ESR), less volatility, less viscosity, non-toxicity, small solvated ion radius and low cost [12].

Aqueous, organic, redox-type, solid or semi-solid electrolytes and ionic liquids (ILs) have been investigated extensively for SCs. Aqueous electrolytes (like KOH, Na_2SO_4, H_2SO_4 and NH_4Cl aqueous solution etc.) provide higher ionic concentration, lower resistance, smaller ionic radius, higher C_s and higher P_d than the organic electrolyte. Moreover, in the case of aqueous electrolytes, there is no strict need of controlling the parameters during their preparation process, whereas in an organic electrolyte, there are strict processes and conditions to get ultra-pure electrolytes. The conductivity of the aqueous electrolyte is ~1 Scm^{-1} and it also has a minimum pore size requirement in comparison to the organic electrolyte [13].

The main shortcoming of the aqueous electrolyte is its small PW (approximately 1.2 V) due to water decomposition at 1.23 V. Organic electrolytes have smaller electrical conductivity (10 to 60 $mScm^{-1}$), so lower P_d, but have higher E_d (due to wide PW of 2.5–2.7 V). ILs are appropriate for making SCs electrolyte because of their properties like high thermal and chemical stability [14–16], low vapor pressure, wide potential window, low flammability and conductivity around 10 $mScm^{-1}$. Ion size in ILs is well-identified because solvation shell is not there due to the solvent-free nature of ILs [13]. With the advancements in ILs, PW of the SCs can be extended up to 4 V, though they have small ionic conductivity and high viscosity. Furthermore, the study of semi-solid electrolytes has led to the growth of flexible or solid-state SCs which have no potential leakage issues. Of late, redox-type electrolytes are introduced because of their additional pseudocapacitance from the redox reactions at the electrode/electrolyte interface [17].

2. Synthesis approach for electrode materials

The method of synthesis of electrode materials plays an important role in controlling the structures and properties of the materials. Some synthesis methods are described here briefly:

2.1. Sol-gel method

Sol-gel is a facile method to prepare materials with greater purity and homogeneity. The sol-gel method is so named, as in it micro-particles in the solution (sol) agglomerate and link together in regulated conditions to form an integrated network (gel). Two basic variations of the sol-gel method are the colloidal method and the polymeric or the alkoxide method, which are different from each other on the type of precursors used. In both methods, the precursor is mixed in a liquid (usually water is used for the colloidal method and alcohol for polymeric method) and is then activated with the addition of an acid or a base. Then, as obtained activated precursor reacts forming a network, which it develops with temperature and time maximally up to the container size [18]. Many TMOs have been prepared by this method. This process provides the advantage of preparing materials of different morphologies. The electrode material prepared by this process possesses high SSA with better electrochemical behaviour which can also be controlled by temperature, change of surfactants, solvents and reaction time [19].

Yusin et al. [20] have reported this method for the production of activated carbon fibre material (ACFM)-$Ni(OH)_2$ composite which exhibits the C_s of ~370–380 Fg^{-1}. Also, the dependence of shape, structure and volume of material on the composition and concentration of the solution was established. Liu et al. [21] have deposited $NiCo_2O_4$ films by a sol-gel method which exhibit the C_s of 2157 Fg^{-1} at a 0.133 $mAcm^{-2}$ current density and good cycling stability (96.5% C_s retained after 10,000 cycles). $NiO/LaNiO_3$ electrode fabricated by spin-coating on $Pt/Ti/SiO_2/Si$ (100) substrate by Liu et al. [22] showed a C_s of 2030 Fg^{-1} at a 0.5 Ag^{-1} and high stability (83% of the C_s retention after 1000 cycles). This superior electrochemical response can be related to high porosity, well-connected network structures with reduced mass-transfer resistance between electrolyte and ion which facilitates the electron hopping in nanoparticles.

2.2. Electro-polymerization/Electrodeposition

This is a common synthesis technique which provides precise regulation over the thickness of films and on the rate of polymerization. By suitable choice of deposition solution, nanostructured films with different mass loading and morphologies can be prepared by this method. This technique involves simple processing conditions and not much toxic chemicals are used in it. It is generally used for preparing CPs such as PANI, PEDOT, PPy etc. Su et al. [23] have prepared MnO_2-PEDOT: PSS composite by co-electrodeposition strategy which exhibits an areal C_s of 1670 m F cm^{-2} at 0.5 $mAcm^{-2}$ and excellent mechanical robustness. Fig. 2 depicts the fabrication process of MnO_2-PEDOT: PSS composite and its scanning electron microscopy (SEM) images. Also, an ultra thin (< 200 μm) asymmetric supercapacitor (ASC) is fabricated with high E_d, P_d and rate capability. Nanosized MnO_2 electrodes on Au nanowire stems are grown electrochemically by Chen et al. [24] which exhibit high C_s (1130 Fg^{-1} at 2 mVs^{-1}), high E_d (15 $Whkg^{-1}$ at 50 Ag^{-1}), high P_d (20 kW kg^{-1} at 50 Ag^{-1}) and long-term stability (90% of C_s left after 5000 cycles). ZnO@Ni_3S_2 core-shell nanorods are formed by the electrodeposition method by Xing et al. [25] which exhibit a C_s of 1529 Fg^{-1} at 2 Ag^{-1} and retain 42% of initial C_s after 2000 cycles. Stretchable CNT-PPy films are deposited by electrochemical deposition by Guo et al. [26].

2.3. In-situ polymerization

In this process, monomers are dispersed into an aqueous solution using the sonication process. Then an oxidizing agent is mixed to initialize the polymerization in the aqueous solution and the sample is obtained by filtering the solution. Earlier this method yielded only irregular aggregates with a little portion of nanofibres, but with slight modification, nanoparticles, nanorods, and nanofibres were reported with better solution processability and better physical and chemical properties. A simple strategy for growth of PEDOT structures on carbon fibre cloth (CFC) by in situ polymerization is reported [27]. When a supercapacitor device is fabricated with these nanostructures, it exhibits a C_s of 203 Fg^{-1} at 5 mVs^{-1}, an E_d of 4.4 $Whkg^{-1}$ and P_d of 40.25 kW kg^{-1} in 1 M H_2SO_4 electrolyte. Also, it possesses 86% C_s retention after 12,000 cycles. Wang et al. [28] have deposited PANI nanowires within the multi-walled carbon nanotubes (MWCNTs) by in situ electro-polymerization. The aligned MWCNTs provide support to the organic polymers along with providing a pathway for the transfer of charge. Also, confined MWCNT channels limit the structural changes in PANI chains while charging-discharging and enhance the lifetime of the structure. The films made with CPs encapsulated in MWCNTs showed a C_s of 296 Fg^{-1} at 1.6 Ag^{-1}. Different Π-conjugated sulfonate templates and additional assistance of graphene and MWCNTs are employed to enquire the polymerization behaviour of PEDOT by Zhou et al. [29]. As prepared PEDOT: MWCNT composite reveals interconnected network due to the Π-Π interaction of PEDOT with non-covalent functionalized MWCNT and exhibits a C_s of 199 Fg^{-1} at 0.5 Ag^{-1}.

2.4. Direct coating

This technique is employed for the fabrication of those SC electrodes in which active material, in the form of slurry, is applied directly on the substrate. Often, additives such as carbon black, polyvinylidene fluoride (PVDF), acetylene black, polytetrafluoroethylene (PTFE) are introduced as binders to provide maximum adhesion along with retaining electrical conductivity. The working electrode is fabricated with 90 wt% electrode materials (NiO) and 10 wt% PVA in millipore water as a solvent and the slurry obtained is pasted on the Pt disc. [30]. Jana et al. [31] prepared supercapacitor electrode slurry by mixing nitric acid treated carbon cloth with 10% PVDF and DMF (*N,N*-dimethyl formamide) and the prepared slurry is coated on a stainless-steel substrate. Du et al. [32] synthesized supercapacitor electrode by coating the slurry formed by adding active material with acetylene black and PTFE onto Ni foam.

2.5. Chemical vapour deposition (CVD)

CVD technique is generally used where the porosity is very important. This process is performed under vapour phase, where the initial material is prepared in vapour form, flowed and subjected to a high temperature (800–1000 °C). The as-prepared structures have even morphology [33]. Among various synthesis methods of graphene for instance, mechanical cleavage of graphite, chemical exfoliation of graphite (in organic solvents), manufacturing of multi-layered graphene by arc discharge, reduction of graphene oxide (GO) synthesized from the oxidation of graphite, graphene synthesized by CVD provides better results owing to their large crystal domains, monolayered structure and fewer defects in the sheets, which are helpful for enhancing carrier mobility [34]. Kalam et al. [35] demonstrated that high-efficiency SCs with improved electrochemical characteristics can be fabricated by CVD grown graphene hybridized with MWCNTs. Lobiak et al. [36] prepared hybrid carbon materials consisting of MWCNTs and graphitic layers, produced by CVD, over MgO assisted metal catalyst, as depicted in Fig. 3. Such materials provide fast charge transport in the cell.

2.6. Vacuum filtration technique

This quick and proficient technique uses the simple concept of vacuum filtration to prepare nanocomposites from a physical combination of different materials. Generally, a mixture of materials is prepared followed by simple vacuum filtration and drying the filtrate. In this method, the composition can be simply altered by varying the concentration or the weight percentage of each constituent in the mixture. Graphene suspension, developed by vacuum filtration deposition by Zhang et al. [37] for fabricating graphene-based Ni foam electrode, shows a higher E_d and P_d along with good cycling performance. Xu et al. [38] have synthesized a nanocomposite of graphene/AC/PPy by vacuum filtration method. As prepared electrode exhibits the C_s of 178 Fg^{-1} at 0.5 $mAcm^{-2}$ and retains 64.4% of C_s after 5000 charge/discharge cycles. Y. Gao [39] has used this technique to prepare graphene/polymer electrode on Ni foam in which the vacuum pressure and its duration controls the distribution of graphene.

2.7. Hydrothermal/solvothermal method

The hydrothermal process can be ascribed as environment-friendly superheated aqueous solution dispensation. In addition, this provides controlled diffusivity within a closed system. The process has superiority over other techniques as it is ideal for preparing designer particulates (particles with high purity, crystallinity, quality and controlled chemical and physical characteristics). Also, this is a low-temperature sintering process with a small energy requirement which is simple to implement and scale up [40]. However, this process has a lesser control over nanoparticle aggregation. The solvent properties (e.g. dielectric constant, solubility) change radically in the supercritical phase. Thus, supercritical phase gives a favourable condition for particle formation owing to increased reaction rate and great supersaturation. If some other solvent is used instead of water, then the method is called solvothermal synthesis. A lot of SC electrodes have been fabricated using this process such as rod-like hollow $CoWO_4/Co_{1-x}S$ [41], Cobalt disulfide-reduced graphene oxide (CoS_2-rGO) [42], hexagonal $NiCo_2O_4$ nanoparticles [43] etc.

2.8. Co-precipitation method

This is a facile method for large-scale production of powder samples. For precipitation to take place, the concentration of one solute

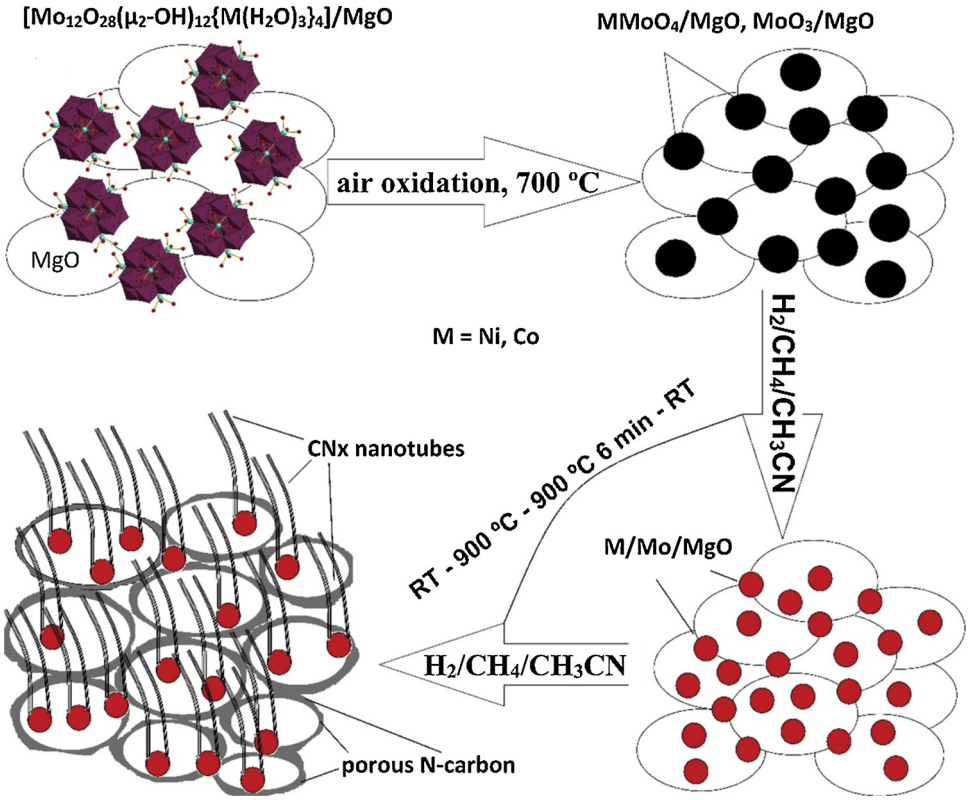

Fig. 3. Schematic representation of the preparation of nitrogen-doped porous MWCNTs hybrid by using Ni or Co polyoxomolybdate clusters [36].

should be more than the solubility limit and temperature should be high enough for fast separation into precipitates. Here, it is difficult to regulate the morphology of prepared samples due to the fast rate of precipitation. Various supercapacitor structures have been reported using this method such as $CoFe_2O_4$-magnetic nanoparticles with different precursors [44], $Ni_3(PO_4)_2$@GO composite [45] which exhibits a C_s of 1329.59 Fg^{-1} at a 0.5 Ag^{-1} and 88% of the C_s retention after 1000 cycles.

2.9. Dealloying method

Dealloying method, also known as selective dissolution, is an easy, flexible and economical technique to produce nanoporous metallic materials (NPMs) with structures like core-shell, hollow core-shell and porous nanoparticles [46]. In this method, more active material is removed from a solution of binary metallic solid by electrolytic dissolution thus producing an interconnected porous structure. Such structures possess higher surface area, good mechanical and compression strength along with size-scale dependent elastic modulus [46–48]. Much attention has been given to NPMs prepared by this method since the important work of Erlebacher et al. [46] and has become a very important method to produce NPMs in the last decade. Li et al. [49] examined the fixed voltage dealloying of AgAu alloy particles in the size range of 2–6 nm and 20–55 nm. They demonstrated that only the core-shell structures (2–6 nm in diameter) evolved above the potential corresponding to Ag^+/Ag equilibrium. CuS nanowire on nanoplate network with improved electrochemical performance has been prepared by Wang et al. [50] using an improved dealloying method at two contrasting reaction temperatures. Cu_2O has been synthesized by oxidation assisted dealloying method [51]. Free-dealloying method has been used for the synthesis of Cu-based metallic glasses in HF and HCl solutions [52]. Lu et al. [53] reported a green and universal technique (vapour-phase dealloying) for fabricating porous materials by using vapour pressure among constituent elements in an alloy, to selectively eliminate a component with high vapour pressure, for producing 3-dimensional bicontinuous open nanoporosity. With this technique, extensive elements can be fabricated with tunable pore sizes along with full recovery of the evaporated component. Flexible electrodes of Co_3O_4 flakes and γ-Fe_2O_3 nanoparticles have been prepared by oxidation assisted dealloying method for the first time by Wang et al. [54].

2.10. Other synthesis methods

Several other synthesis methods have been reported for SC electrodes. The microwave assisted method has been used for rapid synthesis of tin selenide [55]. Nitrogen functionalised carbon nanofibres (N-CNFs) are prepared by carbonizing PPy-coated nanofibres (NFs), which in turn are obtained by 'electrospinning' and deacetylation of electrospun cellulose acetate NFs and PPy polymerization [56]. An additive free, cost-effective and scalable 'successive ionic layer adsorption and reaction (SILAR) method' has been quoted to prepare Ni-Co binary hydroxide on rGO [31] shown in Fig. 4. The pulsed layer deposition method is used to fabricate NiO on graphene foam [57]. Free-standing 3D porous rGO and PANI hybrid foam has been fabricated by 'dipping and dry method' [58]. Hierarchical porous carbon microtubes (HPCNTs) have been synthesized by carbonization along with KOH activation [59].

3. Electrode materials

Electrodes of SCs must have high conductivity, temperature stability, good chemical stability (inertness), high SSA, corrosion resistance, should be environment-friendly and have lower cost. Also, the capability of the material to carry out faradaic charge transfer increases the total C_s. In general, the smaller the pores, the greater is the C_s and hence the E_d. But, smaller pore enhances ESR and hence decrease P_d. So, applications which require more peak currents should have SC electrodes with larger pores, whereas electrode materials having smaller

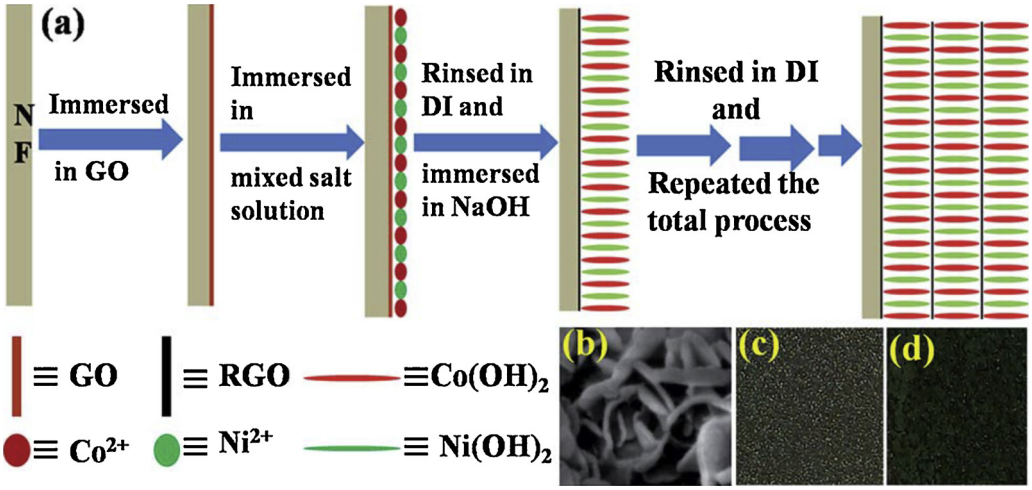

Fig. 4. a) Schematic illustration of Ni-Co binary hydroxide (BH) on a rGO surface by SILAR method (b) SEM images of the prepared composite (c) digital photograph of nickel foam (NF) and (d) NF coated with Ni-Co-BH-G [31]. (Reproduced with permission from Ref. [31] Copyright Royal Society of Chemistry (2016)).

pores are useful in applications which need higher E_d [59,60].

3.1. Nanostructured carbon-based materials

Carbon nanomaterial with high SSA is the suitable electrode material. It provides high electrical conductivity, chemical and electrochemical stability with less cost. Also, the good rectangular shape of Cyclic Voltammetry curves and symmetrical galvanostatic charge-discharge profile of carbon materials suggest that carbon based materials are the suitable capacitive materials. The factors which influence the electrochemical performance are their SSA, structure and shape of the pore, pore-size distribution, electrical conductivity and functionality of the surface [60–63].

ACs are the first material selected for EDLC electrodes. These are porous carbon materials with high SSA. Although their electrical conductivity is less (1250–2500 Sm^{-1}), still it is enough for SCs. Their porous structure consists of micropores (< 20 Å), mesopores (20–500 Å) and macropores (> 500 Å) to attain high SSA [60,61]. For ACs, whole SSA is not useful for the capacitance because electrolyte ions that are very big to enter into smaller micropores do not contribute in charge storage. Research is going to estimate the most suitable pore size for a given ion size and getting better methods to adjust the pore size distribution in the fabrication process. A few studies show that pore size of either 0.4 or 0.7 nm can be suitable for the aqueous electrolyte, while pore size of 0.8 nm may be helpful for organic electrolytes [62,63]. In some papers, the coordination among the pore size and the ion size was confirmed by getting a maximum C_s [17,64]. Also, the functional groups attached to the surface of carbon materials may enhance faradaic redox reactions resulting in about 5–10 % increase in C_s [65]. An electrode having an approximate SSA of 1000 $m^2 g^{-1}$ results in C_s of ~10 μFcm^{-2} (100 Fg^{-1}). Many commercial SCs make use of AC obtained from coconut shells. ACs obtained from coconut shells possess more micropores than AC made from charcoal. ACF obtained from activated carbon (surface area ~2500 $m^2 g^{-1}$) can have micropores with a very narrow pore size distribution which can be conveniently controlled. The advantage of AFC electrode is its small electrical resistance and good contact with the collector [66]. These electrodes possess mainly double-layer capacitance. A little pseudocapacitance arises due to micropores.

Carbon Aerogel (frozen smoke) is a very porous, ultra light, synthetic material made up of a continuous network of carbon nanoparticles with mixed mesopores. It does not require a binding agent as it can itself bond chemically with the current collector. Thus, it has low ESR which provides high P_d [67]. Aerogel electrodes prepared by pyrolysis of resorcinol-formaldehyde aerogels are better conductors than activated carbons. They provide thin and firm electrodes so that they can give mechanical and vibrational constancy for SCs for their use in the high-vibration environment. Carbon aerogel electrodes with the C_s of 104 Fcm^{-3}, yielding an E_d of 90 $Whkg^{-1}$ and P_d of 20 Wkg^{-1} have been obtained [68]. Roldan et al. [69] increased the C_s of many carbon electrodes by adding hydroquinone (HQ) to the electrolyte, but their stability remained a challenge (65% of the C_s retention after 4000 cycles). Wang et al. [70] used rGO electrodes treated with hydrophobic tBu-hydroquinone and achieved good C_s by retaining 94% capacitance after 800 cycles. Anjos et al. [71,72] have studied the capacitive performance of many PAH-quinones adsorbed on carbon and shows their superior cycling stability (97% of the initial Cs retention after 10,000 cycles). Wang et al. [73] have reported an enhancement in capacitance by adding anthraquinone with porous CNT.

Campbell et al. [74] have reported a method to improve the E_d of graphene macro assemblies (GMAs) through non-covalent functionalization with anthraquinone (AQ) and the resulting AQ-GMAs hybrid electrodes possess 2.9 times (up to 23$Whkg^{-1}$) E_d in comparison to untreated GMA electrodes. Fig. 5 shows the synthesis procedure of GMA electrodes by non-covalent functionalization and Thermo-gravimetric analysis (TGA) curves of bulk AQ and AQ-GMA disk.

CDC possesses high SSA with tunable pore diameter to increase ion confinement and hence increasing pseudocapacitance. CDC electrodes with designed pore distribution can give approximately 75% greater E_d than ACs [75]. The theoretical SSA of graphene is 2630 $m^2 g^{-1}$ which can theoretically provide the C_s of 550 Fg^{-1}. El-Kady et al. [76] utilized graphene sheets as electrodes. A graphene-based SC have used curved graphene sheets which do not stack, forming mesopores which were wetted by ionic electrolytes (up to voltages of 4 V). Also, the SC exhibits the E_d of 85.6 $Whkg^{-1}$ (equal to nickel metal hydride battery) with larger P_d greater than that of batteries [77]. The 2-D structure of graphene enhances the charging-discharging process and charge carriers can quickly enter into and out from the deep pores of the electrodes, thus increasing power. Such SCs may be employed for 100/120 Hz filter applications [78]. Chemically modified graphene (CMG) materials prepared from one-atom-thick carbon sheets, functionalized according to our need, exhibits a C_s of 135 Fg^{-1} in aqueous electrolyte and 99 Fg^{-1} in organic electrolyte [79]. Xu et al. [80] showed that flexible SCs with a 120 μm thick graphene film could show good capacitive behaviour with the high C_s of 186 Fg^{-1} (up to 196 Fg^{-1} for a 42 μm thick electrode), small leakage current (10.6 μA), good cycling stability and remarkable mechanical flexibility.

The C_s of Graphene electrodes (in the form of rGO) is only 100-150 Fg^{-1} in organic electrolytes [81,82] and 150–230 Fg^{-1} in inorganic electrolytes [83,84] which is less than theoretical capacitance (550 Fg^{-1}). The lower capacitances are essentially due to the irreversible

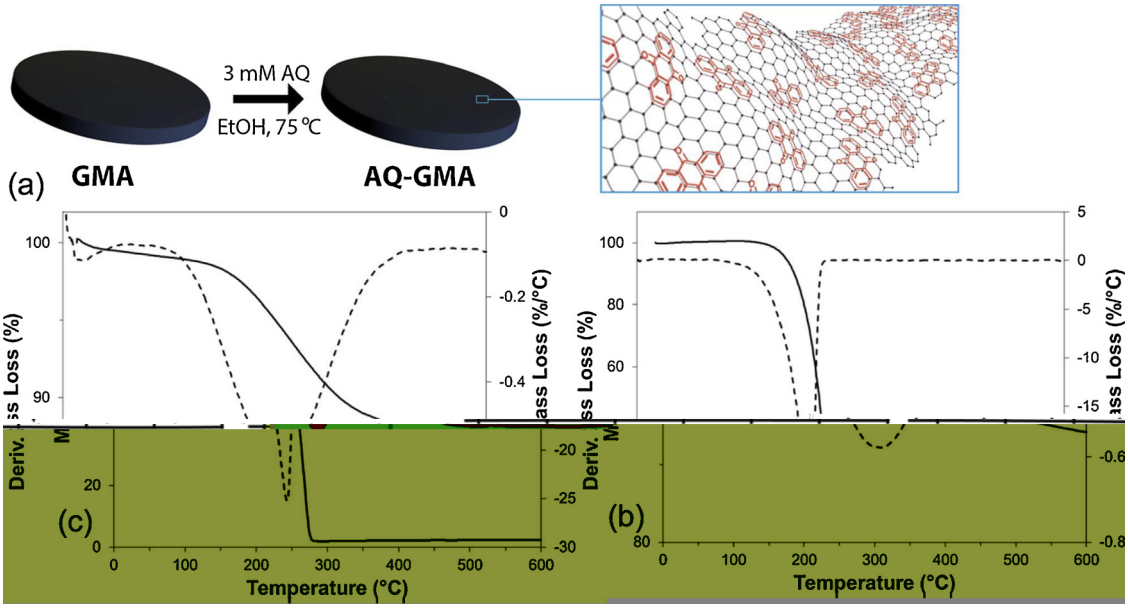

Fig. 5. (a) Schematic of synthesis of non-covalent AQ functionalization of GMA electrodes (b) TGA curve for AQ-GMA disk (c) TGA curve of AQ. Dashed lines show their derivative mass loss curves [74]. (Reproduced with permission from Ref. [74] Copyright Royal Society of Chemistry (2014)).

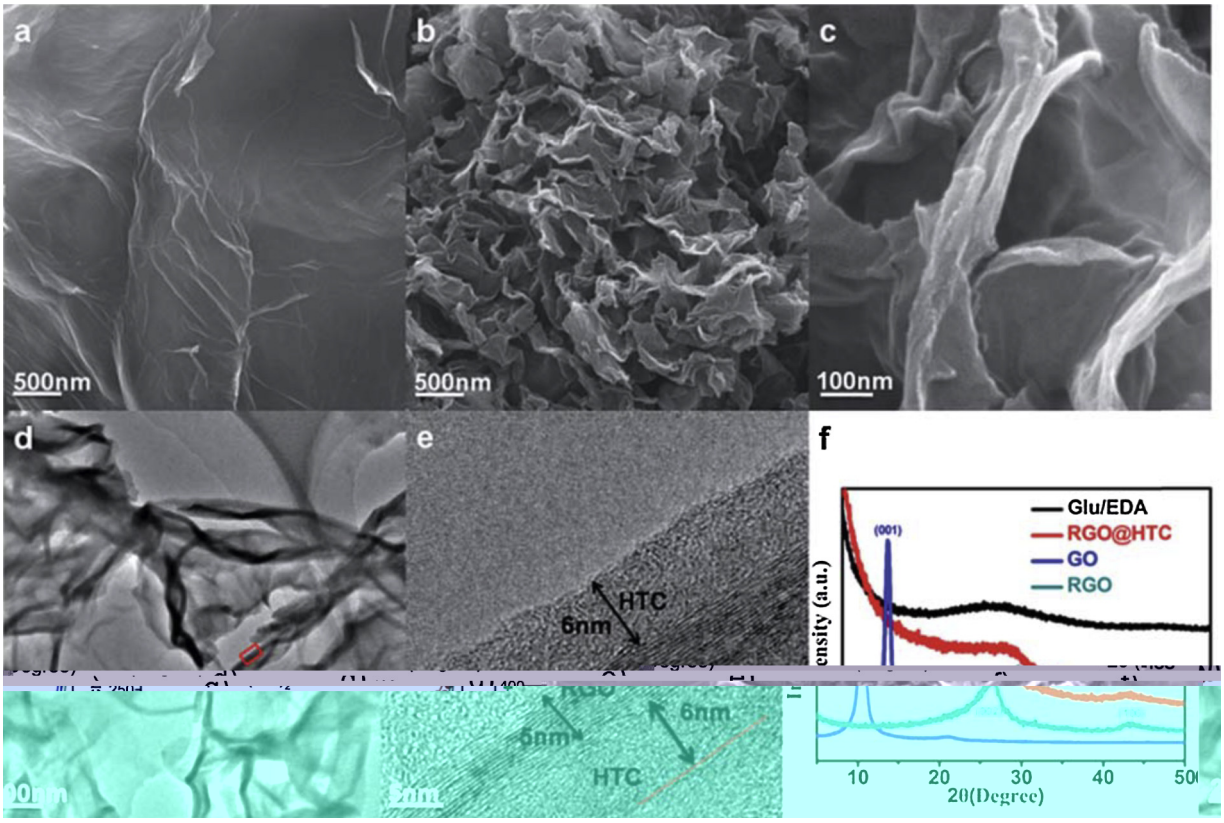

Fig. 6. (a) SEM image of rGO (b) & (c) SEM images of rGO@HTC (d) & (e) TEM and HRTEM images of rGO@HTC (f) XRD pattern of Glu/EDA, rGO@HTC, GO and rGO [86]. (Reproduced with permission from Ref. [86] Copyright Royal Society of Chemistry (2015)).

restacking of individual rGO sheets in the reduction and drying processes [81], which make the major surface of rGO not available for storing charge. Huang et al. [85] explained that a small quantity of GO addition might improve the electrochemical performance of biomass-derived carbon. The rGO@HTC (N-doped hydrothermal carbon coated graphene) composites exhibited high C_s (340 Fg^{-1} at 0.1 Ag^{-1}), high rate capability (203 Fg^{-1} at 50 Ag^{-1}) and good cycling stability (no C_s decay over 2000 cycles) in 6 mol L^{-1} KOH electrolyte solution [86]. Fig. 6 shows the schematic of formation rGO@HTC, SEM, transmission electron microscopy (TEM), high-resolution TEM (HRTEM) and X-ray diffraction (XRD) pattern of the as-prepared composite.

Electrodes of CNTs have been developed as an intertwined mat of carbon nanotubes, with an open and available network of mesopores. The mesopores in CNTs are interconnected, forming a continuous

distribution, thus utilizing the SSA more efficiently [87]. CNT electrode has lower ESR than ACs, as the ions of the electrolyte can easily penetrate into the mesoporous network [88]. Li et al. [89] deduced that the ion size and the electrode/electrolyte accessibility are the prominent factors which affect the performance of flexible single-walled CNTs (SWCNTs) SCs. SWCNTs have a theoretical SSA of 1315 $m^2 g^{-1}$, whereas MWCNTs has lower SSA compared to that of ACs. MWCNTs have mesopores that permit easy flow of ions across the electrode-electrolyte interface. When the pore size becomes comparable to the size of the ion, the molecules of the solvent are partially exposed which results in high ionic packing density. However, their mechanical stability decreases due to significant volume change due to repetitive intercalation and depletion [90]. Peng et al. [91] reported a C_s of 50 Fg^{-1} for MWCNTs. Xie et al. [59] have prepared HPNCTs with willow catkins by an easy carbonization process and exhibit SSA of 1775.7 $m^2 g^{-1}$, C_s of 292 Fg^{-1} at 1 Ag^{-1} and good rate capability with 83.5% of the C_s retention at 10 Ag^{-1} for HPNCT-800. Ogata et al. [92] have proposed a rGO/GO/rGO device which operates as an SC till 1.2 V and as a battery for voltages greater than 1.5 V A high C_s of 185 Fg^{-1} at 0.5 Ag^{-1} for a symmetrical supercapacitor of HSG (hierarchically porous nanocarbon and graphene) has been obtained accompanying an E_d of 78 $Whkg^{-1}$ at P_d of 875 Wkg^{-1} [93].

3.2. CPs based materials

CPs have attained considerable attention as they supply high C_s (due to their redox behaviour), rapid charge-discharge process, lesser cost than carbon-based material and a low ESR value. Particularly, the n/p type polymer configuration has huge potential for high E_d and P_d [15] but, the lack of proficient n-doped conducting material and less cycling stability has delayed the progress of CPs pseudocapacitor. PANI is lightweight, highly conductive, mechanically flexible, low cost, environment-friendly and possesses high theoretical capacitance. The problem is that, because of ion doping/dedoping, PANI shrinks and swells during the charge/discharge process. To surmount this problem, the PANI layer is coated on MOs/carbon materials forming PANI/MOs/nanocarbon ternary hybrid which possesses good cyclic stability and C_s [94]. Also, PANI exhibits a wide range of colours due to their many protonation and oxidation forms. These electrochromic properties can be used for fabrication of electrochromic SCs. Polyacetylene is the most crystalline CP, but it is easily oxidized in air. Polypyrrole and polythiophene can be synthesized directly in doped form and are very stable [15]. PPy has greater density and higher flexibility than other CPs. It has a high electrical conductivity (10–500 Scm^{-1}) and it itself can undergo a rapid redox reaction for charge storage [95]. Lignin-PPy composite has been prepared by coating lignin with PPy by the polymerization of PPy with and without the presence of methyl orange, which leads to the formation of PPy films of globular and nanotubular morphology. Thereafter the composites are converted to carbon materials rich in nitrogen atoms by pyrolysis in N_2 atmosphere. The SSA of the prepared materials has been increased up to 10 times than that of carbon materials [96]. PEDOT is an intrinsically CP (ICP). Although the conductivity of ICP is much less than metals, but still it is useful due to its other properties such as flexibility, easy processing and drying at low temperatures [15].

Polythiophenes (PTs) have been prepared by chemical oxidative polymerization using $FeCl_3$ as an oxidant in the presence and absence of different surfactants. It is observed that surfactants change the morphology of PTs which is clear from the results as PTs prepared with TritronX-100 shows a C_s of 117 Fg^{-1} whereas the C_s for surfactant-free PTs is 78 Fg^{-1} [97]. PVA is a low cost, environment-friendly, water-soluble, colourless and odourless synthetic polymer. It possesses high tensile strength, an excellent capability of film formation, emulsifying and bonding properties along with flexibility. However, the properties described above are humidity dependent. More humidity reduces its tensile strength, but increases its elongation and tear strength [98]. The only conducting polymer which can be converted into highly ordered films is PPV. It has a small band gap and doping can be done to form an electrically conductive polymer with the maximum conductivity of 10^{-3} Scm^{-1}. Its properties can be altered by linking functional side groups [15]. Polyindole (Pind) has gathered attention due to the mixed properties of both poly (p-phenylene) and PPy, such as high redox property, good thermal stability, meager degradation, and better air stability [99] in comparison to PPy and PANI [100]. PANI-Sol nanocrystal, PANI-Eml nanopetal, and PANI-Int nanosphere (depending on the pathway of polymerization: solution (Sol), emulsion (Eml), interfacial (Int)) are reported [101] which exhibit the C_s of 460, 424 and 300 Fg^{-1}, the E_d of 23, 21.2, and 15 $Whkg^{-1}$, respectively at P_d of 200 Wkg^{-1}. Symmetric SCs based on alternate layers of different CPs have been studied by Aradilla et al. [102]. The capacitive properties of as-prepared multilayered system are better than individual CP which may be related to the better porosity of multilayered material. Flexible worm-like SC electrodes are fabricated using cellulose nanofibres (CNFs) and graphite nanoplatelets (GNP), doped with PANI by in situ polymerizations [103]. The C_s of 421.5 Fg^{-1} has been obtained for hybrid PANI electrodes at 1 Ag^{-1} with 20 wt% CNFs loading along with excellent electrochemical properties and C_s retention over 1000 cycles of repeated bending. Also, an all-solid-state symmetric SC has been fabricated using PANI/CNF (20% loading)/ GNP electrodes which shows good C_s retention at various bending angles as shown in Fig. 7. Self-doped PANI nanofibres are fabricated on the Pt electrode by reverse pulse voltammetry which exhibits the C_s of 400 Fg^{-1}, an E_d of 9.4 $Whkg^{-1}$ and P_d of 436 Wkg^{-1} at 5 $mAcm^{-2}$ current density [104]. Stable PPy films with high doping degree have been obtained by pulse polymerization by Sharma et al. [105]. Pulse on time controls the chain size along with chain defects and pulse off time controls orientation and conjugation of the polymer chain. In these films, a C_s of 400 Fg^{-1} has been obtained with E_d of 250 $Whkg^{-1}$ at 5 $mAcm^{-2}$ current density along with long cycle life.

3.3. MOs-based materials

TMOs have been explored a lot as a material for SCs electrodes because they possess high conductivity [6]. B.E. Conway described TMOs such as RuO_2, IrO_2, Fe_3O_4, MnO_2, NiO, Co_3O_4 etc. which possessed high pseudocapacitance [6]. The ESR of RuO_2 is much less than other electrode materials. Thus, it has higher E_d and P_d than EDLCs and CPs supercapacitors, but it is very costly and shows poor performance at high current densities [106]. TMOs are a suitable material for SCs electrode due to their chemical stability and variable valence. Co oxide has been investigated much due to high theoretical C_s (3560 Fg^{-1}), reversibility [107] and better electrochemical performance. Several Co oxide nanostructures are prepared. For instance, ultra layered Co_3O_4 structure synthesized by Rao et al. [108] exhibits a C_s of 548 Fg^{-1} at 8 Ag^{-1}, Wang et al. [109] have reported 3D hollow Co_3O_4 with a C_s of 820 Fg^{-1} at 5 mVs^{-1}, nanoporous Co_3O_4 prepared using solvothermal method exhibits C_s, E_d, and P_d of 476 Fg^{-1}, 42.3$Whkg^{-1}$ and 1.56 kW kg^{-1} respectively [110]. Reddy et al. [111] reported a symmetric $MnO_2//MnO_2$ supercapacitor, Dubal et al. [112] fabricated a symmetric $Mn_3O_4//Mn_3O_4$ supercapacitor and Lu et al. [113] designed a symmetric SC, based on Ni-Co oxide electrodes. Xia et al. [114] prepared a $RuO_2//RuO_2$ supercapacitor with a PW of 1.6 V. Juodkazis et al. [115] suggested a high theoretical C_s of Ru (3800 Fg^{-1})

Das et al. [116] reported C_s of 1715 Fg^{-1} (very close to its predicted theoretical C_s of 2000 Fg^{-1}) for RuO_2 based SCs in which RuO_2 is electrodeposited on the SWCNTs film electrode. RuO_2 deposited on graphene foam exhibits the C_s of 502.78 Fg^{-1}, the E_d of 39.28 $Whkg^{-1}$ and P_d of 128.01 kW kg^{-1} for greater than 8000 cycles with stable performance [117]. Hu et al. [118] have utilized AAO membrane-templates to deposit hydrous RuO_2 arrayed nanotubes onto graphite and obtained a C_s of 1300 Fg^{-1}. Zhang et al. [119] have made a nanotubular hydrous RuO_2 based electrode from manganite nanorods and

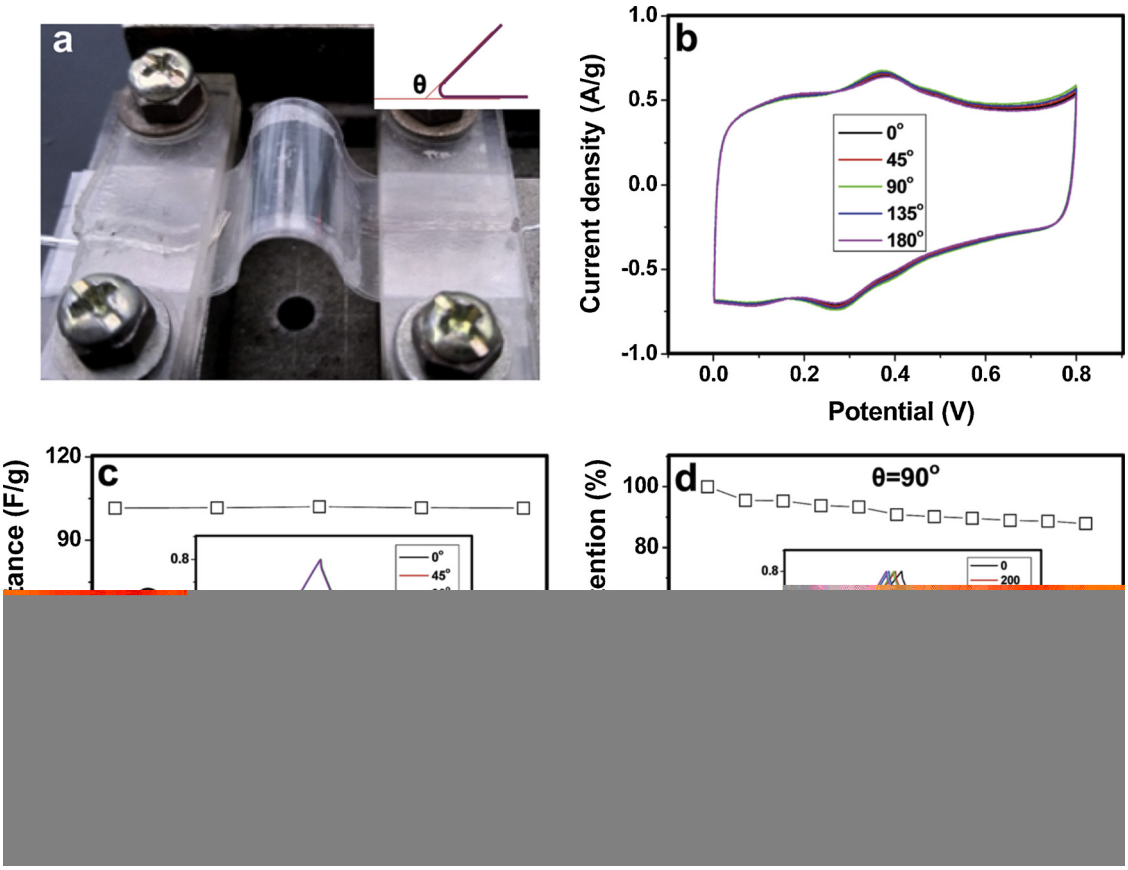

Fig. 7. Electrochemical behavior of all solid state symmetric SC assembled using PANI/CNF (20% loading)/GNP electrodes: (a) Optical image showing bending of SC (b) CV curves at 5 mVs^{-1} scan rate (c) C_s and GCD curves at various bending angles (d)C_s retention at bending angle of 90° [103]. (Reproduced with permission from Ref. [103] Copyright Royal Society of Chemistry (2017)).

a C_s of 861 Fg^{-1} is obtained. Also, low-cost oxides of vanadium, iron, cobalt and nickel have been checked in aqueous electrolytes. NiO nanostructures (E_g = 3.6 to 4.2 eV) may increase C_s due to improved faradic redox reactions [57]. Several methods have been used to synthesize nanostructured NiO by both chemical as well as physical methods, for instance, sol-gel method, wet-chemical solution method, evaporation and oxidation, electrochemical deposition, coprecipitation and reactive pulsed laser ablation. Dutt et al. [30] synthesized porous NiO nanostructures (particle size ~70 nm) by the hydrothermal method which showed a C_s value of 132 Fg^{-1} at 10 mVs^{-1}.

Wang et al. [120] have reported Ni-Zn system materials (Ni_x Zn_{1-x} OH, NiO-ZnO and Ni_xZn_{1-x}). In this system, Ni_x Zn_{1-x} S porous nanoparticles (diameters ~30 nm) with an SSA of 148.4 m^2 g^{-1} exhibit the C_s of 1867 Fg^{-1} at 1 Ag^{-1} along with excellent rate capability. $Cd(OH)_2$ nanowires (NWs) have been fabricated on a stainless-steel substrate by Patil et al. [121]. $Cd(OH)_2$ NWs electrode exhibits the C_s of 267 Fg^{-1} at 5 mVs^{-1} with good cycling life. A symmetric device fabricated using this electrode exhibited an E_d of 11.09 $Whkg^{-1}$ and P_d of 799 Wkg^{-1} at 0.84 Ag^{-1}. Rui et al. [122] have prepared the hydrated V_2O_5 nanosheets by sol-gel technique and used them in organic electrolyte ultracapacitors. Zhu et al. [123] have prepared 3-D nanostructures of V_2O_5 NS by the freeze-drying process and studied their symmetrical device behaviour. Nagaraju et al. [124] have reported the synthesis of 2D V_2O_5 nanosheets (NS) and rGO composite. The V_2O_5 and rGO/V_2O_5 NS delivered a C_s of 253 Fg^{-1} and 635 Fg^{-1} and the corresponding E_d of 39 $Whkg^{-1}$ and 79.5 $Whkg^{-1}$ at a P_d of 900 Wkg^{-1} in an ASC. The E_d is higher than reported for Ppy@V_2O_5 nanoribbon composite (32 $Whkg^{-1}$, 900 Wkg^{-1}) [125], V_2O_5 and PANI nanofibers (26.7 $Whkg^{-1}$, 222 Wkg^{-1}) [126], graphene composites of V_2O_5 nanowires and MnO_2 nanorods (15.4 $Whkg^{-1}$, 436 Wkg^{-1}) [127] etc. MnO_2 doped V_2O_5 nanostructures exhibited a C_s of 450 Fg^{-1} at 0.5 Ag^{-1} and retains 89% of C_s after 500 cycles [128]. An ASC developed using MnO_2 doped V_2O_5 and AC as electrodes exhibits a C_s of 61 Fg^{-1} with an E_d of 8.5 $Whkg^{-1}$.

Compared to monometallic compounds, bimetallic compounds reveal improved performance. $NiCo_2O_4$ shows more electronic conductivity and better electrochemical performance than NiO and Co_3O_4 [129–131]. The Ni-Co hydroxide shows higher C_s along with the improved rate capability than $Ni(OH)_2$ and $Co(OH)_2$ [132–134]. Wang et al. [135] have synthesized $GeSe_2$ nanostructures and obtained a C_s of 300 Fg^{-1} at 1 Ag^{-1}. Zhang et al. [136] synthesized SnSe and obtained a C_s of 228 Fg^{-1} at 0.5 Ag^{-1}. Chen et al. [137] synthesized bimetallic Ni-Co selenides with different Ni-Co ratios and obtained C_s of 535 Fg^{-1} at 1 Ag^{-1} and C_s retention ~82% after 2000 cycles higher than Ni-Co oxides and Ni-Co sulphides. An ASC synthesized using $Ni_{0.67}$ $Co_{0.33}$ Se and rGO as electrodes exhibited a C_s of 176 Fg^{-1} at 1 Ag^{-1} and E_d of 36.7 $Whkg^{-1}$ at a P_d of 750 Wkg^{-1}. Wang et al. [138] have prepared hierarchical $NiCo_2O_4$ electrode material by the hydrothermal method which displays a C_s of 1393 Fg^{-1} at 0.5 Ag^{-1}, a high E_d (21.4 $Whkg^{-1}$) at a P_d of 350 Wkg^{-1} with remarkable stability. Ma et al. [139] have developed $ZnCo_2O_4$@MnO_2 core-shell nanotube arrays as shown in Fig. 8, which possesses C_s of 1981 Fg^{-1} at 5 Ag^{-1}. Also, an ASC with $ZnCo_2O_4$@MnO_2 nanotubes on Ni foam as anode and porous Fe_2O_3 on Fe foil as cathode is fabricated which acquired a C_s of 161 Fg^{-1}, E_d of 37.8 $Whkg^{-1}$ at 2.5 $mAcm^{-2}$ and superior stability with 91% of the C_s retention after 5000 cycles, in voltage window of 1.3 V. $H_2Ti_3O_7$ nanotubes prepared by Yang et al. [140] when employed as an electrode in SC material with non-aqueous electrolyte, possessed the C_s of 414 Fg^{-1} at 0.5 Ag^{-1}. The theoretical values of C_s and electrical conductivity of some TMOs are reported such as NiO (2584 Fg^{-1} [141], 0.01–0.32 Scm^{-1} [142]), MnO_2 (1380 Fg^{-1} [143], 10^{-5}–10^{-6} Scm^{-1}

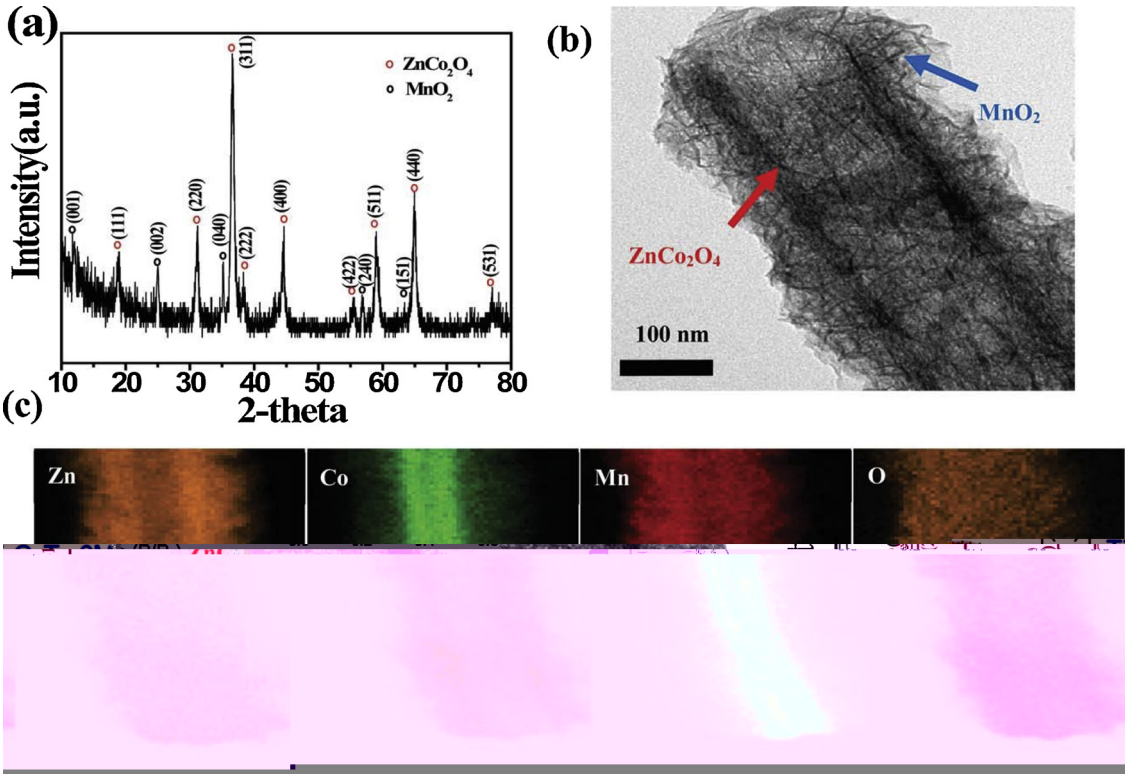

Fig. 8. (a) XRD of $ZnCo_2O_4$@MnO_2 nanotube arrays (b) TEM images of $ZnCo_2O_4$@MnO_2 nanotube arrays (c) EDS (electron diffraction spectroscopy) mapping of individual $ZnCo_2O_4$@MnO_2 nanotube arrays [139]. (Reproduced with permission from Ref. [139] Copyright Royal Society of Chemistry (2015)).

[144], V_2O_5 (2120 Fg^{-1}, 10^{-4}–10^{-2} Scm^{-1} [145]), Co_3O_4 (3560 Fg^{-1} [146,147], 10^{-4}–10^{-2} Scm^{-1} [148] and RuO_2 (1200–2200 Fg^{-1} [149], 10^{3}-1 Scm^{-1} [150]).

3.4. Nanocomposite materials

Generally, the composites contain two or more materials in which each individual component possesses its own properties (physical, chemical and mechanical). Nanocomposite electrodes incorporate carbon materials into MOs or CPs and put together a non-faradaic (physical) and a faradaic (chemical) charge storage mechanism in a single electrode. High SSA is provided by the carbon materials and pseudocapacitive materials further increase the capacitance. CNTs act as a backbone for uniform distribution of MOs or CPs, producing high pseudocapacitance and electric double-layer capacitance. Such type of electrodes attains higher C_s than individual carbon, MOs or CPs electrodes [151].

3.4.1. Carbon materials with CPs

The AC cathode coupled with a CPs anode provides higher E_d and P_d than EDLCs and improved cycling performance than pseudocapacitors [151]. A CNT hydrogel with PANI had a C_s of 680 $mFcm^{-2}$ at 1 $mAcm^{-2}$ [152]. Jaidev and S. Ramaprabhu have prepared poly (phenylenediamine) (PpPD) and hydrogen exfoliated graphene (HEG) sheets which shows a C_s of 248 Fg^{-1} at 2 Ag^{-1} [153]. Also, an ASC is fabricated which exhibits an E_d of 8.6 $Whkg^{-1}$ at a P_d of 0.5 $kW\,kg^{-1}$.

Li et al. [154] have synthesized PANI nanorods on graphite NS which exhibit a C_s of 1665 Fg^{-1} at 1 Ag^{-1}. Zhao et al. [155] synthesized graphene-based PVA composites with 150% better tensile strength and approximately 10 times increase in Young's modulus with graphene loading of 1.8 vol %. Yu et al. [156] prepared PANI/eCFC (etched carbon fibre cloth) composite with C_s of 1035 Fg^{-1} at 1 Ag^{-1}, 88% capacity retention. Wang et al. [157] have investigated the GNS/PANI composite which shows a C_s of 532.3 Fg^{-1} at 2 mVs^{-1}, 99.6% C_s retention at 50 mVs^{-1}. Mao et al. [158] also reported the synthesis of graphene/PANI nanofiber composites with C_s of 526 Fg^{-1} at 0.2 Ag^{-1}. Freestanding PEDOT-PSS/SWCNTs have been reported which exhibit the C_s of 104 Fg^{-1} at 0.2 Ag^{-1}, E_d of 7 $Whkg^{-1}$, P_d of 825 Wkg^{-1} and 90% of the C_s retention after 1000 cycles [159]. Snook et al. [15] prepared PEDOT/PSS and CNTs composite that could reach C_s varying from 85 Fg^{-1} to 150 Fg^{-1}; while the E_d could exceed 0.92 $Whkg^{-1}$ and P_d could range from 100 Wkg^{-1} to 3000 Wkg^{-1}. Frackowiak et al. [160] reported PEDOT/PSS and MWNT composites with a C_s value of 100 Fg^{-1}. Han et al. [161] have reported electrodes of PEDOT/PSS and GO in 1 M H_2SO_4 which yield capacitance of 108 Fg^{-1} with C_s retention of 78% over 1200 cycles. Symmetric (PPy//PPy) and asymmetric (PPy//AC) SCs have been prepared using Cladophora algae-derived cellulose as a binder [162]. These SCs exhibit capacitance values ranging from 0.45 F to 3.8 F. The rGO aerogels generally suffer from low E_d, small life cycle and poor flexibility. Yang et al. [163] have prepared rGO aerogel-PANI composite by electro-deposition of PANI arrays on rGO aerogel which possesses the usefulness of rich open pore and high conductivity of cross-linked framework of 3D aerogel and high capacitance of PANI. The prepared composite exhibits a specific capacitance of 432 Fg^{-1} at a current density of 1 Ag^{-1}, the energy density of 25 $Whkg^{-1}$, 85% capacitance retention after 10,000 cycles with outstanding stability in different bending conditions.

3.4.2. Carbon-based nanomaterials with MOs

TMOs have low electronic conductivity, poor C_s and low electrochemical stability. To improve its performance, nanostructured TMOs are mixed with the carbon material to make composites. This combination of MOs and carbon is useful for high-performance SCs. Various hybrid materials such as Co_3O_4/graphene [164,165], Co_3O_4/CNTs [166], and Co_3O_4/CNFs [167] with improved electrical conductivity and a huge surface area have been prepared. Wang et al. [57] have reported a NiO/GF hybrid electrode which shows a C_s (1225 Fg^{-1} at 2 Ag^{-1}). An ASC has been synthesized using NiO/GF as anode and

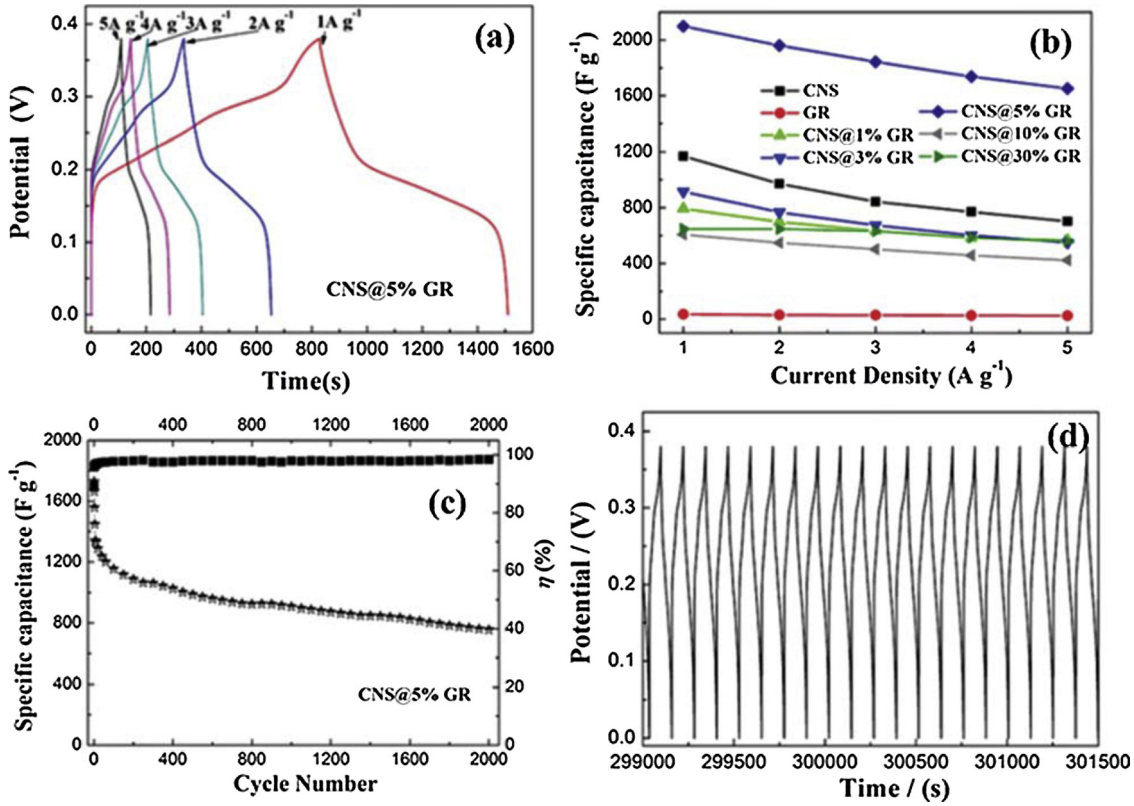

Fig. 9. (a) CD curves of electrodes based on CNS@5%GR nanocomposite (b) C_s comparison of CNS/GR nanocomposite, CNS nanoparticles and GR at diverse current densities (c) Cyclic performance and (d) CD curves for the last 20 cycles at 4 Ag^{-1} current density of CND@5%GR nanocomposite [32]. (Reproduced with permission from Ref. [32] Copyright Royal Society of Chemistry (2014)).

HPNCNTs as a cathode in the KOH solution which exhibits an E_d of 32 $Whkg^{-1}$ at a P_d of 700 Wkg^{-1} with 94% C_s retention after 2000 cycles. Li et al. [168] presented CNTs@NCS@MnO_2 composites which had C_s of 312.5 Fg^{-1} at 1 Ag^{-1} with good cycling stability (92.7% C_s retention after 4000 cycles). An ASC was designed with CNTs@NCS@MnO_2 (+ ve electrode) and ACs (-ve electrode) which possessed a high C_s with a stable PW of 1.8 V, E_d of 27.3 $Whkg^{-1}$ at P_d of 4500 Wkg^{-1}. Perera et al. [169] have assembled a coin cell type ASC using V_2O_5-CNT as an anode and carbon fibre as a cathode which delivers an E_d of around 46.3 $Whkg^{-1}$ and a P_d of 5.26 kW kg^{-1}. Du et al. [32] constructed the $CoNi_2S_4$@graphene (CNS@GR) nanocomposite showing C_s 2009.1 Fg^{-1} at 1 Ag^{-1} and the C_s could be retained at 755.4 Fg^{-1} (4 Ag^{-1}) after 2000 cycles. Fig. 9 shows the CD curves and cycle performance of CNS@GR nanocomposites.

Many single-phase materials or nanocomposites of $Ni_XCo_{3-X}O_4$ have been prepared with superior energy storage properties e.g. nanosheets [170], nanoneedles [171] and nanowires [172] of $NiCo_2O_4$, $Ni_{0.3}Co_{2.7}O_4$ hierarchical structures [173], $NiCo_2O_4$/(CNTs) [174] and $NiCo_2O_4$/graphene oxide (GO) [175] etc. Yuan et al. [176] reported $NiCo_2O_4$ nanosheets with C_s of 1450 Fg^{-1} at 20 Ag^{-1}. Ternary $NiCo_2S_4$ also offer richer redox reactions, as ternary $NiCo_2S_4$ have a higher electronic conductivity than $Ni_XCo_{3-X}O_4$ which can reduce the charge transfer resistance, resulting in a smaller interior resistance (IR) loss at higher current density. Hence, a greater rate capability and P_d can be achieved [177]. The synthesis of $NiCo_2S_4$ nanotubes through sacrificial templates with C_s of 933 Fg^{-1} at 1 Ag^{-1} has been reported [178]. Urchin-like $NiCo_2S_4$, prepared by a precursor transformation method, with C_s of 1050 Fg^{-1} at 2 Ag^{-1} has been reported [179]. However, the two-step transformation method increased the preparation cost. Hence, composite of $NiCo_2S_4$ nanosheets/graphene is again produced by hydrothermal method with a C_s of 760 Fg^{-1} at 20 Ag^{-1} [180].

Xiong et al. [181] have prepared Ni-Co-Mn hydroxide nanoneedles by a hydrothermal method which show the C_s ~1400 Fg^{-1}, higher E_d (30 $Whkg^{-1}$) and P_d (39 kW kg^{-1}) at 100 $mAcm^{-2}$ with no loss of C_s after 3000 cycles. Ratha et al. [182] have reported patronite hybrid, VS_4/rGO, which shows C_s of~ 877 Fg^{-1} at 0.5 Ag^{-1}, an E_d of 117 $Whkg^{-1}$ and P_d of 20.65 kW kg^{-1}. Lu et al. [183] constructed an aqueous sodium-ion ASC by using Mn hexacyanoferrate (HCF) as –ve electrode and Fe_3O_4/rGO nanocomposites as + ve electrode with an extended PW of 1.8 V which exhibited C_s of 96 Fg^{-1}, higher P_d (2183.5 Wkg^{-1}) and E_d (27.9 $Whkg^{-1}$). Guan et al. [184] have presented needle-like Co_3O_4 deposited on graphene as the supercapacitor material with C_s of 157 Fg^{-1} at 0.1 Ag^{-1}.

Liu et al. [185] prepared cobalt-based nanoparticle on mesoporous carbon nanospheres. The synthesis technique used was the 'colloidal amphiphile template oxidative polymerization of dopamine'. Polydopamine possesses enough binding sites to coordinate metal ions. As prepared composite exhibited very fine size, porous structure, complete usage of conductive carbons and manageable chemical compositions which provided high rate capability with long-term cyclic stability. Wu et al. [186] have prepared hybrid structure consisting of graphene-encapsulated carbon and Ni-Al layered double hydroxide which shows a high C_s (1710.5 Fg^{-1} at 1 Ag^{-1}) and E_d of 35.5 $Whkg^{-1}$ at a P_d of 670.7 Wkg^{-1} at 1 Ag^{-1}. Sahoo et al. [187] have prepared $ZnCo_2O_4$/rGO/NiO composite on Ni foam which possesses the C_s of 1256 Fg^{-1} at 3 Ag^{-1}, higher E_d of 62.8 $Whkg^{-1}$, P_d of 7492.5 Wkg^{-1} and low ESR (0.58 Ω). The composite retained 80% of C_s after 3000 charge-discharge cycles. The effect of concentration of electrolyte on the electrochemical behaviour has also been examined.

Table 2 compares supercapacitor electrodes of carbon and its composites in terms of various parameters such as pore size, surface area, C_s, rate capability, stability and cost. It is clear from the table that for obtaining a good performance supercapacitor, composites of carbon materials and MOs is a suitable candidate with high C_s, high rate

Table 2
Comparison of carbon and its composite as SC electrodes [177].

Electrode material	Pore size	SSA	C_s	Rate capability	Stability	Cost
Carbon	Pore size can be designed	High	Low	High	Good	Low
MOs	Difficult to tailor	Low	High	Low	Poor	High
Carbon-MOs composite	Pore size can be tailored	Controlled by the carbon material	High	Good	Good	Moderate

capability and stability with moderate cost.

3.4.3. MOs and CPs composites

The composite of MOs and CPs may give an improved electrochemical performance in SCs due to compatibility between them [188,189]. Therefore, many efforts have been done to develop MOs embedded with CPs that increase the conductivity of electrodes very much by enhancing the C_s, rate capability and cyclic stability. Liu et al. [190] fabricated PPy coated MoO_3 by in-situ polymerization which showed C_s of 110 Fg^{-1} at 100 mAg^{-1} and E_d of 20 $Whkg^{-1}$ at P_d of 75 Wkg^{-1}. The ASC designed with PPy@ MoO_3 as the + ve electrode and AC as the –ve electrode in 0.5 M K_2SO_4 aqueous solution exhibited an E_d of 12 $Whkg^{-1}$ at 3 $kW\,kg^{-1}$. Raj et al. [191] prepared Co_3O_4-Pind which achieved C_s of 1805 Fg^{-1} at 2 Ag^{-1} and C_s of 1625 Fg^{-1} at 25 Ag^{-1}. Table 3 shows some of the latest fabricated SC electrodes (non-flexible) with their various parameters such as C_s, E_d, P_d, capacitance retention etc. Table 4 shows the summary of flexible planar SC electrodes/devices.

4. Asymmetric supercapacitors (ASCs)

ASCs have superiority over symmetrical SCs as these SCs use the faradaic active electrode, which significantly contributes to the pseudocapacitance, besides increasing the PW, along with EDLC electrode which supplies high power. Moreover, the longer discharge times and dissimilar discharge profiles provide higher E_d and P_d to ASCs [237]. As ASCs combine the advantages of both pseudocapacitive electrode and the capacitive electrode, so ASCs can provide higher E_d than symmetric SCs while maintaining cyclic and rate performance [238,239]. Wang et al. [240] fabricated a non-aqueous ASC from two spherical materials: an activated mesocarbon microbead-AMCMB (-ve electrode) and MnO_2 nanowire-sphere (+ve electrode) over a voltage range (0.0–3.0 V) using 1 M Et_4 NBF_4 in acetonitrile as electrolytes. The AMCMB/MnO_2 supercapacitor explored a C_s of 228 Fg^{-1} and E_d of 128 $WhKg^{-1}$ at 10 mVs^{-1}. An asymmetric high voltage SC (1.9 V) had been produced [241] using AC as the -ve electrode and a silicon carbide-MnO_2 (SiC-N-MnO_2) composite as the + ve electrode in Na_2SO_4 electrolyte solution having C_s of 59.9 Fg^{-1} at 2 mVs^{-1} and E_d of 30.06 $Whkg^{-1}$ and P_d of 113.92 Wkg^{-1} with an approximate 3.1% C_s loss after 1000 charge-discharge cycles.

An ASC using Cu_2O as + ve electrode and AC as –ve electrode exhibited an E_d of 20.04 $Whkg^{-1}$ with an extended PW of 1.65 V and retained 93.3% capacitance after 5000 cycles [51]. As-prepared flexible all-solid-state ASC illuminated 52 red coloured LEDs using four charged devices in series. A flexible solid-state ASC has been fabricated by Wang et al. [54] using Co_3O_4 flakes and γ-Fe_2O_3 nanoparticles as electrodes which delivers a high E_d of 38.1 $Whkg^{-1}$ along with extended PW of 1.7 V. Also, the fabricated device illuminated 52 LEDs, for at least 7 min, along with good charge-discharge behaviour under different bending conditions. Wu et al. [242] reported an E_d of 30.4 $Whkg^{-1}$ and P_d of 5 $kW\,kg^{-1}$ using graphene/MnO_2/graphene hybrid cells. An ASC with Carbon Quantum Dots (CQDs)/$NiCo_2O_4$ composite as + ve electrode and the AC as –ve negative electrode has been designed which possesses a C_s of 88.9 Fg^{-1}, E_d of 27.8 $Whkg^{-1}$, P_d of 128 Wkg^{-1}, great cycling stability (101.9% of C_s retention over 5000 cycles) and high coulombic efficiency (η) of almost 100% during the cycling process [243]. Hadi et al. [244] have fabricated an ASC with $Ni_{4.5}Co_{4.5}S_8$ and g-Fe_3C/Fe as the + ve and -ve electrodes which possesses the E_d of 89 $Whkg^{-1}$ at P_d of 1.1 $kW\,kg^{-1}$ and retained 91% of C_s after 2500 cycles. Xie et al. [245] have designed C-$LiFePO_4$ over titanium nitride substrate as the electrode for a Li-ion supercapacitor which exhibits the C_s of 972 Fg^{-1} at 1.0 Ag^{-1}, presenting a C_s improvement of 210% in comparison to 314 Fg^{-1} for $LiFePO_4$/TiN. The C-$LiFePO_4$/TiN nanowires exhibit excellent cyclic stability with a 3.7% loss of C_s after 400 cycles. Table 5 shows the summary of some of the reported asymmetric/symmetric SCs.

5. New materials

5.1. MOFs

TMOs, despite exhibiting attractive properties as good electrical conductivity, superior electrochemical response, less manufacturing cost and simple processability, have limited practical use due to decline in their capacitive response after some time during continuous Faradaic reactions. Hence, there is a requirement of new synthesis techniques, which could provide stable porous structures and control over phase with dimensions of MOs for getting better capacitive performance. Nowadays, MOFs have gathered much attention as templates for the synthesis of porous MOs and nanocomposites of porous carbons and metal/metal oxides [264] first developed by Yaghi et al. in 1995 [265]. MOFs have been prepared by joining inorganic and organic units via strong chemical bonds. The polyvalent organic carboxylates, when associated with metal-containing units, can yield three-dimensional structures which have well-defined pore size distributions and large SSA (1000-10,000 $m^2\,g^{-1}$). Transition metals (eg Zn, Co, Cu, Fe, Ni), alkaline earth elements (eg Ba, Sr), p-block elements (eg In, Ga) and mixed metals are used for the development of MOFs [266]. The annealing time and temperature variation can control the composition, pore size and SSA of MOF derived oxides. MOF based oxides can be combined with different carbon-based materials such as rGO, CNTs, graphene etc. to enhance their electrochemical performance. Few of the porous TMOs obtained from MOFs are cupric oxide, zinc oxide, iron oxide, nickel oxide, cerium oxide, cobalt oxide, titanium dioxide, manganese oxide, magnesium oxide. Also, MOFs may be favourable for the synthesis of mixed MOs and their composites, such as Co_3O_4 /$NiCo_2O_4$, Co_3O_4/$ZnFe_2O_4$, CuO/Cu_2O, Cu/Cu_2O@TiO_2, CuO@NiO, Fe_2O_3@TiO_2, Fe_2O_3/$NiCo_2O_4$, $NiFe_2O_4$/Fe_2O_3, ZnO@ Co_3O_4, ZnO/$ZnFe_2O_4$ [267]. Thus, these materials can be employed for manufacturing SCs electrodes because of the multiple functions and high SSA, but still face some major hurdles, such as low electrical conductivity at higher charge-discharge rates, short cycle life at higher rates, shortcomings in the diffusion distance of the electrolyte within porous MOs owing to high crystallinity [268].

The capacitive performance of MOF-derived MOs can be enhanced by: (a) mixing the MOF-derived MOs with conductive carbon materials as rGO, CNTs, graphene etc. along with a secondary metal oxide, thereby improving the electrical conductivity (b) increasing the SSA of MOF-derived MOs by heating the MOF precursors under N_2 atmosphere prior to heating them in air, which is beneficial for stopping the fast release of volatile gases which would have resulted in the collapse of the frameworks (c) optimizing the pore size of MOF-derived materials with size of electrolyte ion by matching the heating conditions so that the ions can enter in to the pores of MOs up to larger distances which

Table 3
Summary of the latest fabricated SC electrodes.

Electrode material	Electrolyte	Preparation method	C_s (Fg^{-1})	E_d ($Whkg^{-1}$)	P_d ($kWkg^{-1}$)	Retention (cycles)	Ref
Porous Au/MnO_2	–	–	1145 at 50 mVs^{-1}	–	–	80%(500)	[192]
Ni Co_2O_4 nanoneedle arrays	–	–	1118.6	–	–	89.4%(2000)	[193]
CuO@ AuPd@MnO_2 core-shell Whiskers	1 M KOH	Electrodeposition	1376 at 5 mVs^{-1}	0.55 $mWhcm^{-3}$	413 $mWcm^{-3}$	99%(5000)	[194]
$Ni_{0.61}Co_{0.39}$oxide on Ni foam	–	Electrodeposition	1523 at 2 Ag^{-1}	36.46	0.142	95.3%(1000)	[195]
CoO-PPY on 3D Ni foam	–	–	2223 at 1 $mAcm^{-2}$	–	–	99.8%(2000)	[95]
Mn/MnO_2 core-shell 3D porous structure	–	Electrodeposition	1200 at 5 mVs^{-1}	–	–	96%(2000)	[196]
VA-CNT-graphene with $Ni(OH)_2$ coating	2 M KOH	–	1065 at 22.1 Ag^{-1}	–	–	96%(20,000)	[197]
B-$Ni(OH)_2$/GO /CNTs	–	Phase transformation method	1815 at 2 Ag^{-1}	–	–	97%(2000)	[198]
Ni Co_2O_4	–	Hydrothermal method with annealing at 300 °C	1393 at 0.5 Ag^{-1}	21.4	0.35	–	[138]
$CoNi_2S_4$/ grapheme	–	–	2009.1 at 1 Ag^{-1}	–	–	–	[32]
Ni-Co-Mn triple hydroxide (NCMTH)/(GPs) graphitic petals	–	Hydrothermal method	1400	30	39	˜100% (10,000)	[181]
$Ni(OH)_2$-MnO_2-rGO	–	–	1985	54	–	–	[199]
$Ni(OH)_2$/rGO on Ni foam	–	Hydrothermal method	3328.7 at 1.5 Ag^{-1} 15.65 Fcm^{-2}	–	–	90.6%(5000)	[200]
N-CNF/N-CNF and $Ni(OH)_2$	6 M KOH	Electro-spinning	1045	51	117	84%(5000)	[56]
$Co(OH)_2$ –NPG	–	–	1800	–	–	–	[201]
Ni-CO-BH (binary hydroxide)/rGO	–	SILAR method	2130 at 2 Ag^{-1}	92	7.0	80%(10,000)	[31]
GF/Ni foam/$Co(OH)_2$	0.08 M $K_3Fe(CN)_6$/ 1 M KOH	–	7514 at 16 Ag^{-1}	–	–	–	[202]
Co_3O_4 /NH_2-GS	–	Hydrothermal method	2108.4 at 1 Ag^{-1} 1356.7 at 15 Ag^{-1}	59.3	.225	–	[203]
Ni-Mn LDH/rGO	–	Co-precipitation method	1635 at 1 Ag^{-1}	33.8 (at potential 1.7 V)	–	–	[204]
nickel-based metal organic frameworks (MOFs)	–	–	1698 at 1 Ag^{-1}	–	–	94.8%(1000)	[205]
Manganese molybdate nanosheet/Ni foam	–	Hydrothermal	1271 at 5mVs^{-1}	31.6	.935	84.5%(2000)	[206]
NiO/$LaNiO_3$	–	Spin coating	2030 at 0.5 Ag^{-1}	–	–	83%(1000)	[22]
nanopore $NiCo_2O_4$	–	Sol-gel	2157 (mass Cs) 40.6 $mFcm^{-2}$ (areal capacitance)	–	–	96.5%(10,000)	[21]
Ni_3S_2/$NiCo_2O_4$	–	–	4569.1 $mFcm^{-2}$ at 1$mAcm^{-2}$	–	–	89.2%(1000)	[207]
Co_3O_4 NCs	–	–	1913 at 8 Ag^{-1}	–	–	–	[208]
V_2O_5 nanosheets/rGO	1 M KCl	–	635 at 1 Ag^{-1}	–	–	–	[124]
RuO_2 decorated TiO_2 nanotube	–	–	1263	–	–	–	[209]
VS_4/Rgo	–	Hydrothermal synthesis	877 at 0.5 Ag^{-1}	117	20.65	–	[182]
Co_3O_4/ polyindole	1 M KOH	In situ cathodic electrodeposition	1805 at 2 Ag^{-1}	–	–	83%(1000)	[191]
NiO/GF	–	Pulsed laser deposition	1225 at 2 Ag^{-1}	–	–	89%(1000)	[57]
$Ni_xZn_{1-x}S$	3 M KOH	Hydrothermal method	1867 at 1 Ag^{-1}	–	–	77.4%(1000)	[120]
ZnO@Ni_3S_2	–	Electrodeposition	1529 at 2 Ag^{-1}	–	–	42%(1000)	[25]
$ZnCo_2O_4$/rGo/NiO	6 M KOH		1256 at 3 Ag^{-1}	62.8	7.4925	–	[187]
$Ni(OH)_2$/CNS	–	–	2218 at 1.0 Ag^{-1}	–	–	–	[210]

Table 4
Summary of the fabricated flexible planar SC electrodes/devices.

Electrode material	Electrolyte	Preparation method	C_s (Fg^{-1})	E_d ($Whkg^{-1}$)	P_d ($kWkg^{-1}$)	Retention (cycles)	Ref
CNT-graphene films	1 M H_2SO_4	Drop casting, vacuum filtration, air brush spraying	~140 at 0.1 Ag^{-1}	–	–	–	[211]
rGO/carbon black	PVA/H_2SO_4	–	79 at 1 Ag^{-1}	–	–	–	[212]
Carbon black pillared graphene film	1 M H_2SO_4	vacuum filtration	215 at 0.1 Ag^{-1}	–	414	97%(10,000)	[213]
Functionalized rGO film	Nafion	vacuum filtration	118.5 at 0.1 Ag^{-1}	–	–	90%(1000)	[214]
Macroporous graphene film	–	Hard template, vacuum filtration	92.7 at 3 mVs^{-1}	–	–	–	[215]
Graphene/PANI composite paper	1 M H_2SO_4	Vacuum filtration& electro- polymerization	233 at 2 mVs^{-1}	–	–	–	[216]
Graphene/PANI hybrid paper	1 M H_2SO_4	Vacuum filtration& polymerization	489 at 0.4 Ag^{-1}	–	33.9	96%(500)	[217]
NiO-graphene 3D networks	3 M KOH	CVD & sacrificial template	~816 at 5 mVs^{-1}	–	–	~100%(2000)	[218]
Graphene-MnO_2 -CNTs nanocomposite films	1 M Na_2SO_4	Co-precipitation & vacuum filtrarion	372	2.2	42	~95%(1000)	[219]
Embossed rGO-MnO_2 hybrid films	1 M Na_2SO_4	Vacuum filteration & sacrificial template	389 at 1 Ag^{-1}	44	25	95%(1000)	[220]
PPy/graphene	KCl	–	237 at 0.01 Vs^{-1}	–	–	–	[221]
Functionalized graphene hydrogel	1 M H_2SO_4	Hydrothermal treatment	441 at 1 Ag^{-1}	–	–	86%(10,000)	[222]
3D N&B co-doped graphene hydrogel	1 M H_2SO_4	Hydrothermal treatment	239 at 1 mVs^{-1}	8.7 (all solid state)	1.65(all solid state)	100%(1000)	[223]
PANI-oriented graphene hybrid film	–	Vacuum filtration & in situ polymerization	574	–	–	93%(10,000)	[224]
Graphene - PANI composite	1 M H_2SO_4	Coating & electro- polymerization	763 at 1 Ag^{-1}	–	–	82%(1000)	[225]
3D graphene -MnO_2 composite networks	0.5 M Na_2SO_4	CVD & electro- chemical deposition	465 at 2 mVs^{-1}	6.8	2.5	81.2%(5000)	[226]
Graphene-MnO_2 nano structured textiles	0.5 M Na_2SO_4	Dip drying & electro- chemical deposition	~315 at 2 mVs^{-1}	12.5	110	~95%(5000)	[227]
Co-Al LDH/rGO films	1 M KOH	Layer by layer assembly	1240 at 5 mVs^{-1} (90 $mFcm^{-2}$)	–	–	99%(2000)	[228]
Graphene- MnO_2 nanostructured sponges	1 M Na_2SO_4	Dip-drying	~450 at 2 mVs^{-1}	8.34	94	90%(10,000)	[229]
PANI nanowire-carbon cloth	–	–	1079 at 1.73 Ag^{-1}	–	–	86%(2100)	[230]
PANI nanowire arrays-Au coated PET films	–	–	588 F cm^{-3}	–	–	–	[231]
Ultra-thin MnO_2 / Zn_2SnO_4 nanowire-carbon microfibers	–	–	621.6 at 2 mVs^{-1}	–	–	98.8%(1000)	[232]
PANI nanoparticles-carbon nanofiber	–	–	638 at 2 Ag^{-1}	–	–	90%(1000)	[233]
$Ni(OH)_2$ nanosheet-graphene	–	–	660.8 F cm^{-3}	–	–	98.2%(2000)	[234]
$NiCo_2O_4$@ polypyrrole core-shell nanowire on hemp-derived carbon (HDC) microfiber	–	–	2055	17.5	0.5	90%(5000)	[235]
3D rGO-F/ PANI	–	Dipping and drying method	790	17.6	98	80%(5000)	[58]
NiAs-type Cobalt sulphide	–	Hydrothermal method	867	–	–		[236]
Cu_2O	1 M KOH	Dealloying method	210.9 at 0.5 Ag^{-1}			94.5%(5000)	[51]
Co_3O_4 flakes	1 M KOH	Dealloying method	410 at 0.7 Ag^{-1}	–	–	80.5%(5000)	[54]
γ – Fe_2O_3 nanoparticles	1 M KOH	Dealloying method	187 at 0.7 Ag^{-1}	–	–	93.2%(5000)	[54]

Table 5
Summary of some of the reported asymmetric/symmetric SCs.

Electrodes	C_s (Fg^{-1})	E_d ($Whkg^{-1}$)	P_d ($kWkg^{-1}$)	Capacitance retention	Ref
CNT/PANI//CNT/MnO_2/GR, by vacuum filtration method in 1 M Na_2SO_4/PVP	–	24.8 at 1.6 V	–	–	[246]
e-CMG/MnO_2//e-CMG in 1 M Na_2SO_4	–	44	11.2	95% after 1000 cycles	[247]
MnO_2/OCN/PVDF//MnO_2/OCN/PVDF	363.28	64.39	3.87		[248]
Co_2AlO_4@MnO_2 nanosheet//Fe_3O_4 nanoflakes	99.1	35.3 24.11	0.8001 8.033	92.4% after 5000 cycles	[249]
MnO_2 -V_2O_5//AC(activated carbon) in 0.5 M K_2SO_4	61	8.5	–	–	[128]
NiO-GF//HPN CNTs in 1 M KOH	116 at $1Ag^{-1}$	17	42	94% after 2000 cycles	[57]
NiO//porous carbon	–	11.6	0.028	–	[250]
$Ni(OH)_2$ nanosphere//AC	120 at 4.8 Ag^{-1}	–	–	–	[251]
$Ni_{0.67}$ $Co_{0.33}$ Se//RGO	176 at $1Ag^{-1}$	36.7	0.750		[142]
Ni Co_2 O_4 -RGO//AC	–	–	–	83% after 2500 cycles	[252]
Ni-Co oxide//AC	–	7.4	1.9	85% after 2000 cycles	[253]
V_2O_5 NS//RGO	95 at $1Ag^{-1}$	39	0.900	92% after 3000 cycles	[124]
rGO - V_2O_5 NS//RGO	195 at 1 Ag^{-1}	75.9	0.900	94% after 3000 cycles	[124]
Ni Co_2 O_4//AC in 2 M KOH	135 at 1 Ag^{-1}	21.4	0.350	95.6% after 1000 cycles	[138]
Ni Co_2 O_4 - MnO_2//activated graphene	–	5.8	2.5	–	[254]
Ni Co_2 O_4//AC	–	6.8	2.8	–	[255]
Ni-Zn-Co oxide/ hydroxide//AC	–	16.62	2.9	–	[256]
$ZnCo_2O_4$@MnO_2// Fe_2O_3 in 1 M KOH by hydrothermal method	161 at 2.5 $mAcm^{-2}$	37.8	0.648	91% after 5000 cycles at 20 Ag^{-1}	[139]
NiO//AC	73.4	15	0.447	–	[257]
Ni Co_2 O_4 @MnO_2//AC	–	35	0.163	–	[258]
Co_3O_4@MnO_2//AC	–	17.7	0.600	–	[259]
Ni-Co sulphide//AC	–	25	0.447	–	[260]
CNT@NCS@MnO_2//AC in 1 M Na_2SO_4	–	27.3	4.5 at 1.8 V	78.8% after 2000 cycles	[168]
$H_2Ti_6O_{13}$//CMK-3 (mesoporous carbon)	–	90	11	–	[140]
PPy@MoO_3//AC in 0.5 M K_2SO_4	–	12	3	–	[190]
Mn HCF//Fe_3O_4@rGO	96 at 1 $mAcm^{-1}$	27.9	2.183 at 1.8 V	82.2% after 1000 cycles	[183]
CNT/graphene//Mn_3O_4/graphene	72.6 at 0.5 Ag^{-1}	22.9	9	86% after 10,000 cycles	[261]
MnO_2// MnO_2	26 mF cm^{-2} at 0.7 V	–	–	–	[262]
Ru//Ru	68 mF cm^{-2} at 1 $mAcm^{-2}$	–	–	–	[115]
$Cd(OH)_2$//$Cd(OH)_2$, by chemical bath deposition in 1 M NaOH	51 at $5mVs^{-1}$	11.09	0.799 at 0.84 Ag^{-1}	–	[121]
HPCNTs//HPCNTs in 1 M $LiPF_6$	139 at 1 Ag^{-1}	37.9	0.700 at 1 A g^{-1}	90.6% after 4000 cycles	[59]
RGO//RGO		6.8	49.8	–	[263]
Ni-Mn LDH/rGO//AC	82.26 at $1Ag^{-1}$	33.8 at 1.7 V	–	–	[204]
$MnMoO_4.nH_2O$//AC	–	31.6	0.935	–	[206]
CNG@NCH//rGO	–	78.75	0.473	–	[213]
RuO_2-NPG//$Co(OH)_2$-NPG	350	120	–	–	[21]
N-CNFs/$Ni(OH)_2$//N-CNFs	–	51	117	84% after 5000 cycles	[22]
Ni-Co-BH-G//CCN	340	92	7	–	[31]
$Ni(OH)_2$-CNS//AC	198	56.7	4.0	93% after 10,000 cycles	[217]
$CoWO_4$/$Co_{1-x}S_4$//AC	103.1	22.5	4	87.27% after 5000 cycles	[41]
Cu_2O//AC by dealloying method	53 at 0.5 Ag^{-1}	20.04	7.1	93.3% after 5000 cycles	[51]
Co_3O_4 flakes//γ-Fe_2O_3 nanoparticles by dealloying method	94.7 at 0.7 Ag^{-1}	38.1	–	80.1% after 5000 cycles	[54]

can be made feasible by reducing the crystallinity of material [268].

Wang et al. [264] reported MOF (polyhedral ZIF-8) for SC application with enhanced values of E_d, P_d and cycling life in comparison to current hybrid capacitors. Kaur et al. [269,270] assembled graphene-MOF composite on TiO_2/FTO substrate and QD-MOF (quantum dot-MOF) nanocomposite. The 1-D and 2-D materials can facilitate easy highways for ion intercalation and deintercalation, thus improving charge-discharge. Thus, higher E_d and P_d may be obtained by using 3-D materials which can supply many reaction sites in their 3-D networks. But, very few methods provide control over the dimensions of the prepared metal oxides which illustrates the significance of MOF-derived materials. Hence an extensive understanding of the charge-discharge process of MOF-derived MOs is needed to get better electrochemical performance.

5.2. COFs

COFs, novel microporous materials, which have molecularly ordered structures formed by the covalent linking of organic building blocks, are gaining importance because of their well-defined structures, high porosity, versatile molecular design and precise control over the placement and character of redox-active groups [271]. The first COF was reported by Yaghi and co-workers in 2005, utilizing boronate ester with boroxine linkages. It resulted in porous materials with good crystallinity [272]. The COFs are synthesized by using solvent conditions that result in a suspension or slurry [273]. By designing the solvent conditions, the COF formation rate can be obtained by turbidity measurements. In this study, the COF formation rate is related to the aromatic stacking capacity of the monomer. Another report explored the effect of dihedral angles among aromatic rings of the monomers on the crystallinity and porosity in COFs [274]. However, the lesser electrical conductivity and less stability of COFs put hurdles in their practical application. A strategy has been planned to eradicate these limitations by confining conducting polymers within porous frameworks which results in improved cycle stability along with maintaining electrical conductivity and mechanical stability.

Recently, Dichtel et al. [275] have developed this process by using PEDOT-modified COF (DAAQ-TFP COF) to obtain very high-rate charging with higher E_d. Xu et al. [276] have explained that the PEDOT-modified DAAQ-TFP COF films possess a better current response in CV than pristine DAAQ-TFP COF film which can be ascribed to the wiring effect of PEDOT chains. However, ion transport is improved by vertical pore channels by reducing the diffusion length. Chandra et al. [277] reported COFs [TpPa-$(OH)_2$, TpBD-$(OH)_2$] for SCs. Fig. 10 shows the

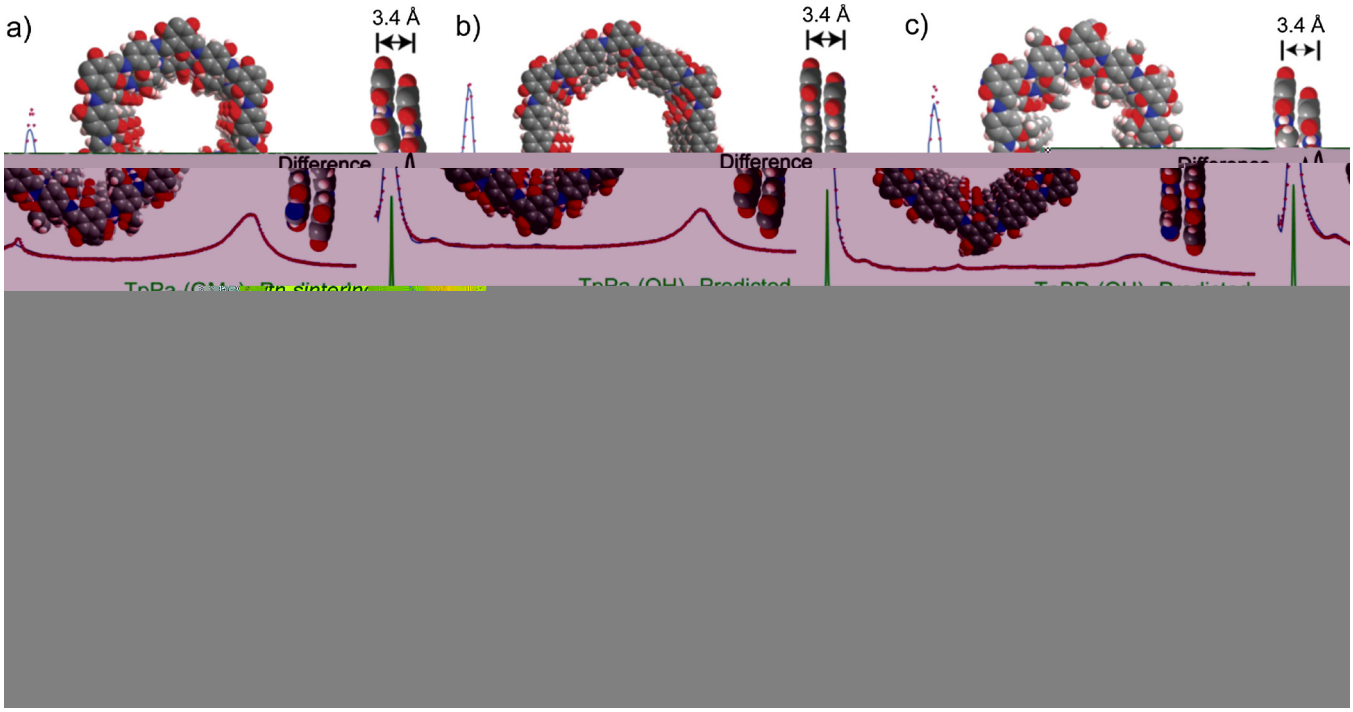

Fig. 10. Comparision of XRD pattern for (a) TaPa-$(OH)_2$ (b)TpBD-$(OH)_2$ and (c) TaPa-$(OMe)_2$; Inset of (a), (b), and (c) shows the pore structure and л-л stacking distance for COFs Comparision of N_2 adsorption isotherms at 77 K for (d) TaPa series and (e) TpBD series (f) Pore size distribution and (g) TEM images for TaPa-$(OH)_2$, TpBD-$(OH)_2$, TaPa-$(OMe)_2$, and TpBD-$(OM)_2$ [277]. (Reproduced with permission from Ref. [277] Copyright American Chemical Society (2017)).

XRD, N_2 adsorption curves, pore size distribution and TEM images of COFs. TpPa-$(OH)_2$ exhibited C_s of 416 Fg^{-1} at 0.5 Ag^{-1} with 66% C_s retention after 10,000 cycles. High C_s is due to the exact molecular control of redox functionalities in the COF. Han et al. [278] fabricated nanocoatings of COFs on Ni NWs which exhibited C_s of 314 Fg^{-1} at 50 Ag^{-1} with 74% of the C_s retention at 2 Ag^{-1}. The high current density made the charge-discharge phenomenon very rapid. Kim et al. [271] fabricated N-doped carbon by carbonization of COFs through an azine-linked 2-D network (ACOF1). In ACOF1, micropores (diameters < 1 nm) have been formed with high SSA (1596 $cm^2 g^{-1}$). The C_s of carbonized ACOF1 is 234 Fg^{-1} at the 1.0 Ag^{-1} which is greater than the carbonized COF1 (191 Fg^{-1}). Romero et al. [279] fabricated COFs of polyimine with many metal ions (Fe^{III}, $Co^{II,}$ and Ni^{II}).

5.3. MXenes

MXenes (2-D inorganic compounds) were first developed in 2011 by Yury Gogotsi [280] and comprise few atom deep layers of transition metal nitrides, carbides or carbonitrides. MXenes provide an exclusive amalgamation of conductivity and hydrophilicity (because of their hydroxyl surfaces) along with the superior mechanical properties. MXenes have the general formula $M_{n+1}AX_n$, where M is a transition metal, A is group 13 or 14 element, X is C and/or N and n = 1, 2, or 3. These are produced by selective etching of element A from their 3D layered MAX phase. So far, approximately 20 MXenes have been produced which have shown superior C_s for the reversible intercalation of metal cations (eg. Li^+, Na^+, K^+, Mg^{2+}, Al^{3+}, etc.) [281].

Fu et al. [282] prepared a flexible paper electrode using layered 2D $Ti_3C_2T_x$ which achieved a high volumetric capacitance of 892 F cm^{-3} along with excellent cycling performance (no capacitance loss after 10,000 cycles). Yarn SCs are fabricated using MXenes and PEDOT-PSS which show excellent stability and device performance even during bending and twisting [283]. Shah et al. [284] demonstrated the scrolling, bending and folding of $Ti_3C_2T_x$ nanosheets into 3D crumpled structures and also the change was found to be reversible on rehydration. Rakhi et al. [285] reported the formation of nanocrystalline ε-MnO_2on MXene nanosheets (ε-MnO_2/Ti_2CT_x and ε-MnO_2/$Ti_3C_2T_x$) by chemical synthesis. The ε-MnO_2 nanocrystalline whiskers enhance the SSA of the nanocomposite electrode and hence improve the C_s by approximately three times in comparison to that of pure MXene-based symmetric SCs. The fabricated ε-MnO_2/MXene SCs possess good cycling stability (~88% of the C_s retention after 10,000 cycles). Hu et al. [286] studied $Ti_3C_2T_x$ MXenes obtained by etching Ti_3AlC_2 in HF aqueous solution (at different concentrations-6 M and 15 M) as shown in Fig. 11. A higher C_s had been obtained in 6 M HF-etched MXene ($Ti_3C_2T_x$-6 M).

5.4. Metal nitrides (MNs)

MNs have captured the interest as SC electrode material due to their good electrochemical properties, high chemical stability and standard technological approach [287]. Zhu et al. [288] grew two MNs: TiN porous layers and Fe_2N nanoparticles on vertical-aligned graphene sheets and used as the electrodes for solid-state SCs. Das et al. [289] prepared MNs (M = Co, Cr) nanoparticles (particle size approximately 20–30 nm) in NH_3 + N_2 atmosphere at small temperature. The Cr-urea complex directly changes to CrN, however, CoN has been obtained from Co_3O_4. The ASC fabricated using MNs and AC as electrodes shows high C_s of 37 and 75 Fg^{-1} for M = Co, Cr, respectively at 30 mA g^{-1}.

5.5. Black phosphorus (BP)

BP (newest members in the 2D material family), has recently gathered much attraction due to its higher theoretical C_s (2596 $mAhg^{-1}$), distinct structures with corrugated planes of P atoms which are linked by strong interlayer P—P bonding and weak interlayer Vander Waals forces [290]. The bulk BP may be converted into thin sheets (few layers to even a single layer) by breaking the weak interactions. Few layered BP (phosphorene) has a direct band gap of 0.3 eV–2.2 eV which can be controlled by the number of layers. Also, BP has an interlayer spacing of 5.3 Å, greater than graphite (3.6 Å) and comparable to that of 1 T MoS_2 phase (6.15 Å) [291]. Hao et al. [292] fabricated flexible SC using liquid-exfoliated BP nanoflakes which

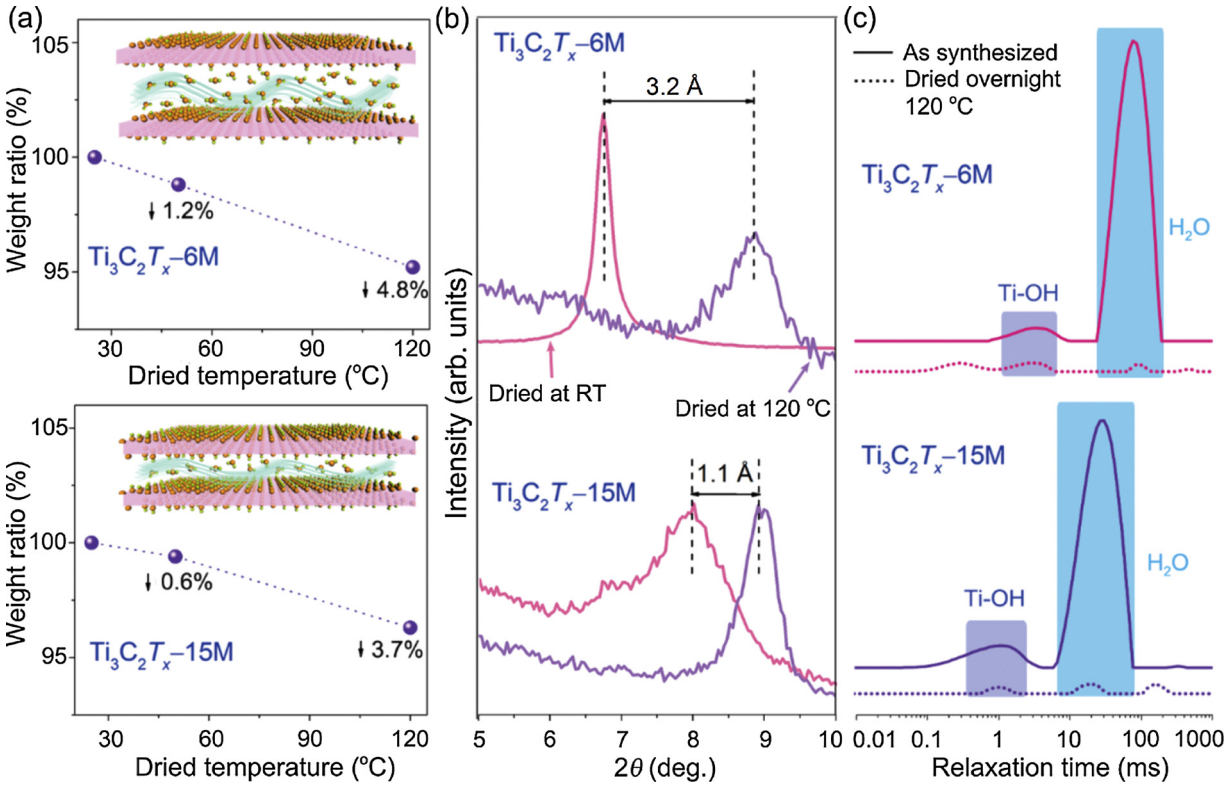

Fig. 11. (a) Normalized weight of $Ti_3C_2T_x$-6 M and $Ti_3C_2T_x$-15 M dried at different temperatures, Inset shows the schematic of $Ti_3C_2T_x$-6 M and $Ti_3C_2T_x$-15 M dried at room temperature (b) (0002) peaks of XRD pattern shows the shrinkage of interlayer spacing upon drying at 120 °C for $Ti_3C_2T_x$-6 M and $Ti_3C_2T_x$-15 M (c) 1H NMR spectra of as-synthesized MXenes and those dried at 120 °C overnight [286]. (Reproduced with permission from Ref. [286] Copyright American Chemical Society (2018)).

delivered C_s (volumetric) of 13.75 Fcm^{-3}, P_d of 8.83 Wcm^{-3} and E_d of 2.47 $mWhcm^{-3}$ and a very long lifespan of over 30,000 cycles.

Yang et al. [293] fabricated all-solid-state SC using flexible BP nanoflake/CNT composite paper as electrodes. CNTs increase electrolyte shuttling and forbid the restacking of BP nanoflakes. The prepared SC with BP/CNTs (ratio 1:4) exhibited C_s (volumetric) of 41.1 Fcm^{-3} at 0.005 Vs^{-1}, a high P_d of 821.62 Wcm^{-3}, high E_d of 5.71 $mWhcm^{-3}$, excellent mechanical flexibility and high cycle stability (91.5% C_s retention after 10,000 cycles). Chen et al. [294] have synthesized a heterostructure of BP and red phosphorus through the sonochemical process. The C_s of BP/Red Phosphorus hybrid is approximately 60.1 Fg^{-1} retaining 83.3% of C_s after 2000 cycles.

6. New Devices/Applications for SCs

6.1. Electrochromic SC

Along with improving electrochemical performance of SCs, research has been focussed on the integration of SCs with multiple functions such as flexibility, wearability for their use in portable devices and adding smart functionalities so that people can easily determine the electrical energy storage (EES) [295]. The most striking change is the visual change which can be easily identified. Among SC materials, WO_3 has been found to be smart material due to its good contrast amid the bleached transparent state and blue coloured state. The change in colour with potential or EES of the electrode demonstrates its smart function [296]. Zhu et al. [297] synthesized WO_3 by electro-deposition method (e- WO_3) as a smart electrode material. Optical density has been used for investigation of colour change of WO_3 film based SCs. A linear dependence between optical density and EES is discovered. Then hybrid SC is fabricated to integrate the color-change based EES indicators to various high-performance SCs. As the EES of SCs is visually apparent by the color change of WO_3 so e-WO_3 can be integrated with other materials to form a smart hybrid SC.

6.2. Battery-supercapacitor hybrid (BSH) device

BSH devices are of immense interest due to their future applications in smart electric grids, electric vehicles and miniaturized electronic-optoelectronic devices etc. Along with traditional Pb-acid, Ni-MH, Ni-Cd, Li-ion batteries (LIBs), several advanced batteries such as Li-air, Li-sulfur, Na-ion, Al-ion batteries and aqueous metal ion batteries are emerging. Energy storage using a high C_s battery-type electrode and high P_d capacitive electrode called BSH provides a potential way to fabricate a device with the qualities of both batteries and SCs [298].

In Li-ion BSH, the SC electrode materials are carbon materials (such as ACs, CNTs, graphene etc.) and battery material are MOs, intercalation compounds, and their composites. Zheng et al. [298] combined EDLC type + ve electrode with battery type -ve electrode which achieved an E_d of 147 $Whkg^{-1}$ at a P_d of 150 Wkg^{-1} and also retained an E_d of 86 $Whkg^{-1}$ at a P_d of 2587 Wkg^{-1}. Peng et al. [299] have introduced a new SC/Li-ion battery (SC/BT) topology hybrid energy storage system (HESS) for electric vehicle (EV) using ADVISOR simulator. In this braking regeneration energy is harvested by SC pack. The constraint on Li resources has forced researchers to use other elements abundant on earth. In this context, Na-ion SCs have been explored which couples battery electrode with high C_s and surface adsorption based SC electrode with good rate capability. Lu et al. [183] constructed an advanced Na-ion SC using Mn hexacyanoferrate as the cathode and Fe_3O_4/rGO as an anode in the aqueous electrolyte with an extended PW of 1.8 V, P_d of 2183.5 Wkg^{-1}, E_d of 27.9 $Whkg^{-1}$ and good cycling stability (82.2% C_s retention after 1000 cycles). Along with Na-ion based BSH, potassium-ion based BSH is also attractive due to its low cost and abundance of potassium (K) in nature.

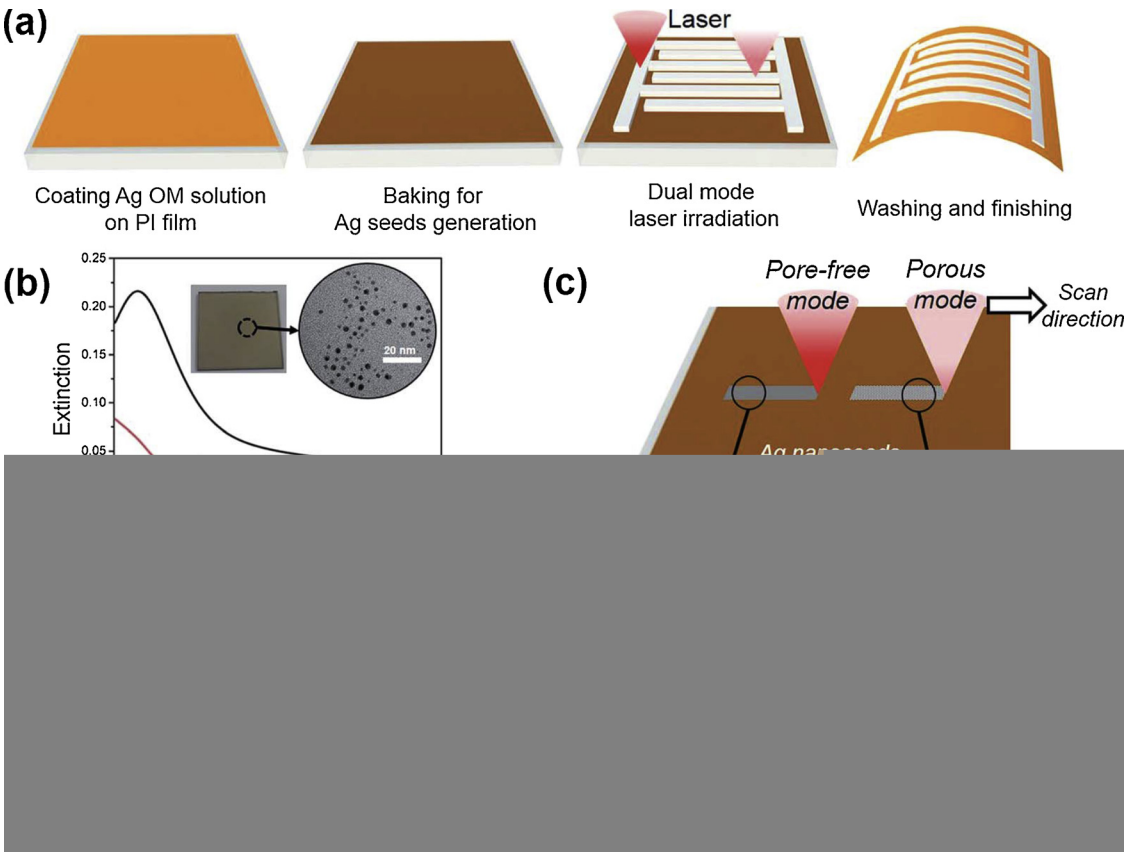

Fig. 12. (a) Schematic explanation of nanoporous silver (NPS) electrode and current collector (b)Extinction efficiency of pre-baked organometallic solution and procedure of a laser-sintering process (c) Change in structure of silver conductor based on the laser energy [313]. (Reproduced with permission from Ref. [313] Copyright Royal Society of Chemistry (2017)).

Komaba et al. [300] proposed a graphite-polyacrylate electrode as a –ve electrode for 4 V K-ion SC. Multivalent metal ion (e.g. Al^{3+}) based BSH devices are also of concern along with monovalent metal ions, due to their high E_d. Li et al. [301] reported a BSH system with an E_d of 13 $Whkg^{-1}$ using $Al_{0.2}CuFe$-PBA as the + ve electrode, AC as the -ve electrode. Another Al-ion BSH system using PPy@MoO_3 as the -ve electrode with AC as the + ve electrode has been reported with an E_d of 30 $Whkg^{-1}$ and operating voltage up to 1.5 V in aqueous electrolyte [302].

6.3. Electrochemical flow capacitor (EFC)

In EFC, energy is stored in electric double layers formed by charging carbon particles. Here, a slurry type carbon-electrolyte mixture is deployed as the active material for the charge storage. EFC consists of a cell having two external reservoirs which possess a blend of electrolyte and carbon material. The uncharged mixture is passed from reservoir tanks to flow cell, where the energy is given to the carbon material. After being charged, the slurry can be kept in big tanks until the need for energy arises and at the time of need, the complete process is reversed. EFCs can sustain a large number (hundreds of thousands) of charge-discharge cycles [303,304]. A flowable electrode made up of HQ/carbon spheres yielded a C_s of 64 Fg^{-1} which was 50% more than that of only carbon-based flowable electrodes [305].

6.4. Alternating current (ac) line-filtering SCs

A supercapacitor can replace bulky Al electrolytic capacitors (AECs) used exhaustively in ac line filtering, resulting in the miniaturization of the devices. However, the SCs developed for this purpose, have restricted applied voltage range of ˜20 V. To enhance the voltage range, designing of carbon electrodes with appropriate pore structure is necessary. Yoo et al. [306] reported graphitic mesoporous carbon as an electrode in SCs and fabricated a 2.5 V SC with a C_s (areal) of (□560 $mFcm^{-2}$) and rapid frequency response (ϕ ˜ -80°) at 120 Hz. Also, mixing a small amount of CNTs to the electrode material enhanced the voltage to □40 V. Rangom et al. [307] fabricated superior-performance, self-standing composite electrodes with SWCNTs. The 3-D mesoporous SWCNT-based electrodes permitted unimpaired ionic transport in thick films and provided better results in an ac line frequency of 120 Hz. Measurements of 601 μFcm^{-2} with a -81° phase angle and a time constant of 199 μs had been obtained and as fabricated electrodes were capable of cycling at higher than 200 Vs^{-1} showing a parallelepipedic CV shape at 1 kVs^{-1}. Current densities were greater than 6400 Ag^{-1} and the electrodes preserved greater than 98% of C_s over 1 million cycles. Preparation of graphene-based ac line-filters on a large scale has been reported by Wu et al. [308]. Here, GO reduced by patterned metal interdigits has been employed as the electrode and the fabricated device explored a phase angle of -75.4° at 120 Hz, a time constant of 0.35 ms, a C_s of 316 μFcm^{-2} and retains 97.2% of the C_s after 10,000 charge-discharge cycles. Kurra et al. [309] have reported PEDOT micro-supercapacitor with ultra-high scan rate capability of 500 Vs^{-1} and a cross over frequency of 400 Hz at a phase angle of -45° which exhibits C_s (areal) of 9 m F cm^{-2} in 1 M H_2SO_4. These devices retain the C_s of 80% after 10,000 cycles, maintained efficiency (η) of 100% and exhibit an E_d of 7.7 $mWhcm^{-3}$.

6.5. Micro-supercapacitors (Micro-SCs)

Thin film batteries and microsized batteries suffer from certain limitations, for instance, short lifetime, small P_d and complex architecture, which restrict their integration in portable and miniaturized

devices. Micro-SCs with planar architecture have the advantage of easy fabrication into miniaturized electronics [310]. Shao et al. [311] reported a quasi-solid state micro-SC with cellular graphene films as an active material and PVA/H_3PO_4 as the gel electrolyte. The 3D graphene films served as high-performance SC electrodes as well as an ion reservoir for the electrolyte. Liu et al. [312] have reported a photoswitchable micro-SC based on the diarylethene-graphene film which exhibits the C_s modulation up to 20% demonstrating a photoswitchable micro-SC. Terahertz spectroscopy explored that the photoswitching is related to charge transfer at the graphene-diarylethene interface on light modulation. A flexible micro-SC of the self-generated silver layer has been designed by Lee et al. [313] using the laser-induced growth-sintering technique. As designed SC exhibits a high E_d (volumetric) of 16.3 mWhcm^{-3} and a P_d of 3.54 Wcm^{-3} as shown in Fig. 12.

6.6. Photo-supercapacitors (photo-SCs)

Photovoltaic energy generation is among the fastest growing power sector. In photo-SCs, the fluctuating electricity generated from solar cells is integrated with SCs. SCs with a photoactive layer along with a supercapacitive layer into a single device have been presented [314]. This device exhibits the capabilities of self-charging upon illumination with self-storage of charge. The photogenerated current is about 2 mAg^{-1} along with the C_s of ˜140 Fg^{-1}. Xu et al. [315] reported a stack-integrated photo-SC`, composed of DSSC (dye-sensitized solar cells) and a SC fabricated on anodic titanium oxide (ATO) nanotube array, where an enhanced SC output was obtained by plasma-assisted hydrogenation process. The C_s (areal) of selectively hydrogenated ATO had been 1.0 mFcm^{-2} at 1mAcm^{-2}. The optimized photo-SCs showed good photoelectric conversion efficiency with storage efficiency (approximately 1.64%) with quick response and better cycling capability.

6.7. Thermally chargeable SCs

Low-grade thermal energy, which at present is wasted, can be stored for powering devices such as wearable electronics and sensors. Thermoelectric energy conversion is a good method for waste heat management, but impediments like low output voltage with no energy storing capability require other components (e.g. voltage boosters and capacitors). Thermal self-charging SC uses the Seebeck effect, thermally activated ion diffusion and temperature dependent electrochemical redox potential. It comprises two electrodes kept at dissimilar temperatures [316]. An innovative process of producing a large voltage from the temperature gradient like conventional thermoelectronics is reported [317]. The PANI coated graphene and CNT electrodes sandwich the polystyrene sulphonic acid (PSSH) film in which thermally excited electrochemical reactions result in charging without the requirement of any external source for power supply. With little temperature difference (5 K), the thermally chargeable supercapacitor produces a voltage of 38 mV and a large C_s (areal) (1200 Fm^{-2}). Al-zubaidi et al. [318] examined the thermally-induced phenomena of an ionic electrolyte and solid-liquid interface and also reviewed the studies on thermally excited self-charging in SCs. Wang et al. [319] explored a thermal charging process to restore the energy wasted in SCs after electrical charging and discharging. Zhao et al. [320] used an asymmetric polymer electrolyte prepared from NaOH-treated polyethylene oxide (PEO-NaOH) to generate a thermally-induced voltage in SCs. They employed electrodes of Au and of MWCNTs deposited on Au and obtained a thermopotential of 10 mV K^{-1}, the C_s (areal) of 1.03 mFcm^{-2} and E_d of 1.35 mJcm^{-2} at the temperature difference of 4.5 K.

6.8. Self-healing SCs

A self-healing SC has been fabricated by Li et al. [321] which exhibits higher E_d by employing biochar-based electrodes and polyampholyte gel electrolyte. Polyampholyte is a tough hydrogel which provides self-healing capability along with mechanical flexibility. Biochar (BC), obtained from pyrolysis (low-temperature) of biological wastes along with the inclusion of the rGO, is a carbon material that provides mechanical strength and electrical conductivity. The SC fabricated using BC-rGo electrodes, exhibit higher E_d of 30 Whkg^{-1} with ˜90% C_s retention after 5000 cycles at P_d of 50 Wkg^{-1} at room temperature and an E_d of 10.5 Whkg^{-1} at a P_d of 500 Wkg^{-1} at −300 °C. The low-temperature behaviour excellence may be linked to non-freezable water near hydrophilic polymer chains. This can further inspire researchers to explore the phase performance of water close to polyampholyte chains. Wang et al. [322] reported rGO based spring electrodes for stretchable SCs synthesized by casing fibre springs in a self-healing polymer which show 82.4% C_s retention after almost 100% stretch, and 54.2% C_s retention after third healing.

6.9. Shape memory SC (SMSC)

Flexible wearable SCs experience deformations which do not reverse after long-term stress, leading to structural and functional fatigue. For solving this problem, an SMSC has been fabricated by Huang et al. [323] which is flexible and gets easily deformed but when heated above a specific temperature, it recuperates its original shape by restoring all deformations. Also, a shape memory textile fabricated with these SMSCs can act as smart sleeves which can remember its previous shape and register automatic cooling when overheated.

6.10. Piezoelectric SCs

The advancement in the integration level along with minimizing energy losses in power management circuits is the need of the hour. Generally, a full wave rectifier is employed among the piezoelectric nanogenerator and the storage device which reduces integration density and enhances energy loss. Recently, Xing et al. [324] demonstrated a self-charging cell for energy conversion and storage by integrating piezoelectric separator and Li-ion battery. However, due to slow charging and reduced cyclability of Li-ion battery, the SCs have gained immense attention. The integration of pseudocapacitor and piezoelectric material in the energy storage device has been reported by Ramadoss et al. [325]. Song et al. [326] integrated a PVDF film in SC as the energy harvester and separator. An SC has been formed by using PVDF film coated with H_2SO_4/PVA gel as anode and carbon cloth with H_2SO_4/PVA electrolyte as a cathode. The piezoelectric PVDF film due to mechanical force showed the charging of the SC and possessed a C_s of 357.6 Fm^{-2}, an E_d of 400 mW m^{-2} and a P_d of 49.67 mWhm^{-2}. Maitra et al. [327] have fabricated a bio-piezoelectric run self-charging ASC consisting of NiCoOH-CuO@Cu foil as a + ve electrode and rGO@Cu foil as -ve electrode with a PVA-KOH gel electrolyte dipped porous fish swim bladder as a bio-piezoelectric separator. This SC can be charged up to 281.3 mV in ˜80 s.

7. Conclusions and challenges for SCs

Electrochemical SCs are developing as promising devices for energy storage. In this review, a detailed description of electrode materials based on carbon materials, CPs, MOs and their composites has been given. Further research is needed for high-performance SC electrodes which can simultaneously assure high capacitance, cyclic stability and excellent rate. The authors believe that more research should be focussed on different nanocomposite materials made up of carbon, MOs and CPs for fabricating high-performance SC electrodes. Also, the state-of-the-art developments in SC electrode materials have been incorporated in this article along with some novel materials and new devices for SCs. Continuous research efforts are needed to allow these materials and novel devices to meet the growing energy demands. Also, it is essential to improve synthesis parameters and material properties for full capability exploration of the SC electrode materials. MOFs,

COFs, MXenes and metal nitrides are new materials with great potential for SC application. Phosphorene, because of reduced diffusion pathway and highly dense structure, is also a promising candidate for SCs. In the energy industry, fabrication of new devices for SCs such as BSH device, EFC, micro-SC, electrochromic SC, photo-SC, thermally chargeable SC, self-healing SC, shape memory SC and piezoelectric SC have gained attention.

Although encouraging results have been attained in this field; yet the evolution of a new generation of SCs is at its premature stage. To improve the supercapacitor performance, the focus should be on the following parameters: (i) An in-depth knowledge of energy storage mechanisms should be gained for interfacial reactions at the electrode and the electrolyte (ii) Design the electrodes to form hierarchical interconnected porous microstructures and avoid the creation of dead volume (iii) Control the interfacial interactions to obtain a structure with high electrochemical performance.

The main developmental goals are:

- More novel manufacturing techniques should be developed to prepare highly porous material with hollow structures so that a large amount of charge can be stored resulting in increase in E_d.
- Moreover, to improve the E_d, along with electrode material, electrolytes with stable and wide potential window along with good ionic conductivity are needed. Also, the compatibility issues between pore size of electrode material and ion size of the electrolyte should be taken into account in order to fully explore the utilization of porous surface of electrode material.
- In addition to the selection of electrode material and electrolyte several other issues such as improvement of the operating temperature range, self-discharge rate, long lifetime, degradation of the current collectors, separators, packaging etc. should be vigorously investigated for improving overall cell performance.
- More focus should be on the development of ASCs as these SCs provide higher E_d and P_d simultaneously.

Conflicts of interest

There are no conflicts to declare.

Acknowledgments

Ms. Poonam is thankful to UGC, New Delhi, India for providing Teacher Fellowship under 'Faculty Development Programme' to complete Ph.D. at Panjab University, Chandigarh.

References

[1] L.L. Zhang, X.S. Zhao, Carbon-based materials as supercapacitor electrodes, Chem. Soc. Rev. 38 (2009) 2520–2531.
[2] A. Balducci, R. Dugas, P. Taberna, P. Simon, D. Plee, M. Mastragostino, S. Passerini, High temperature carbon-carbon supercapacitor using ionic liquid as electrolyte, J. Power Sources 165 (2007) 922–927.
[3] C. Largeot, C. Portet, J. Chmiola, P. Taberna, Y. Gogotsi, P. Simon, Relation between the ion size and pore size for an electric double-layer capacitor, J. Am. Chem. Soc. 130 (2008) 2730–2731.
[4] S. Kandalkar, D. Dhawale, C. Kim, C. Lokhande, Chemical synthesis of cobalt oxide thin film electrode for supercapacitor application, Synth. Met. 160 (2010) 1299–1302.
[5] M. Winter, R.J. Brodd, What are batteries, fuel cells and supercapacitors? Chem. Rev. 104 (2004) 4245–4269.
[6] B.E. Conway, Transition from "Supercapacitor" to "Battery" behavior in electrochemical energy storage, J. Electrochem. Soc. 138 (1991) 1539–1548.
[7] Z. Mingjia, X. Chengcheng, L. Jiaangtian, L. Ming, W. Nianqiang, Nanostructured carbon-metal oxide composite electrodes for supercapacitors: a review, Nanoscale 5 (2013) 72–88.
[8] Z.S. Wu, Y. Zheng, S. Zheng, S. Wang, C. Sun, K. Parvez, T. Ikeda, X. Bao, K. Mullen, X. Feng, Stacked-layer heterostructure films of 2D thiophene nanosheets and graphene for high-rate all-solid-state pseudocapacitors with enhanced volumetric capacitance, Adv. Mater. 29 (2017) 1602960.
[9] S. Kondrat, A.A. Kornyshev, Pressing a spring: what does it take to maximize the energy storage in nanoporous supercapacitors? Nanoscale Horiz. 1 (2016) 45–52.
[10] J. Tang, Y. Yamauchi, Carbon materials: MOF morphologies in control, Nat. Chem. 8 (2016) 638–639.
[11] S. Zheng, Z.S. Wu, S. Wang, H. Xiao, F. Zhou, C. Sun, X. Bao, H.M. Cheng, Graphene-based materials for high-voltage and high-energy asymmetric supercapacitors, Energy Storage Mater. 6 (2017) 70–97.
[12] G. Wang, L. Zhang, J. Zhang, A review of electrode materials for electrochemical supercapacitors, Chem. Soc. Rev. 41 (2012) 797–828.
[13] W.G. Pell, B.E. Conway, Voltammetry at a de Levie brush electrode as a model for electrochemical supercapacitor behavior, J. Electroanal. Chem. 500 (2001) 121–133.
[14] H. Ohno, K. Fukumoto, Progress in ionic liquids for electrochemical reaction matrices, Electrochemistry 76 (2008) 16–23.
[15] G.A. Snook, P. Kao, A.S. Best, Conducting-polymer-based supercapacitor devices and electrodes, J. Power Sources 196 (2011) 1–12.
[16] M. Galinsky, A. Lewandowski, I. Stepniak, Ionic liquids as electrolytes, Electrochim. Acta 51 (2006) 5567–5580.
[17] C. Zhong, Y. Deng, W. Hu, J. Qiao, L. Zhang, J. Zhang, A review of electrolyte materials and compositions for electrochemical supercapacitors, Chem. Soc. Rev. 44 (2015) 7484–7539.
[18] D.P. Dubal, P.G. Romero, B.R. Sankapal, R. Holze, Nickel cobaltite as an emerging material for supercapacitors: an overview, Nano Energy 11 (2015) 377–399.
[19] G.E. Goikolea, J.A. Barrena, R. Mysyk, Review on supercapacitors: technologies and materials, Sustain. Eng. Rev. 58 (2016) 1189–1206.
[20] A.I. Yusin, A.G. Bannov, Synthesis of composite electrodes for Supercapacitors based on carbon materials and the metal oxide/metal hydroxide system, Prot. Met. Phys. Chem. Surf. 53 (2017) 475–482.
[21] Y. Liu, N. Wang, C. Yang, W. Hu, Sol-gel synthesis of nanoporous $NiCo_2O_4$ thin films on ITO glass as high-performance supercapacitor electrodes, Ceram. Int. 42 (2016) 11411–11416.
[22] X. Liu, G. Du, J. Zhu, Z. Zeng, X. Zhu, $NiO/LaNiO_3$ film electrode with binder-free for high performance supercapacitor, Appl. Surf. Sci. 384 (2016) 92–98.
[23] Z. Su, C. Yang, C. Xu, H. Wu, Z. Zhang, T. Liu, C. Zhang, Q. Yang, B. Li, F. Kang, Co-electro-deposition of the MnO_2-PEDOT: PSS nanostructured composite for high areal mass, flexible asymmetric supercapacitor devices, J. Mater. Chem. A 1 (2013) 12432–12440.
[24] Y.L. Chen, P.C. Chen, T.L. Chen, C.Y. Lee, H.T. Chiu, Nanosized MnO_2 spines on Au stem for high-performance flexible supercapacitor electrodes, J. Mater. Chem. A 1 (2013) 13301–13307.
[25] Z. Xing, Q. Chu, X. Ren, C. Ge, A.H. Qusti, A.M. Asiri, A.A. -Youbi, X. Sun, Ni_3S_2 coated ZnO array for high-performance supercapacitors, J. Power Sources 245 (2014) 463–467.
[26] F.M. Guo, R.Q. Xu, X. Cui, L. Zhang, K.L. Wang, Y.W. Yao, J.Q. Wei, High performance of stretchable carbon nanotube-polypyrrole fiber supercapacitors under dynamic deformation and temperature variation, J. Mater. Chem. A 4 (2016) 9311–9318.
[27] M. Rajesh, C.J. Raj, R. Manikandan, B.C. Kim, S.Y. Park, K.H. Yu, A high performance PEDOT/PEDOT symmetric supercapacitor by facile in-situ hydrothermal polymerization of PEDOT nanostructures on flexible carbon fibre cloth electrodes, Mater. Today 6 (2017) 96–104.
[28] R. Wang, Q. Wu, X. Zhang, Z. Yang, L. Gao, J. Ni, O.K.C. Tsui, Flexible supercapacitors based on a polyaniline nanowire-infilled 10 nm-diameter carbon nanotube porous membrane by in situ electrochemical polymerization, J. Mater. Chem. A 4 (2016) 12602–12608.
[29] H. Zhou, G. Liu, J. Liu, Y. Wang, Q. Ai, J. Huang, Z. Yuan, L. Tan, Y. Chen, Effective network formation of PEDOT by in-situ polymerization using novel organic template and nanocomposite supercapacitor, Electrochim. Acta 247 (2017) 871–879.
[30] R. Datt, J. Gangwar, S.K. Tripathi, R.K. Singh, A.K. Srivastava, Porous nickel oxide nanostructures for supercapacitor applications, Quantum Matter 5 (2016) 1–7.
[31] M. Jana, S. Saha, P. Samanta, N.C. Murmu, N.H. Kim, T. Kuila, J.H. Lee, Growth of Ni-Co binary hydroxide on a reduced graphene oxide surface by a successive ionic layer adsorption and reaction (SILAR) method for high performance asymmetric supercapacitor electrodes, J. Mater. Chem. A 4 (2016) 2188–2197.
[32] W. Du, Z. Wang, Z. Zhu, S. Hu, X. Zhu, Y. Shi, H. Pang, X. Qian, Facile synthesis and superior electrochemical performances of $CoNi2S_4$/graphene nanocomposite suitable for supercapacitor electrodes, J. Mater. Chem. A 2 (2014) 9613–9619.
[33] W.K. Chee, H.N. Lim, Z. Zainal, N.M. Huang, I. Harrison, Y. Andou, Flexible graphene-based supercapacitors: a review, J. Phys. Chem. C 120 (2016) 4153–4172.
[34] Q. Ke, J. Wang, Graphene-based materials for supercapacitor electrodes-a review, J. Materiomics 2 (2016) 37–54.
[35] A.A. Kalam, S. Park, Y. Seo, J. Bae, High-efficiency supercapacitor electrodes of CVD-grown graphenes hybridized with multiwalled carbon nanotubes, Bull. Korean Chem. Soc. 36 (2015) 2111–2115.
[36] E.V. Lobiak, L.G. Bulusheva, E.O. Fedorovskaya, Y.V. Shubin, P.E. Plyusnin, P. Lonchambon, B.V. Senkovskiy, Z.R. Ismagilov, E. Flahaut, A.V. Okotrub, One-step chemical vapor deposition synthesis and supercapacitor performance of nitrogen-doped porous carbon-carbon nanotube hybrids, Beilstein J. Nanotechnol. 8 (2017) 2669–2679.
[37] S. Zhang, Y. Li, N. Pan, Graphene based supercapacitor fabricated by vacuum filtration deposition, J. Power Sources 206 (2012) 476–482.
[38] L. Xu, M. Jia, Y. Li, S. Zhang, X. Jin, Design and synthesis of graphene/activated carbon/polypyrrole flexible supercapacitor electrodes, RSC Adv. 7 (2017) 31342–31351.
[39] Y. Gao, Graphene and polymer composites for supercapacitor applications: a review, Nanoscale Res. Lett. 12 (2017) 387–404.

[40] H. Hayashi, Y. Hakuta, Hydrothermal synthesis of metal oxide nanoparticles in supercritical water, Materials 3 (2010) 3794–3817.
[41] J. Ge, J. Wu, J. Dong, J. Jia, B. Ye, S. Jiang, J. Zeng, Q. Bao, A high energy density asymmetric supercapacitor utilizing a nickel phosphate/graphene foam composite as the cathode and carbonized iron cations adsorbed onto polyaniline as the anode, Chem. Electro. Chem. 5 (2018) 1–10.
[42] S. Venkateshalu, D. Rangappa, A.N. Grace, Hydrothermal synthesis and electrochemical properties of CoS_2-reduced graphene oxide nanocomposite for supercapacitor application, Int. J. Nanosci. 17 (2018) 1760020–1760028.
[43] Poonam, K. Sharma, N. Singh, S.K. Tripathi, Characterization of nickel cobalt oxide: a potential material for supercapacitor, Mater. Res. Express (2018), https://doi.org/10.1088/2053-1591/aae9c1.
[44] H. Kennaz, A. Harat, O. Guellati, D.Y. Momodu, F. Barzegar, J.K. Dangbegnon, N. Manyala, M. Guerioune, Synthesis and electrochemical investigation of spinel cobalt ferrite magnetic nanoparticles for supercapacitor application, J. Solid State Electrochem. 22 (2018) 835–847.
[45] J.J. Li, M.C. Li, L.B. Kong, D. Wang, Y.M. Hu, W. Han, L. Kang, Advanced asymmetric supercapacitors based on $Ni_3(PO_4)_2$@GO and Fe_2O_3@GO electrodes with high specific capacitance and high energy density, RSC Adv. 5 (2015) 41721–41728.
[46] J. Erlebacher, M.J. Aziz, A. Karma, N. Dimitrov, K. Sieradzki, Evolution of nanoporosity in dealloying, Nature 410 (2001) 450–453.
[47] E. Seker, M.L. Reed, M.R. Begley, Nanoporous gold: fabrication, characterization, and applications, Materials 2 (2009) 2188–2215.
[48] J.W. Lang, L.B. Kong, W.J. Wu, Y.C. Luo, L. Kang, Facile approach to prepare loose-packed NiO nano-flakes materials for supercapacitors, Chem. Commun. 35 (2008) 4213–4215.
[49] X. Li, Q. Chen, I. McCue, J. Snyder, P. Crozier, J. Erlebacher, K. Sieradzki, Dealloying of noble-metal alloy nanoparticles, Nano Lett. 14 (2014) 2569–2577.
[50] Z. Wang, X. Zhang, Y. Zhang, M. Li, C. Qin, Z. Bakenov, Chemical dealloying synthesis of CuS nanowire-on-nanoplate network as anode materials for Li-ion batteries, Metals 8 (2018) 252.
[51] R. Wang, Y. Sui, F. Yang, J. Qi, F. Wei, Y. He, Q. Meng, Z. Sun, Synthesis of Cu_2O by oxidation-assisted dealloying method for flexible all-solid-state asymmetric supercapacitors, J. Mater. Sci.: Mater. Electron. 29 (2018) 2080–2090.
[52] Z. Wang, J. Liu, C. Qin, H. Yu, X. Xia, C. Wang, Y. Zhang, Q. Hu, W. Zhao, Dealloying of Cu-based metallic glasses in acidic solutions: products and energy storage applications, Nanomaterials 5 (2015) 697–721.
[53] Z. Lu, C. Li, J. Han, F. Zhang, P. Liu, H. Wang, Z. Wang, C. Cheng, L. Chen, A. Hirata, T. Fujita, J. Erlebacher, M. Chen, Three-dimensional bicontinuous nanoporous materials by vapor phase Dealloying, Nat. Commun. 9 (2018) 276.
[54] R. Wang, Y. Sui, S. Huang, Y. Pu, P. Cao, High-performance flexible all-solid-state asymmetric supercapacitors from nanostructured electrodes prepared by oxidation-assisted dealloying protocol, Chem. Eng. J. 331 (2018) 527–535.
[55] D. Ni, Y. Chen, X. Yang, C. Liu, K. Cai, Microwave-assisted synthesis method for rapid synthesis of tin selenide electrode material for supercapacitors, J. Alloy Compd. 737 (2018) 623–629.
[56] J. Cai, H. Niu, Z. Li, Y. Du, P. Cizek, Z. Xie, H. Xiong, T. Lin, High-performance supercapacitor electrode materials from cellulose-derived carbon nanofibers, ACS Appl. Mater. Interfaces 7 (2015) 14946–14953.
[57] H. Wang, H. Yi, X. Chen, X. Wang, Asymmetric supercapacitors based on nano-architectured nickel oxide/graphene foam and hierarchical porous nitrogen-doped carbon nanotubes with ultrahigh-rate performance, J. Mater. Chem. A 2 (2014) 3223–3230.
[58] P. Yu, X. Zhao, Z. Huang, Y. Li, Q. Zhang, Free-standing three-dimensional graphene and polyaniline nanowire arrays hybrid foams for high-performance flexible and lightweight supercapacitors, J. Mater. Chem. A 2 (2014) 14413–14420.
[59] L. Xie, G. Sun, F. Su, X. Guo, Q. Kong, X. Li, X. Huang, L. Wan, W. Song, K. Li, C. Lv, C.M. Chen, Hierarchical porous carbon microtubes derived from willow catkins for supercapacitor applications, J. Mater. Chem. A 4 (2016) 1637–1646.
[60] E. Frackowiak, F. Beguin, Carbon materials for the electrochemical storage of energy in capacitors, Carbon 39 (2001) 937–950.
[61] C. Arbizzani, M. Mastragostino, New trends in electrochemical supercapacitors, J. Power Sources 100 (2001) 164–170.
[62] E.R. Pinero, K. Kierzek, J. Machnikowski, F. Beguin, Relationship between the nanoporous texture of activated carbons and their capacitance properties in different electrolytes, Carbon 44 (2006) 2498–2507.
[63] G. Salitra, A. Soffer, L. Eliad, Y. Cohen, D. Aurbach, Carbon electrodes for double-layer capacitors I. Relations between ion and pore dimensions, J. Electrochem. Soc. 147 (2000) 2486–2493.
[64] O. Ania, V. Khomenko, E.R. Pinero, J.B. Para, F. Beguin, The large electrochemical capacitance of microporous doped carbon obtained by using a zeolite template, Adv. Funct. Mater. 17 (2007) 1828–1836.
[65] R. Kotz, M. Carleen, Principles and applications of electrochemical capacitors, Electrochim. Acta 45 (2000) 2483–2498.
[66] A.G. Pandolfo, A.F. Hollenkamp, Carbon properties and their role in supercapacitors, J. Power Sources 157 (2006) 11–27.
[67] A.S. Aricò, P. Bruce, Nanostructured materials for advanced energy conversion and storage devices, Nat. Mater. 4 (2005) 366–377.
[68] H.C. Chien, W.Y. Cheng, Y.H. Wang, S.Y. Lu, Ultrahigh specific capacitance for supercapacitors achieved by nickel cobaltite/carbon aerogel composites, Adv. Funct. Mater. 22 (2012) 5038–5043.
[69] S. Roldan, C. Blanco, M. Granda, R. Menendez, R. Santamaria, Towards a further generation of high-energy carbon-based capacitors by using redox-active electrolytes, Angew. Chem. Int. Ed. 50 (2011) 1699–1701.
[70] H. Wang, H. Wu, Y. Chang, Z. Hu, Tert-butylhydroquinone-decorated graphene nanosheets and their enhanced capacitive behaviours, Chin. Sci. Bull. 56 (2011) 2092–2097.
[71] D.M. Anjos, J.K. McDonough, E. Perre, G.M. Brown, S.H. Overbury, Y. Gogotsi, V. Presser, Pseudocapacitance and performance stability of quinone-coated carbon on ions, Nano Energy 2 (2013) 702–712.
[72] D.M. Anjos, A.I. Kolesnikov, Z. Wu, Y. Cai, M. Neurock, G.M. Brown, S.H. Overbury, Inelastic neutron scattering, Raman and DFT investigations of the adsorption of phenanthrenequinone on onion-like carbon, Carbon 52 (2013) 150–157.
[73] X. Chen, H. Wang, H. Li, X. Wang, X. Yan, Z. Guo, Anthraquinone on porous carbon nanotubes with improved supercapacitor performance, J. Phys. Chem. C 118 (2014) 8262–8270.
[74] P.G. Campbell, M.D. Merrill, B.C. Wood, E. Montalvo, M.A. Worsley, T.F. Baumann, J. Biener, Battery/supercapacitor hybrid via non-covalent functionalization of graphene macro-assemblies, J. Mater. Chem. A 2 (2014) 17764–17770.
[75] V. Presser, M. Heon, Y. Gogotsi, Carbide-derived carbons-from porous networks to nanotubes and graphene, Adv. Funct. Mater. 21 (2011) 810–833.
[76] M.F.E. -Kady, V. Strong, S. Dubin, R.B. Kaner, Laser scribing of high-performance and flexible graphene-based electrochemical capacitors, Science 335 (2012) 1326–1330.
[77] C. Liu, Z. Yu, D. Neff, A. Zhamu, B.Z. Jang, Graphene-based supercapacitor with an ultrahigh energy density, Nano Lett. 10 (2010) 4863–4868.
[78] J.R. Miller, R.A. Outlaw, B.C. Holloway, Graphene double-layer capacitor with ac line-filtering performance, Science 329 (2010) 1637–1639.
[79] M.D. Stoller, S. Park, Y. Zhu, J. An, R.S. Ruoff, Graphene-based ultracapacitors, Nano Lett. 8 (2008) 3498–3502.
[80] Y. Xu, Z. Lin, X. Huang, Y. Liu, Y. Huang, X. Duan, Flexible solid-state supercapacitors based on three-dimensional graphene hydrogel films, Nano Lett. 7 (2013) 4042–4049.
[81] Z. Wen, X. Wang, S. Mao, Z. Bo, H. Kim, S. Cui, G. Lu, X. Feng, J. Chen, Crumpled nitrogen-doped graphene nanosheets with ultrahigh pore volume for high--performance supercapacitor, Adv. Mater. 24 (2012) 5610–5616.
[82] C. Liu, Z. Yu, D. Neff, A. Zhamu, B.Z. Jang, Graphene-based supercapacitor with an ultrahigh energy density, Nano Lett. 10 (2010) 4863–4868.
[83] Z. Lei, L. Lu, X.S. Zhao, The electrocapacitive properties of graphene oxide reduced by urea, Energy Environ. Sci. 5 (2012) 6391–6399.
[84] H. Wang, D. Zhang, T. Yan, X. Wen, L. Shi, J. Zhang, Graphene prepared via a novel pyridine-thermal strategy for capacitive deionization, J. Mater. Chem. 22 (2012) 23745–23748.
[85] D. Krishnan, K. Raidongia, J. Shao, J. Huang, Graphene oxide assisted hydrothermal carbonization of carbon hydrates, ACS Nano 8 (2013) 449–457.
[86] H. Luo, Z. Liu, L. Chao, X. Wu, X. Lei, Z. Chang, X. Sun, Synthesis of hierarchical porous N-doped sandwich-type carbon composites as high-performance supercapacitor electrodes, J. Mater. Chem. A 3 (2015) 3667–3675.
[87] E. Frackowiak, K. Metenier, Supercapacitor electrodes for multiwalled carbon nanotubes, Appl. Phys. Lett. 77 (2000) 2421–2423.
[88] K.H. An, W.S. Kim, Electrochemical properties of high-power supercapacitors using single-walled carbon nanotube electrodes, Adv. Funct. Mater. 11 (2001) 387–392.
[89] X. Li, J. Rong, B. Wei, Electrochemical behavior of single-walled carbon nanotube supercapacitors under compressive stress, ACS Nano 4 (2010) 6039–6049.
[90] A.C. Dillon, Carbon nanotubes for photoconversion and electrical energy storage, Chem. Rev. 110 (2010) 6856–6872.
[91] C. Peng, J. Jin, G.Z. Chen, A comparative study on electrochemical co-deposition and capacitance of composite films of conducting polymers and carbon nanotubes, Electrochim. Acta 53 (2007) 525–537.
[92] C. Ogata, R. Kurogi, K. Hatakeyama, T. Taniguchi, M. Koinumaa, Y. Matsumoto, All-graphene oxide device with tunable supercapacitor and battery behaviour by the working voltage, Chem. Commun. 52 (2016) 3919–3922.
[93] H. Zhang, K. Wang, X. Zhang, H. Lin, X. Sun, C. Li, Y. Ma, Self-generating graphene and porous nanocarbon composites for capacitive energy storage, J. Mater. Chem. A 3 (2015) 11277–11286.
[94] G. Han, Y. Liu, L. Zhang, E. Kan, S. Zhang, J. Tang, W. Tang, MnO_2 nanorods intercalating graphene oxide/polyaniline ternary composites for robust high-performance supercapacitors, Sci. Rep. 4 (2014) 4824.
[95] C. Zhou, Y. Zhang, Y. Li, J. Liu, Construction of high-capacitance 3D CoO@polypyrrole nanowire array electrode for aqueous asymmetric supercapacitor, Nano Lett. 13 (2013) 2078–2085.
[96] P. Bober, N. Gavrilov, A. Kovalcik, M. Mičušík, C. Unterweger, I.A. Pašti, I. Šeděnková, U. Acharya, J. Pfleger, S.K. Filippov, J. Kuliček, M. Omastová, S. Breitenbach, G.Ć. Marjanović, J. Stejskal, Electrochemical properties of lignin/polypyrrole composites and their carbonized analogues, Mater. Chem. Phys. 213 (2018) 352–361.
[97] B. Senthilkumar, P. Thenamirthan, R.K. Selvan, Structural and electrochemical properties of polythiophene, Appl. Surf. Sci. 257 (2011) 9063–9067.
[98] T.S. Gaaz, A.B. Sulong, M.N. Akhtar, A.A.H. Kadhum, A.B. Mohamad, A.A. Al-Amiery, Properties and applications of polyvinyl alcohol, halloysite nanotubes and their nanocomposites, Molecules 20 (2015) 22833–22847.
[99] A. Kumar, A.C. Pandey, R. Prakash, Electro-oxidation of formic acid using polyindole-SnO2 nanocomposite, Catal. Sci. Technol. 2 (2012) 2533–2538.
[100] V.Q. Trung, D.N. Huyen, Progress in conjugated polyindoles: synthesis, polymerization mechanisms, properties, and applications, J. Phys. Conf. Ser. 187 (2009) 012058–012063.
[101] B. Rajendera, S. Palaniappan, Organic solvent soluble methyltriphenylphosphonium peroxodisulfate: a novel oxidant for the synthesis of polyaniline and the

thus prepared polyaniline in high performance supercapacitors, New J. Chem. 39 (2015) 5382–5388.
[102] D. Aradilla, F. Estrany, C. Aleman, Symmetric supercapacitors based on multilayers of conducting polymers, J. Phys. Chem. C 115 (2011) 8430–8438.
[103] W. Zheng, R. Lv, B. Na, H. Liu, T. Jin, D. Yuan, Nanocellulose-mediated hybrid polyaniline electrodes for high performance flexible supercapacitors, J. Mater. Chem. A 5 (2017) 12969–12976.
[104] H.R. Ghenaatian, M.F. Mousavi, S.H. Kazemi, M. Shamsipur, Electrochemical investigations of self-doped polyaniline nanofibers as a new electroactive material for high performance redox supercapacitor, Syn. Metal. 159 (2009) 1717–1722.
[105] R.K. Sharma, C. Rastogi, S.B. Desu, Pulse polymerized polypyrrole electrodes for high energy density electrochemical supercapacitor, Electrochem. Commun. 10 (2008) 268–272.
[106] I.H. Kim, K.B. Kim, Ruthenium oxide thin film electrodes for supercapacitors, Electrochem. Solid State Lett. 4 (2001) A62–A64.
[107] S. Farhadi, J. Safabaksh, P. Zaringhadam, Synthesis, characterization, and investigation of optical and magnetic properties of cobalt oxide (Co_3O_4) nanoparticles, J. Nanostruct. Chem. 3 (2013) 69–78.
[108] S.K. Meher, G.R. Rao, Ultralayered Co_3O_4 for high-performance supercapacitor applications, J. Phys. Chem. C 115 (2011) 15646–15654.
[109] Y. Wang, Y. Lei, J. Li, L. Gu, H. Yuan, D. Xiao, Synthesis of 3D-nanonet hollow structured Co_3O_4 for high capacity supercapacitor, ACS Appl. Mater. Interfaces 6 (2014) 6739–6747.
[110] K. Deori, S.K. Ujjain, R.K. Sharma, S. Deka, Morphology controlled synthesis of nanoporous Co_3O_4 nanostructures and their charge storage characteristics in supercapacitors, ACS Appl. Mater. Interfaces 5 (2013) 10665–10672.
[111] A.L.M. Reddy, M.M. Shaijumon, S.R. Gowda, P.M. Ajayan, Multisegmented Au-MnO_2/carbon nanotube hybrid coaxial arrays for high-power supercapacitor applications, J. Phys. Chem. C 114 (2010) 658.
[112] D.P. Dubal, A.D. Jagadale, C.D. Lokhande, Big as well as light weight portable, Mn_3O_4 based symmetric supercapacitive devices: fabrication, performance evaluation and demonstration, Electrochim. Acta 80 (2012) 160–170.
[113] X.H. Lu, X. Huang, S.L. Xie, T. Zhai, C.S. Wang, P. Zhang, M.H. Yu, W. Li, C.L. Liang, Y.X. Tong, Controllable synthesis of porous nickel-cobalt oxide nanosheets for supercapacitors, J. Mater. Chem. 22 (2012) 13357–13364.
[114] H. Xia, Y.S. Meng, G.L. Yuan, C. Cui, L. Lu, A symmetric RuO_2/RuO_2 supercapacitor operating at 1.6 V by using a neutral aqueous electrolyte, Electrochem. Solid-State Lett. 15 (2012) A60–A63.
[115] K. Juodkazis, J. Juodkazyte, V. Sukiene, A. Griguceviciene, A. Selskis, On the charge storage mechanism at RuO_2/0.5 M H_2SO_4 interface, J. Solid State Electrochem. 12 (2008) 1399–1404.
[116] R.K. Das, B. Liu, J.R. Reynolds, A.G. Rinzler, Engineered macroporosity in single-wall carbon nanotube films, Nano Lett. 9 (2009) 677–683.
[117] W. Wang, S. Guo, C.S. Ozkan, Hydrous ruthenium oxide nanoparticles anchored to graphene and carbon nanotube hybrid foam for supercapacitors, Sci. Rep. 4 (2014) 4452.
[118] C.C. Hu, K.H. Chang, M.C. Lin, Y.T. Wu, Design and tailoring of the nanotubular arrayed architecture of hydrous RuO_2 for next generation supercapacitors, Nano Lett. 6 (2006) 2690–2695.
[119] J.T. Zhang, J.Z. Ma, L.L. Zhang, P.Z. Guo, J.W. Jiang, X.S. Zhao, Template synthesis of tubular ruthenium oxides for supercapacitor applications, J. Phys. Chem. C 114 (2010) 13608–13613.
[120] X. Wang, J. Hu, W. Liu, G. Wang, J. An, J. Lian, Ni-Zn binary system hydroxide, oxide and sulfide materials: synthesis and high supercapacitor performance, J. Mater. Chem. A 3 (2015) 23333–23344.
[121] S. Patil, S. Raut, R. Gorea, B. Sankapal, One-dimensional cadmium hydroxide nanowires towards electrochemical supercapacitor, New J. Chem. 39 (2015) 9124–9131.
[122] X. Rui, Z. Lu, Z. Yin, D.H. Sim, N. Xiao, T.M. Lim, H.H. Hng, H. Zhang, Q. Yan, Oriented molecular attachments through sol-gel chemistry for synthesis of ultrathin hydrated vanadium pentoxide nanosheets and their applications, Small 9 (2013) 716–721.
[123] J. Zhu, L. Cao, Y. Wu, Y. Gong, Z. Liu, H.E. Hoster, Y. Zhang, S. Zhang, S. Yang, Q. Yan, P.M. Ajayan, R. Vajtai, Building 3D structures of vanadium pentoxide nanosheets and application as electrodes in supercapacitors, Nano Lett. 13 (2013) 5408–5413.
[124] D.H. Nagaraju, Q. Wang, P. Beaujuge, H.N. Alshareef, Two-dimensional heterostructures of $V2O_5$ and reduced graphene oxide as electrodes for high energy density asymmetric supercapacitors, J. Mater. Chem. A 2 (2014) 17146–17152.
[125] Q. Qu, Y. Zhu, X. Gao, Y. Wu, Core-shell structure of polypyrrole grown on $V2O_5$ nanoribbon as high performance anode material for supercapacitors, Adv. Energy Mater. 2 (2012) 950–955.
[126] Q.T. Qu, Y. Shi, L.L. Li, W.L. Guo, Y.P. Wu, H.P. Zhang, S.Y. Guan, R. Holze, $V_2O_5{\cdot}0.6H_2O$ nanoribbons as cathode material for asymmetric supercapacitor in K_2SO_4 solution, Electrochem. Commun. 11 (2009) 1325–1328.
[127] S.D. Perera, M. Rudolph, R.G. Mariano, N. Nijem, J.P. Ferraris, Y.J. Chabal, K.J. Balkus, Manganese oxide nanorod-graphene/vanadium oxide nanowire-graphene binder-free paper electrodes for metal oxide hybrid supercapacitors, Nano Energy 2 (2013) 966–975.
[128] B.S. Kumar, K.K. Purushothamanb, G. Muralidharan, MnO_2 grafted V_2O_5 nanostructures: formation mechanism, morphology and supercapacitive features, Cryst. Eng. Comm. 16 (2014) 10711–10720.
[129] T.Y. Wei, C.H. Chen, H.C. Chien, S.Y. Lu, C.C. Hu, A cost-effective supercapacitor material of ultrahigh specific capacitances: spinel nickel cobaltite aerogels from an epoxide-driven sol-gel process, Adv. Mater. 22 (2010) 347–351.
[130] H.C. Chen, J.J. Jiang, L. Zhang, T. Qi, D.D. Xia, H.Z. Wan, Facilely synthesized porous $NiCo_2O_4$ flowerlike nanostructure for high-rate supercapacitors, J. Power Sources 248 (2014) 28–36.
[131] H. Wang, Q. Gao, L. Jiang, Facile approach to prepare nickel cobaltite nanowire materials for supercapacitors, Small 7 (2011) 2454–2459.
[132] H. Chen, L. Hu, M. Chen, Y. Yan, L. Wu, Nickel-cobalt layered double hydroxide nanosheets for high-performance supercapacitor electrode materials, Adv. Funct. Mater. 24 (2014) 934–942.
[133] H.C. Chen, J.J. Jiang, L. Zhang, Y.D. Zhao, D.Q. Guo, Y.J. Ruan, D.D. Xia, High-stable α-phase NiCo double hydroxide microspheres via microwave synthesis for supercapacitor electrode materials, Chem. Plus Chem. 80 (2015) 181–187.
[134] Y. Bai, W. Wang, R. Wang, J. Sun, L. Gao, Controllable synthesis of 3D binary nickel-cobalt hydroxide/graphene/nickel foam as a binder-free electrode for high-performance supercapacitors, J. Mater. Chem. A 3 (2015) 12530–12538.
[135] X. Wang, B. Liu, Q. Wang, W. Song, X. Hou, D. Chen, Y.B. Cheng, G. Shen, Three-dimensional hierarchical $GeSe_2$ nanostructures for high performance flexible all-solid-state supercapacitors, Adv. Mater. 25 (2013) 1479–1486.
[136] C. Zhang, H. Yin, M. Han, Z. Dai, H. Pang, Y. Zheng, Y.Q. Lan, J. Bao, J. Zhu, Two-dimensional tin selenide nanostructures for flexible all-solid-state supercapacitors, ACS Nano 8 (2014) 3761–3770.
[137] H. Chen, S. Chen, M. Fan, C. Li, D. Chen, G. Tian, K. Shu, Bimetallic nickel cobalt selenides: a new kind of electroactive material for high-power energy storage, J. Mater. Chem. A 3 (2015) 23653–23659.
[138] S. Wang, S. Sun, S. Li, F. Gong, Y. Li, Q. Wu, P. Song, S. Fang, P. Wang, Time and temperature dependent multiple hierarchical $NiCo_2O_4$ for high-performance supercapacitors, Dalton Trans. 45 (2016) 7469–7475.
[139] W. Ma, H. Nan, Z. Gu, B. Geng, X. Zhang, Superior performance asymmetric supercapacitors based on $ZnCo_2O_4$@MnO_2 core-shell electrode, J. Mater. Chem. A 3 (2015) 5442–5448.
[140] J. Yang, L. Lian, P. Xiong, M. Wei, Pseudo-capacitive performance of titanate nanotubes as a supercapacitor electrode, Chem. Commun. 50 (2014) 5973–5975.
[141] D.S. Kong, J.M. Wang, H.B. Shao, J.Q. Zhang, C.N. Cao, Electrochemical fabrication of a porous nanostructured nickel hydroxide film electrode with superior pseudocapacitive performance, J. Alloys Compd. 509 (2011) 5611–5616.
[142] S. Nandy, U.N. Maiti, C.K. Ghosh, K.K. Chattopadhyay, Enhanced p-type conductivity and band gap narrowing in heavily Al doped NiO thin films deposited by RF magnetron sputtering, J. Phys. Condens. Matter 21 (2009) 115804–115811.
[143] M. Toupin, D. Belanger, Charge storage mechanism of MnO_2 electrode used in aqueous electrochemical capacitor, Chem. Mater. 16 (2004) 3184–3190.
[144] D. Belanger, T. Brousse, J.W. Long, Manganese oxides: battery materials make the leap to electrochemical capacitors, Electrochem. Soc. Interface 17 (2008) 49–52.
[145] W. Pan, J.H. Gong, Nanostructured carbon metal oxide composite electrodes for supercapacitors: a review, Key Eng. Mater. 336 (2007) 2134–2137.
[146] R.B. Rakhi, W. Chen, D.K. Cha, H.N. Alshareef, Substrate dependent self-organization of mesoporous cobalt oxide nanowires with remarkable pseudocapacitance, Nano Lett. 12 (2012) 2559–2567.
[147] C.Z. Yuan, L. Yang, L.R. Hou, L.F. Shen, X.G. Zhang, X.W. Lou, Growth of ultrathin mesoporous Co_3O_4 nanosheet arrays on Ni foam for high-performance electrochemical capacitors, Energy Environ. Sci. 5 (2012) 7883–7887.
[148] Mohamed Hamdani, R.N. Singh, P. Chartier, Co_3O_4 and Co-based spinel oxides bifunctional oxygen electrodes, Int. J. Electrochem. Sci. 5 (2010) 556–577.
[149] C.C. Hu, W.C. Chen, K.H. Chang, How to achieve maximum utilization of hydrous ruthenium oxide for supercapacitors, J. Electrochem. Soc. 151 (2004) A281–A290.
[150] A. Adeyemo, G. Hunter, P.K. Dutt, Interaction of CO with hydrous ruthenium oxide and development of a chemoresistive ambient CO sensor, Sens. Actuators B 152 (2011) 307–315.
[151] M. Mastragostino, C. Arbizzani, Conducting polymers as electrode materials in supercapacitors, Solid State Ion. 148 (2002) 493–498.
[152] S. Zeng, H. Chen, F. Cai, Y. Kang, M. Chen, Q. Li, Electrochemical fabrication of carbon nanotube/polyaniline hydrogel film for all-solid-state flexible supercapacitor with high areal capacitance, J. Mater. Chem. A 3 (2015) 23864–23870.
[153] Jaidev, S. Ramaprabhu, Poly(p-phenylenediamine)/graphene nanocomposites for supercapacitor applications, J. Mater. Chem. 22 (2012) 18775–18783.
[154] Y. Li, X. Zhao, P. Yu, Q. Zhang, Oriented arrays of polyaniline nanorods grown on graphite nanosheets for an electrochemical supercapacitor, Langmuir 29 (2012) 493–500.
[155] X. Zhao, Q. Zhang, D. Chen, Alternate multilayer films of poly(vinyl alcohol) and exfoliated graphene oxide fabricated via a facial layer-by-layer assembly, Macromolecules 43 (2010) 9411–9416.
[156] P. Yu, Y. Li, X. Yu, X. Zhao, L. Wu, Q. Zhang, Polyaniline nanowire arrays aligned on nitrogen-doped carbon fabric for high-performance flexible supercapacitors, Langmuir 29 (2013) 12051–12058.
[157] R. Wang, M. Han, Q. Zhao, Z. Ren, X. Guo, X. Xu, N. Hu, L. Lu, Hydrothermal synthesis of nanostructured graphene/polyaniline composites as high-capacitance electrode materials for supercapacitors, Sci. Rep. 7 (2017) 44562.
[158] L. Mao, K. Zhang, H.S.O. Chan, J. Wu, Surfactant-stabilized graphene/polyaniline nanofiber composites for high performance supercapacitor electrode, J. Mater. Chem. 22 (2012) 80–85.
[159] D. Antiohos, G. Folkes, P. Sherrell, S. Ashraf, G.G. Wallace, P. Aitchison, A.T. Harris, J. Chen, A.I. Minett, Compositional effects of PEDOT-PSS/single walled carbon nanotube films on supercapacitor device performance, J. Mater. Chem. 21 (2011) 15987–15994.
[160] E. Frackowiak, V. Khomenko, K. Jurewicz, K. Lota, F. Béguin, Supercapacitors based on conducting polymers/nanotubes composites, J. Power Sources 153 (2006) 413–418.
[161] Y. Han, B. Ding, H. Tong, X. Zhang, Capacitance properties of graphite oxide/poly (3,4-ethylene dioxythiophene) composites, J. Appl. Polym. Sci. 121 (2011)

892–898.
[162] J. Keskinen, S. Tuurala, M. Sjödin, K. Kiri, L. Nyholm, T. Flyktman, M. Strømme, M. Smolander, Asymmetric and symmetric supercapacitors based on polypyrrole and activated carbon electrodes, Syn. Metal. 203 (2015) 192–199.
[163] Y. Yang, Y. Xi, J. Li, G. Wei, N.I. Klyui, W. Han, Flexible supercapacitors based on polyaniline arrays coated graphene aerogel electrodes, Nanoscale Res. Lett. 12 (2017) 394.
[164] C. Xiang, M. Li, M. Zhi, A. Manivannan, N. Wu, A reduced graphene oxide/Co_3O_4 composite for supercapacitor electrode, J. Power Sources 226 (2013) 65–70.
[165] G. He, J. Li, H. Chen, J. Shi, X. Sun, S. Chen, X. Wang, Hydrothermal preparation of Co_3O_4@graphene nanocomposite for supercapacitor with enhanced capacitive performance, Mater. Lett. 82 (2012) 61–63.
[166] Y. Shan, L. Gao, Formation and characterization of multi-walled carbon nanotubes/Co_3O_4 nanocomposites for supercapacitors, Mater. Chem. Phys. 103 (2007) 206–210.
[167] S. Abouali, M.A. Garakani, B. Zhang, Z.L. Xu, E.K. Heidari, J.Q. Huang, J. Huang, J.K. Kim, Electrospun carbon nanofibers with in situ encapsulated Co_3O_4 nanoparticles as electrodes for high-performance supercapacitors, ACS Appl. Mater. Interfaces 7 (2015) 13503–13511.
[168] L. Li, R. Li, S. Gai, P. Gao, F. He, M. Zhang, Y. Chen, P. Yang, Hierarchical porous CNTs@NCS@MnO_2 composites: rational design and high asymmetric supercapacitor performance, J. Mater. Chem. A 3 (2015) 15642–15649.
[169] S.D. Perera, B. Patel, N. Nijem, K. Roodenko, O. Seitz, J.P. Ferraris, Y.J. Chabal, K.J. Balkus, Vanadium oxide nanowire-carbon nanotube binder-free flexible electrodes for supercapacitors, Adv. Energy Mater. 1 (2011) 936–945.
[170] G. Zhang, X.W. Lou, General solution growth of mesoporous $NiCo_2O_4$ nanosheets on various conductive substrates as high-performance electrodes for supercapacitors, Adv. Mater. 25 (2013) 976–979.
[171] G.Q. Zhang, H.B. Wu, H.E. Hoster, M.B. Chan-Park, X.W. Lou, Single-crystalline $NiCo_2O_4$ nanoneedle arrays grown on conductive substrates as binder-free electrodes for high-performance supercapacitors, Energy Environ. Sci. 5 (2012) 9453–9456.
[172] C.Z. Yuan, J.Y. Li, L.R. Hou, L. Yang, L.F. Shen, X.G. Zhang, Facile template-free synthesis of ultralayered mesoporous nickel cobaltite nanowires towards high-performance electrochemical capacitors, J. Mater. Chem. 22 (2012) 16084–16090.
[173] H.B. Wu, H. Pang, X.W. Lou, Facile synthesis of mesoporous $Ni_{0.3}Co_{2.7}$ O_4 hierarchical structures for high-performance supercapacitors, Energy Environ. Sci. 6 (2013) 3619–3626.
[174] X. Wang, X.D. Han, M. Lim, N. Singh, C.L. Gan, M. Jan, P.S. Lee, Nickel cobalt oxide-single wall carbon nanotube composite material for superior cycling stability and high-performance supercapacitor application, J. Phys. Chem. C 116 (2012) 12448–12454.
[175] D. Carriazo, J. Patino, M.C. Gutierrez, M.L. Ferrer, F.D. Monte, Microwave-assisted synthesis of $NiCo_2O_4$-graphene oxide nanocomposites suitable as electrodes for supercapacitors, RSC Adv. 3 (2013) 13690–13695.
[176] C. Yuan, J. Li, L. Hou, X. Zhang, L. Shen, X.W. Lou, Ultrathin mesoporous $NiCo_2O_4$ nanosheets supported on Ni foam as advanced electrodes for supercapacitors, Adv. Funct. Mater. 22 (2012) 4592–4597.
[177] M. Zhi, C. Xiang, J. Li, M. Li, N. Wu, Nanostructured carbon-metal oxide composite electrodes for supercapacitors: a review, Nanoscale 5 (2013) 72–88.
[178] H. Wan, J. Jiang, J. Yu, K. Xu, L. Miao, L. Zhang, H. Chen, Y. Ruan, $NiCo_2S_4$ porous nanotubes synthesis via sacrificial templates: high-performance electrode materials of supercapacitors, Cryst. Eng. Comm. 15 (2013) 7649–7651.
[179] H. Chen, J. Jiang, L. Zhang, H. Wan, T. Qi, D. Xia, Highly conductive $NiCo_2S_4$ urchin-like nanostructures for high-rate pseudocapacitors, Nanoscale 5 (2013) 8879–8883.
[180] S. Peng, L. Li, C. Li, H. Tan, R. Cai, H. Yu, S. Mhaisalkar, M. Srinivasan, S. Ramakrishna, Q. Yan, In situ growth of $NiCo_2S_4$ nanosheets on graphene for high-performance supercapacitors, Chem.Commun. 49 (2013) 10178–10180.
[181] G. Xiong, P. He, L. Liu, T. Chen, T.S. Fisher, Plasma-grown graphene petals templating Ni-Co-Mn hydroxide nanoneedles for high-rate and long-cycle-life pseudocapacitive electrodes, J. Mater. Chem. A 3 (2015) 22940–22948.
[182] S. Ratha, S.R. Marri, N.A. Lanzillo, S. Moshkalev, S.K. Nayak, J.N. Behera, C.S. Rout, Supercapacitors based on patronite-reduced graphene oxide hybrids: experimental and theoretical insights, J. Mater. Chem. A 3 (2015) 18874–18881.
[183] K. Lu, D. Li, X. Gao, H. Dai, N. Wang, H. Ma, An advanced aqueous sodium-ion supercapacitor with a manganous hexacyanoferrate cathode and a $Fe3O_4$/rGO anode, J. Mater. Chem. A 3 (2015) 16013–16019.
[184] Q. Guan, J. Cheng, B. Wang, W. Ni, G. Gu, X. Li, L. Huang, G. Yang, F. Nie, Needle-like Co_3O_4 anchored on the graphene with enhanced electrochemical performance for aqueous supercapacitors, ACS Appl. Mater. Interfaces 6 (2014) 7626–7632.
[185] B. Liu, L. Jin, H. Zheng, H. Yao, Y. Wu, A. Lopes, J. He, Ultrafine Co-based nanoparticle@mesoporous carbon nanospheres toward high-performance supercapacitors, ACS Appl. Mater. Interfaces 9 (2017) 1746–1758.
[186] S. Wu, K.S. Hui, K.N. Hui, K.H. Kim, Electrostatic-induced assembly of graphene-encapsulated carbon@nickel-aluminum layered double hydroxide core-shell spheres hybrid structure for high-energy and high-power-density asymmetric supercapacitor, ACS Appl. Mater. Interfaces 9 (2017) 1395–1406.
[187] S. Sahoo, J.J. Shim, Facile synthesis of three-dimensional ternary $ZnCo_2O_4$/reduced graphene oxide/NiO composite film on nickel foam for next generation supercapacitor electrodes, ACS Sustainable Chem. Eng. 5 (2017) 241–251.
[188] H. Chen, T.N. Cong, W. Yang, C. Tan, Y. Li, Y. Ding, Progress in electrical energy storage system: a critical review, Prog. Nat. Sci. 19 (2009) 291–312.
[189] K. Xie, B. Wei, Materials and structures for stretchable energy storage and conversion devices, Adv. Mater. 26 (2014) 3592–3617.
[190] Y. Liu, B. Zhang, Y. Yang, Z. Chang, Z. Wen, Y. Wu, Polypyrrole-coated α-MoO_3 nanobelts with good electrochemical performance as anode materials for aqueous supercapacitors, J. Mater. Chem. A 1 (2013) 13582–13587.
[191] R.P. Raj, P. Ragupathy, S. Mohan, Remarkable capacitive behavior of a $Co3O_4$-polyindole composite as electrode material for supercapacitor applications, J. Mater. Chem. A 3 (2015) 24338–24348.
[192] X. Lang, A. Hirata, T. Fujita, M. Chen, Nanoporous metal/oxide hybrid electrodes for electrochemical supercapacitors, Nat. Nanotechnol. 6 (2011) 232–236.
[193] G.Q. Zhang, H.B. Wu, H.E. Hoster, M.B. Chan-Park, X.W.D. Lou, Single-crystalline $NiCo_2O_4$ nanoneedle arrays grown on conductive substrates as binder-free electrodes for high-performance supercapacitors, Energy Environ. Sci. 5 (2012) 9453–9456.
[194] Z. Yu, J. Thomas, Energy storing electrical cables: integrating energy storage and electrical conduction, Adv. Mater. 26 (2014) 4279–4285.
[195] Y.M. Wang, X. Zhang, C.Y. Guo, Y.Q. Zhao, C.L. Xu, H.L. Li, Controllable synthesis of 3D $Ni_{\chi}Co_{1-\chi}$ oxides with different morphologies for high-capacity supercapacitors, J. Mater. Chem. A 1 (2013) 13290–13300.
[196] M.J. Deng, P.J. Ho, C.Z. Song, S.A. Chen, J.F. Lee, J.M. Chen, K.T. Lu, Fabrication of Mn/Mn oxide core-shell electrodes with three-dimensionally ordered macroporous structures for high-capacitance supercapacitors, Energy Environ. Sci. 6 (2013) 2178–2185.
[197] F. Du, D. Yu, L. Dai, S. Ganguli, V. Varshney, A.K. Roy, Preparation of tunable 3D pillared carbon nanotube-graphene networks for high-performance capacitance, Chem. Mater. 23 (2011) 4810–4816.
[198] X. Ma, J. Liu, C. Liang, X. Gong, R. Che, A facile phase transformation method for the preparation of 3D flower-like β-Ni(OH)2/GO/CNTs composite with excellent supercapacitor performance, J. Mater. Chem. A 2 (2014) 12692–12696.
[199] H. Chen, S. Zhou, L. Wu, Porous nickel hydroxide-manganese dioxide-reduced graphene oxide ternary hybrid spheres as excellent supercapacitor electrode materials, ACS Appl. Mater. Interfaces 6 (2014) 8621–8630.
[200] S. Min, C. Zhao, Z. Zhang, G. Chen, X. Qiana, Z. Guo, Synthesis of $Ni(OH)_2$/RGO pseudocomposite on nickel foam for supercapacitors with superior performance, J. Mater. Chem. A 3 (2015) 3641–3650.
[201] L.Y. Chen, Y. Hou, J.L. Kang, A. Hirata, M.W. Chen, Asymmetric metal oxide pseudocapacitors advanced by three-dimensional nanoporous metal electrodes, J. Mater. Chem. A 2 (2014) 8448–8455.
[202] J. Luo, J. Liu, Z. Zeng, C.F. Ng, L. Ma, H. Zhang, J. Lin, Z. Shen, H.J. Fan, Three-dimensional graphene foam supported Fe_3O_4 lithium battery anodes with long cycle life and high rate capability, Nano Lett. 13 (2013) 6136–6143.
[203] X. Sun, Z. Jiang, C. Li, Y. Jiang, X. Sun, X. Tian, L. Luo, X. Hao, Z.J. Jiang, Facile synthesis of Co_3O_4 with different morphologies loaded on amine modified graphene and their application in supercapacitors, J. Alloys Compd. 685 (2016) 507–517.
[204] M. Lia, J.P. Cheng, J. Wang, F. Liu, X.B. Zhang, The growth of nickel-manganese and cobalt-manganese layered double hydroxides on reduced graphene oxide for supercapacitor, Electrochim. Acta 206 (2016) 108–115.
[205] J. Xu, C. Yang, Y. Xue, C. Wang, J. Cao, Z. Chen, Facile synthesis of novel metal-organic nickel hydroxide nanorods for high performance supercapacitor, Electrochim. Acta 211 (2016) 595–602.
[206] X. Mu, Y. Zhang, H. Wang, B. Huang, P. Sun, T. Chen, J. Zhou, E. Xie, Z. Zhang, A high Ed asymmetric supercapacitor from ultrathin manganese molybdate nanosheets, Electrochim. Acta 212 (2016) 217–224.
[207] Y. Chang, Y.W. Sui, J.Q. Qi, L.Y. Jiang, Y.Z. He, F.X. Wei, Q.K. Meng, Hierarchical Ni_3S_2 nanosheets coated on mesoporous $NiCo_2O_4$ nanoneedle arrays as high-performance electrode for supercapacitor, Mater. Lett. 176 (2016) 274–277.
[208] M. Pal, R. Rakshit, A.K. Singh, K. Mandal, Ultra high supercapacitance of ultra small Co_3O_4 nanocubes, Energy 103 (2016) 481–486.
[209] W. Yong-gang, Z. Xiao-gang, Preparation and electrochemical capacitance of RuO_2/TiO_2nanotubes composites, Electrochim. Acta 49 (2004) 1957–1962.
[210] M. Xie, Z. Xu, S. Duan, Z. Tian, Y. Zhang, K. Xiang, M. Lin, X. Guo, W. Ding, Facile growth of homogeneous $Ni(OH)_2$ coating on carbon nanosheets for high-performance asymmetric supercapacitor applications, Nano Res. 11 (2018) 216–224.
[211] L. Qiu, X. Yang, X. Gou, W. Yang, Z.-F. Ma, G.G. Wallace, D. Li, Dispersing carbon nanotubes with graphene oxide in water and synergistic effects between graphene derivatives, Chem. Eur. J. 16 (2010) 106593–110658.
[212] Y. Wang, J. Chen, J. Cao, Y. Liu, Y. Zhou, J.H. Ouyang, D. Jia, Graphene/carbon black hybrid film for flexible and high rate performance supercapacitor, J. Power Sources 271 (2014) 269–277.
[213] X. Yang, J. Zhu, L. Qiu, D. Li, Bioinspired effective prevention of restacking in multilayered graphene films: towards the next generation of high-performance supercapacitors, Adv. Mater. 23 (2011) 2833–2838.
[214] B.G. Choi, J. Hong, W.H. Hong, P.T. Hammond, H. Park, Facilitated ion transport in all-solid-state flexible supercapacitors, ACS Nano 5 (2011) 7205–7213.
[215] C.M. Chen, Q. Zhang, C.H. Huang, X.C. Zhao, B.S. Zhang, Q.Q. Kong, M.Z. Wang, Y.G. Yang, R. Cai, D.S. Su, Macroporous 'bubble' graphene film via template-directed ordered-assembly for high rate supercapacitors, Chem. Commun. 48 (2012) 7149–7151.
[216] D.W. Wang, F. Li, J. Zhao, W. Ren, Z.G. Chen, J. Tan, Z.S. Wu, I. Gentle, G.Q. Lu, H.M. Cheng, Fabrication of graphene/polyaniline composite paper via in situ anodic electropolymerization for high-performance flexible electrode, ACS Nano 3 (2009) 1745–1752.
[217] X. Yan, J. Chen, J. Yang, Q. Xue, P. Miele, Fabrication of free-standing, electrochemically active, and biocompatible graphene oxide-polyaniline and graphene-polyaniline hybrid papers, ACS Appl. Mater. Interfaces 2 (2010) 2521–2529.
[218] X. Cao, Y. Shi, W. Shi, G. Lu, X. Huang, Q. Yan, Q. Zhang, H. Zhang, Preparation of novel 3D graphene networks for supercapacitor applications, Small 7 (2011) 3163–3168.

[219] Y. Cheng, S. Lu, H. Zhang, C.V. Varanasi, J. Liu, Synergistic effects from graphene and carbon nanotubes enable flexible and robust electrodes for high-performance supercapacitors, Nano Lett. 12 (2012) 4206–4211.
[220] B.G. Choi, M. Yang, W.H. Hong, J.W. Choi, Y.S. Huh, 3D Macroporous graphene frameworks for supercapacitors with high energy and power densities, ACS Nano 6 (2012) 4020–4028.
[221] A. Davies, P. Audette, B. Farrow, F. Hassan, Z. Chen, J.Y. Choi, A. Yu, Graphene-based flexible supercapacitors: pulse-electropolymerization of polypyrrole on free-standing graphene films, J. Phys. Chem. C 115 (2011) 17612–17620.
[222] Y. Xu, Z. Lin, X. Huang, Y. Wang, Y. Huang, X. Duan, Functionalized graphene hydrogel-based high-performance supercapacitors, Adv. Mater. 25 (2013) 5779–5784.
[223] Z.S. Wu, A. Winter, L. Chen, Y. Sun, A. Turchanin, X. Feng, K. Mullen, Three-dimensional nitrogen and boron co-doped graphene for high-performance all-solid-state supercapacitors, Adv. Mater. 24 (2012) 5130–5135.
[224] Y. Wang, X. Yang, L. Qiu, D. Li, Revisiting the capacitance of polyaniline by using graphene hydrogel films as a substrate: the importance of nano-architecturing, Energy Environ. Sci. 6 (2013) 477–481.
[225] H.P. Cong, X.C. Ren, P. Wang, S.H. Yu, Flexible graphene-polyaniline composite paper for high-performance supercapacitor, Energy Environ. Sci. 6 (2013) 1185–1191.
[226] Y. He, W. Chen, X. Li, Z. Zhang, J. Fu, C. Zhao, E. Xie, Freestanding three-dimensional graphene/MnO_2 composite networks as ultralight and flexible supercapacitor electrodes, ACS Nano 7 (2012) 174–182.
[227] G. Yu, L. Hu, M. Vosgueritchian, H. Wang, X. Xie, J.R. McDonough, X. Cui, Y. Cui, Z. Bao, Solution-processed graphene/MnO_2 nanostructured textiles for high-performance electrochemical capacitors, Nano Lett. 11 (2011) 2905–2911.
[228] X. Dong, L. Wang, D. Wang, C. Li, J. Jin, Layer-by-layer engineered Co-Al hydroxide nanosheets/graphene multilayer films as flexible electrode for supercapacitor, Langmuir 28 (2011) 293–298.
[229] J. Ge, H.B. Yao, W. Hu, X.F. Yu, Y.X. Yan, L.B. Mao, H.H. Li, S.S. Li, S.H. Yu, Facile dip coating processed graphene/MnO_2nanostructured sponges as high performance supercapacitor electrodes, Nano Energy 2 (2013) 505–513.
[230] Y.Y. Horng, Y.C. Lu, Y.K. Hsu, C.C. Chen, L.C. Chen, K.H. Chen, Flexible supercapacitor based on polyaniline nanowires/carbon cloth with both high gravimetric and area-normalized capacitance, J. Power Sources 195 (2010) 4418–4422.
[231] K. Wang, W. Zou, B. Quan, A. Yu, H. Wu, P. Jiang, Z. Wei, An all-solid-state flexible micro-supercapacitor on a chip, Adv. Energy Mater. 1 (2011) 1068–1072.
[232] L. Bao, J. Zang, X. Li, Flexible Zn_2SnO_4/MnO_2 core/shell nanocable-carbon microfiber hybrid composites for high-performance supercapacitor electrodes, Nano Lett. 11 (2011) 1215–1220.
[233] X. Yan, Z. Tai, J. Chen, Q. Xue, Fabrication of carbon nanofiber-polyaniline composite flexible paper for supercapacitor, Nanoscale 3 (2011) 212–216.
[234] J. Xie, X. Sun, N. Zhang, K. Xu, M. Zhou, Y. Xie, Layer-by-layer β-$Ni(OH)_2$/graphene nanohybrids for ultraflexible all-solid-state thin-film Supercapacitors with high electrochemical performance, Nano Energy 2 (2013) 65–74.
[235] W. Xiong, X. Hu, X. Wu, Y. Zeng, B. Wang, G. Hea, Z. Zhu, A flexible fiber-shaped supercapacitor utilizing hierarchical $NiCo_2O_4$@polypyrrole core-shell nanowires on hemp-derived carbon, J. Mater. Chem. A 3 (2015) 17209–17216.
[236] C. Ranaveera, Z. Wang, E. Alqurashi, P.K. Kahol, P. Dvornic, B.K. Gupta, K. Ramasamy, A.D. Mohite, G. Gupta, R.K. Gupta, Highly stable hollow bifunctional cobalt sulfides for flexible supercapacitor and hydrogen evolution, J. Mater. Chem. A 00 (2016) 1–3.
[237] M. Rajkumar, C.–T. Hsu, T.–H. Wu, M.–G. Chen, C.–C. Hu, Advanced materials for aqueous supercapacitors in the asymmetric design, Proc. Nat. Sci.-Mater. 25 (2015) 527–544.
[238] J. Lin, H. Liang, H. Jia, S. Chen, J. Guo, J. Qi, C. Qu, J. Cao, W. Fei, J. Feng, In situ encapsulated Fe_3O_4 nanosheet arrays with Graphene layers as an anode for high-performance asymmetric supercapacitors, J. Mater. Chem. A 5 (2017) 24594–24601.
[239] J. Li, J. Guo, X. Zhang, Y. Huang, L. Guo, Asymmetric supercapacitors with high energy and power density fabricated using $LiMn_2O_4$ nano-rods and activated carbon electrodes, Int. J. Electrochem. Sci. 12 (2017) 1157–1166.
[240] H.Q. Wang, Z.S. Li, Y.G. Huang, Q.Y. Li, X.Y. Wang, A novel hybrid supercapacitor based on spherical activated carbon and spherical MnO_2 in a non-aqueous electrolyte, J. Mater. Chem. 20 (2010) 3883–3889.
[241] M. Kim, J. Kim, Development of high power and Ed microsphere silicon carbide-MnO_2 nanoneedles and thermally oxidized activated carbon asymmetric electrochemical supercapacitors, Phys. Chem. Chem. Phys. 16 (2014) 11323–11336.
[242] Z.S. Wu, W. Ren, D.W. Wang, F. Li, B. Liu, H.M. Cheng, High-energy MnO_2 nanowire/graphene and graphene asymmetric electrochemical capacitors, ACS Nano 4 (2010) 5835–5842.
[243] Y. Zhu, Z. Wu, M. Jing, H. Hou, Y. Yang, Y. Zhang, X. Yang, W. Song, X. Jia, X. Ji, Porous $NiCo_2O_4$ spheres tuned through carbon quantum dots utilized as advanced materials for an asymmetric supercapacitor, J. Mater. Chem. A 3 (2015) 866–877.
[244] H. Khani, D. Wipf, Iron oxide nanosheets and pulse-electrodeposited Ni-Co-S nanoflake arrays for high-performance charge storage, ACS Appl. Mater. Interfaces 9 (2017) 6967–6978.
[245] Y. Xie, F. Song, C. Xia, H. Du, Preparation of carbon-coated lithium iron phosphate/titanium nitride for a lithium-ion supercapacitor, New J. Chem. 39 (2015) 604–613.
[246] Y. Jin, H. Chen, M. Chen, N. Liu, Q. Li, Graphene-patched CNT/MnO_2 nanocomposite papers for the electrode of high-performance flexible asymmetric supercapacitors, ACS Appl. Mater. Interfaces 5 (2013) 3408–3416.
[247] B.G. Choi, M.H. Yang, W.H. Hong, J.W. Choi, Y.S. Huh, 3D macroporous graphene frameworks for supercapacitors with high energy and power densities, ACS Nano 6 (2012) 4020–4028.
[248] N. Phattharasupakun, J. Wutthiprom, P. Chiochan, P. Suktha, M. Suksomboon, S. Kalasina, M. Sawangphruk, Turning conductive carbon nanospheres into nanosheets for high-performance supercapacitors of MnO_2 nanorods, Chem. Commun. 52 (2016) 2585–2588.
[249] F. Li, H. Chen, X.Y. Liu, S.J. Zhu, J.Q. Jia, C.H. Xu, F. Dong, Z.Q. Wend, Y.X. Zhang, Low-cost high-performance asymmetric supercapacitors based on Co_2AlO_4@MnO_2 nanosheets and Fe_3O_4 nanoflakes, J. Mater. Chem. A 4 (2016) 2096–2104.
[250] D.W. Wang, F. Li, H.M. Cheng, Hierarchical porous nickel oxide and carbon as electrode materials for asymmetric supercapacitor, J. Power Sources 185 (2008) 1563–1568.
[251] H.B. Li, M.H. Yu, F.X. Wang, P. Liu, Y. Liang, J. Xiao, C.X. Wang, Y.X. Tong, G.W. Yang, Amorphous nickel hydroxide nanospheres with ultrahigh capacitance and energy density as electrochemical pseudocapacitor materials, Nat. Commun. 4 (2013) 1894–1901.
[252] X. Wang, W.S. Liu, X.H. Lu, P.S. Lee, Dodecyl sulfate-induced fast faradic process in nickel cobalt oxide-reduced graphite oxide composite material and its application for asymmetric supercapacitor device, J. Mater. Chem. 22 (2012) 23114–23119.
[253] C.H. Tang, Z. Tang, H. Gong, Hierarchically porous Ni-Co oxide for high reversibility asymmetric full-cell supercapacitors, J. Electrochem. Soc. 159 (2012) A651–A656.
[254] M. Kuang, Z.Q. Wen, X.L. Guo, S.M. Zhang, Y.X. Zhang, Engineering firecracker-like beta-manganese dioxides@spinel nickel cobaltates nanostructures for high-performance supercapacitors, J. Power Sources 270 (2014) 426–433.
[255] R. Ding, L. Qi, M. Jia, H. Wang, Facile and large-scale chemical synthesis of highly porous secondary submicron/micron-sized $NiCo_2O_4$ materials for high-performance aqueous hybrid AC-$NiCo_2O_4$ electrochemical capacitors, Electrochim. Acta 107 (2013) 494–502.
[256] H. Wang, Q. Gao, J. Hu, Asymmetric capacitor based on superior porous Ni-Zn-Co oxide/hydroxide and carbon electrodes, J. Power Sources 195 (2010) 3017–3024.
[257] X. Lu, M. Yu, T. Zhai, G. Wang, S. Xie, T. Liu, C. Liang, Y. Tong, Y. Li, High energy density asymmetric quasi-solid-state supercapacitor based on porous vanadium nitride nanowire anode, Nano Lett. 13 (2013) 2628–2633.
[258] Z.S. Wu, W.C. Ren, D.W. Wang, F. Li, B.L. Liu, H.M. Cheng, High performance porous nickel cobalt oxide nanowires for asymmetric supercapacitor, ACS Nano 4 (2010) 5835–5842.
[259] Z. Lei, J. Zhang, X.S. Zhao, Ultrathin MnO_2 nanofibers grown on graphitic carbon spheres as high-performance asymmetric supercapacitor electrodes, J. Mater. Chem. 22 (2012) 153–160.
[260] H.L. Wang, C.M.B. Holt, Z. Li, X.H. Tan, B.S. Amirkhiz, Z.W. Xu, B.C. Olsen, T. Stephenson, D. Mitlin, Graphene-nickel cobaltite nanocomposite asymmetrical supercapacitor with commercial level mass loading, J. Nano Res. 5 (2012) 605–617.
[261] H. Gao, F. Xiao, C. Ching, H. Duan, Flexible all-solid-state asymmetric supercapacitors based on free-standing carbon nanotube/graphene and Mn_3O_4 nanoparticle/graphene paper electrodes, ACS Appl. Mater. Interfaces 4 (2012) 7020–7026.
[262] P.H. Yang, X. Xiao, Y.Z. Li, Y. Ding, P.F. Qiang, X.H. Tan, W.J. Mai, Z.Y. Lin, W.Z. Wu, T.Q. Li, H.Y. Jin, P.Y. Liu, J. Zhou, C.P. Wong, Z.L. Wang, Hydrogenated ZnO core-shell nanocables for flexible supercapacitors and self-powered systems, ACS Nano 7 (2013) 2617–2626.
[263] J.T. Zhang, J.W. Jiang, H.L. Li, X.S. Zhao, A high-performance asymmetric supercapacitor fabricated with graphene-based electrodes, Energy Environ. Sci. 4 (2011) 4009–4015.
[264] R. Wang, D. Jin, Y. Zhang, S. Wang, J. Lang, X. Yan, L. Zhang, Engineering metal organic framework derived 3D nanostructures for high performance hybrid supercapacitors, J. Mater. Chem. A 5 (2017) 292–302.
[265] L. Wang, Y. Han, X. Feng, J. Zhou, P. Qi, B. Wang, Metal-organic frameworks for energy storage: batteries and supercapacitors, Coord. Chem. Rev. 307 (2016) 361–381.
[266] Y. Zhao, Z. Song, X. Li, Q. Sun, N. Cheng, S. Lawes, X. Sun, Metal organic frameworks for energy storage and conversion, Energy Storage Mater. 2 (2016) 35–62.
[267] Y. Zhao, X. Li, B. Yan, D. Li, S. Lawes, X. Sun, Significant impact of 2D graphene nanosheets on large volume change tin-based anodes in lithium-ion batteries: a review, J. Power Sources 15 (2015) 869–884.
[268] R.R. Salunkhe, Y.V. Kaneti, Y. Yamauchi, Metal-organic framework-derived nanoporous metal oxides towards supercapacitor applications: progress and prospects, ACS Nano 11 (2017) 5293–5308.
[269] R. Kaur, K.H. Kim, A. Deep, A convenient electrolytic assembly of graphene-MOF composite thin film and its photoanodic application, Appl. Surf. Sci. 396 (2017) 1303–1309.
[270] R. Kaur, A. Rana, R.K. Singh, V.A. Chhabra, K.H. Kim, A. Deep, Efficient photocatalytic and photovoltaic applications with nanocomposites between CdTe QDs and an NTU-9 MOF, RSC Adv. 7 (2017) 29015–29024.
[271] G. Kim, J. Yang, N. Nakashima, T. Shiraki, Highly microporous nitrogen-doped carbon synthesized from azine-linked covalent organic framework and its supercapacitor function, Chem. Eur. J. 23 (2017) 17504–17510.
[272] S.B. Alahakoon, C.M. Thompson, G. Occhialini, R.A. Smaldone, Design principles for covalent organic frameworks in energy storage applications, Chem. Sus. Chem. 10 (2017) 2116–2129.
[273] B.J. Smith, A.C. Overholts, N. Hwang, W.R. Dichtel, Insight into the crystallization of amorphous imine-linked polymer networks to 2D covalent organic frameworks, Chem. Commun. 52 (2016) 3690–3693.

[274] T. Patsahan, J.M. Ilnytskyi, O. Pizio, On the properties of a single OPLS-UA model curcumin molecule in water, methanol and dimethyl sulfoxide molecular dynamics computer simulation results, Condens. Matter Phys. 20 (2017) 1–20.
[275] C.R. Mulzer, L. Shen, R.P. Bisbey, J.R. McKone, N. Zhang, H.D. Abruna, W.R. Dichtel, Superior charge storage and power density of a conducting polymer-modified covalent organic framework, ACS Cent. Sci. 2 (2016) 667–673.
[276] Q. Xu, S. Dalapati, D. Jiang, Charge up in wired covalent organic frameworks, ACS Cent. Sci. 2 (2016) 586–587.
[277] S. Chandra, D.R. Chowdhury, M. Addicoat, T. Heine, A. Paul, R. Banerjee, Molecular level control of the capacitance of two-dimensional covalent organic frameworks: role of hydrogen bonding in energy storage materials, Chem. Mater. 29 (2017) 2074–2080.
[278] Y. Han, N. Hu, S. Liu, Z. Hou, J. Liu, X. Hua, Z. Yang, L. Wei, L. Wang, H. Wei, Nanocoating covalent organic frameworks on nickel nanowires for greatly enhanced performance supercapacitors, Nanotechnology 28 (2017) 1–8.
[279] J. Romero, D.R.S. Miguel, A. Ribera, R.M. Balleste, T.F. Otero, I. Manet, F. Licio, G. Abellan, F. Zamora, E. Coronado, Metal-functionalized covalent organic frameworks as precursors of supercapacitive porous N-doped graphene, J. Mater. Chem. A 5 (2017) 4343–4351.
[280] M. Naguib, M. Kurtoglu, V. Presser, J. Lu, J. Niu, M. Heon, L. Hultman, Y. Gogotsi, M.W. Barsoum, Two-dimensional nanocrystals produced by exfoliation of Ti_3AlC_2, 2011, Adv. Mater. 23 (2011) 4248–4253.
[281] N.K. Chaudhari, H. Jin, B. Kim, D.S. Baek, S.H. Joo, K. Lee, MXene: an emerging two-dimensional material for future energy conversion and storage applications, J. Mater. Chem. A 5 (2017) 24564–24579.
[282] Q. Fu, J. Wen, N. Zhang, L. Wu, M. Zhang, S. Lin, H. Gao, X. Zhang, Free-standing $Ti_3C_2T_x$ electrode with ultrahigh volumetric capacitance, RSC Adv. 7 (2017) 11998–12005.
[283] J. Zhang, S. Seyedin, Z. Gu, W. Yang, X. Wang, J.M. Razal, MXene: a potential candidate for yarn supercapacitors, Nanoscale 9 (2017) 18604–18608.
[284] S.A. Shah, T. Habib, H. Gao, P. Gao, W. Sun, M.J. Green, M. Radovic, Template-free 3D titanium carbide ($Ti_3C_2T_x$) MXene particles crumpled by capillary forces, Chem. Commun. 53 (2017) 400–403.
[285] R.B. Rakhi, B. Ahmed, D. Anjum, H.N. Alshareef. Direct chemical synthesis of MnO_2 nanowhiskers on transition-metal carbide surfaces for supercapacitor applications, ACS Appl. Mater. Interfaces 8 (2016) 18806–18814.
[286] M. Hu, T. Hu, Z. Li, Y. Yang, R. Cheng, J. Yang, C. Cui, X. Wang, Surface functional groups and interlayer water determine the electrochemical capacitance of Ti_3C_2 T_x MXene, ACS Nano 12 (2018) 3578–3586.
[287] M.S. Balogun, W. Qiu, W. Wang, P. Fang, X. Lu, Y. Tong, Recent advances in metal nitrides as high-performance electrode materials for energy storage devices, J. Mater. Chem. A 3 (2015) 1364–1387.
[288] C. Zhu, P. Yang, D. Chao, X. Wang, X. Zhang, S. Chen, B.K. Tay, H. Huang, H. Zhang, W. Mai, H.J. Fan, All metal nitrides solid-state asymmetric supercapacitors, Adv. Mater. 27 (2015) 4566–4571.
[289] B. Das, M. Behm, G. Lindbergh, M.V. Reddy, B.V.R. Chowdari, High performance metal nitrides, MN (M = Cr, Co) nanoparticles for non-aqueous hybrid supercapacitors, Adv. Powder Technol. 26 (2015) 783–788.
[290] S. Lin, Y. Chui, Y. Li, S.P. Lau, Liquid-phase exfoliation of black phosphorus and its applications, Flat. Chem. 2 (2017) 15–37.
[291] X. Ren, P. Lian, D. Xie, Y. Yang, Y. Mei, X. Huang, Z. Wang, X. Yin, Properties, preparation and application of black phosphorus/phosphorene for energy storage: a review, J. Mater. Sci. 52 (2017) 10364–10386.
[292] C. Hao, B. Yang, F. Wen, J. Xiang, L. Li, W. Wang, Z. Zeng, B. Xu, Z. Zhao, Z. Liu, Y. Tian, Flexible all-solid-state supercapacitors based on liquid-exfoliated black--phosphorus nanoflakes, Adv. Mater. 28 (2016) 3194–3201.
[293] B. Yang, C. Hao, F. Wen, B. Wang, C. Mu, J. Xiang, L. Li, B. Xu, Z. Zhao, Z. Liu, Y. Tian, Flexible black-phosphorus nanoflake/carbon nanotube composite paper for high-performance all-solid-state supercapacitors, ACS Appl. Mater. Interfaces 9 (2017) 44478–44484.
[294] X. Chen, G. Xu, X. Ren, Z. Li, X. Qi, K. Huang, H. Zhang, Z. Huang, J. Zhong, A black/red phosphorus hybrid as an electrode material for high-performance Li-ion batteries and supercapacitors, J. Mater. Chem. A 5 (2017) 6581–6588.
[295] Y. Huang, M. Zhu, W. Meng, Y. Fu, Z. Wang, Y. Huang, Z. Pie, C. Zhi, Robust reduced graphene oxide paper fabricated with a household non-stick frying pan: a large-area freestanding flexible substrate for supercapacitors, RSC Adv. 43 (2015) 33981–33989.
[296] G. Cai, X. Wang, M. Cui, P. Darmawan, J. Wang, A. Eh, P. Lee, Electrochromo-supercapacitor based on direct growth of NiO nanoparticles, Nano Energy 12 (2015) 258–267.
[297] M. Zhu, Y. Huang, Y. Huang, W. Meng, Q. Gong, G. Li, C. Zhi, An electrochromic supercapacitor and its hybrid derivatives: quantifiably determining their electrical energy storage by an optical measurement, J. Mater. Chem. A 3 (2015) 21321–21327.
[298] F. Zhang, T. Zhang, X. Yang, L. Zhang, K. Leng, Y. Huang, Y. Chen, A high-performance supercapacitor-battery hybrid energy storage device based on graphene-enhanced electrode materials with ultrahigh energy density, Energy Environ. Sci. 6 (2013) 1623–1632.
[299] X. Peng, Q. Shuhai, X. Changjun, A new supercapacitor and Li-ion battery hybrid system for electric vehicle in ADVISOR, J. Phys. Conf. Ser. (2017) 1–6.
[300] S. Komaba, T. Hasegawa, M. Dahbi, K. Kubota, Potassium intercalation into graphite to realize high-voltage/high-power potassium-ion batteries and potassium-ion capacitors, Electrochem. Commun. 60 (2015) 172–175.
[301] Z. Li, K. Xiang, W. Xing, W.C. Carter, Y.M. Chiang, Reversible aluminum-ion intercalation in prussian blue analogs and demonstration of a high-power aluminum-ion asymmetric capacitor, Adv. Energy Mater. 5 (2015) 1401410–1401415.
[302] F. Wang, Z. Liu, X. Wang, X. Yuan, X. Wu, Y. Zhu, L. Fu, Y. Wu, A conductive polymer coated MoO_3 anode enables an Al-ion capacitor with high performance, J. Mater. Chem. A 4 (2016) 5115–5123.
[303] V. Presser, C.R. Dennison, J. Campos, K.W. Kneher, E.C. Kumber, Y. Gogotsi, The electrochemical flow capacitor: a new concept for rapid energy storage and recovery, Adv. Energy Mater. 2 (2012) 895–902.
[304] M. Boota, K.B. Hatzell, E.C. Kumbur, Y. Gogotsi, Towards high-energy-density pseudocapacitive flowable electrodes by the incorporation of hydroquinone, Chem. Sus. Chem. 8 (2015) 835–843.
[305] F. Wang, X. Wu, X. Yuan, Z. Liu, Y. Zhang, L. Fu, Y. Zhu, Q. Zhou, Y. Wu, W. Huang, Latest advances in supercapacitors: from new electrode materials to novel device designs, Chem. Soc. Rev. 46 (2017) 6816–6854.
[306] Y. Yoo, M.S. Kim, J.K. Kim, Y.S. Kim, W. Kim, Fast-response supercapacitors with graphitic ordered mesoporous carbons and carbon nanotubes for AC line filtering, J. Mater. Chem. A 4 (2016) 5062–5068.
[307] Y. Rangom, X.S. Tang, L.F. Nazar, Carbon nanotube-based supercapacitors with excellent ac line filtering and rate capability via improved interfacial impedance, ACS Nano 9 (2015) 7248–7255.
[308] Z. Wu, L. Li, Z. Lin, B. Song, Z. Li, K.S. Moon, C.P. Wong, S.L. Bai, Alternating current line-filter based on electrochemical capacitor utilizing template-patterned graphene, Sci. Rep. 5 (2015) 10983.
[309] N. Kurra, M.K. Hota, H.N. Alshareef, Conducting polymer micro-supercapacitors for flexible energy storage and Ac line-filtering, Nano Energy 13 (2015) 500–508.
[310] D. Qi, Y. Liu, Z. Liu, L. Zhang, X. Chen, Design of architectures and materials in in-plane micro-supercapacitors: current status and future challenges, Adv. Mater. 29 (2017) 1602802–1602821.
[311] Y. Shao, J. Li, H. Wang, Q. Zhang, R.B. Kaner, Flexible quasi-solid-state planar micro-supercapacitor based on cellular graphene films, Mater. Horiz. 4 (2017) 1145–1150.
[312] Z. Liu, H.I. Wang, A. Narita, Q. Chen, Z. Misc, D. Turchinovich, M. Klaui, M. Bonn, K. Mullen, Photoswitchable micro-supercapacitor based on a diarylethene-graphene composite film, J. Am. Chem. Soc. 139 (2017) 9443–9446.
[313] J. Lee, J.Y. Seok, S. Son, M. Yang, B. Kang, High-energy, flexible micro-supercapacitors by one-step laser fabrication of a self-generated nanoporous metal/oxide electrode, J. Mater. Chem. A 5 (2017) 24585–24593.
[314] Y. Yin, K. Feng, C. Liu, S. Fan, A polymer supercapacitor capable of self-charging under light illumination, J. Phys. Chem. C 119 (2015) 8488–8491.
[315] J. Xu, H. Wu, L. Lu, S.F. Leung, D. Chen, X. Chen, Z. Fan, G. Shen, D. Li, Integrated photo-supercapacitor based on bi-polar TiO_2 nanotube arrays with selective one-side plasma-assisted hydrogenation, Adv. Funct. Mater. 24 (2014) 1840–1846.
[316] A. Hartel, M. Janssen, D. Weingarth, V. Presser, R. Roij, Heat-to-current conversion of low-grade heat from a thermocapacitive cycle by supercapacitors, Energy Environ. Sci. 8 (2015) 2396–2401.
[317] S.L. Kim, H.T. Lin, C. Yu, Thermally chargeable solid-state supercapacitor, Adv. Energy Mater. 6 (2016) 1600546–1600553.
[318] A. Al-zubaidi, X. Ji, J. Yu, Thermal charging of supercapacitors: a perspective, Sustain. Energy Fuels 1 (2017) 1457–1474.
[319] J. Wang, S.P. Feng, Y. Yang, N.Y. Hau, M. Munro, E.F. Yang, G. Chen, "Thermal Charging" phenomenon in electrical double layer capacitors, Nano Lett. 15 (2015) 5784–5790.
[320] D. Zhao, H. Wang, Z.U. Khan, J. Chen, R. Karlsson, M.P. Jonsson, M. Berggren, X. Crispin, Ionic thermoelectric supercapacitors, Energy Environ. Sci. 9 (2016) 1450–1457.
[321] X. Li, L. Liu, X. Wang, Y.S. Ok, J.A.W. Elliott, S.X. Chang, H.J. Chung, Flexible and self-healing aqueous supercapacitors for low temperature applications: poly-ampholyte gel electrolytes with biochar electrodes, Sci. Rep. 7 (2017) 1685.
[322] S. Wang, N. Liu, J. Su, L. Li, F. Long, Z. Zou, X. Jiang, Y. Gao, Highly stretchable and self-healable supercapacitor with reduced graphene oxide based fiber springs, ACS Nano 11 (2017) 2066–2074.
[323] Y. Huang, M. Zhu, Z. Pei, Q. Xue, Y. Huang, C. Zhi, A shape memory supercapacitor and its application in smart energy storage textiles, J. Mater. Chem. A 4 (2016) 1290–1297.
[324] L. Xing, Y. Nie, X. Xue, Y. Zhang, PVDF mesoporous nanostructures as the piezo-separator for a self-charging power cell, Nano Energy 10 (2014) 44–52.
[325] A. Ramadoss, B. Saravanakumar, S.W. Lee, Y.S. Kim, S.J. Kim, Z.L. Wang, Piezoelectric-driven self-charging supercapacitor power cell, ACS Nano 9 (2015) 4337–4345.
[326] R. Song, H. Jin, X. Li, L. Fei, Y. Zhao, H. Huang, H.L. Chan, Y. Wang, Y. Chai, A rectification-free piezo-supercapacitor with a polyvinylidene fluoride separator and functionalized carbon cloth electrodes, J. Mater. Chem. A 3 (2015) 14963–14970.
[327] A. Maitra, S.K. Karan, S. Paria, A.K. Das, R. Bera, L. Halder, S.K. Si, A. Bera, B.B. Khatua, Fast charging self-powered wearable and flexible asymmetric supercapacitor power cell with fish swim bladder as an efficient natural bio-piezoelectric separator, Nano Energy 40 (2017) 633–645.